On the development of a surge bin

A vertical hydraulic transport model to predict concentration profiles

by

Alke Alexander de Boer

Delft University of Technology

Section of Dredging Engineering

July 28th , 2015

Master Thesis

Offshore & Dredging Engineering

On the development of a surge bin

A vertical dynamic transport model to predict concentration profiles

Graduation Committee:

ir. R. Lotman

Prof. Dr. ir. C. van Rhee

Dr. ir. A.M. Talmon

Under the authority of:

Royal IHC

Acknowledgements

This is the final part of the Master in Offshore & Dredging Engineering, at Delft University of Technology. The research carried out, was under the authority of Royal IHC Mining B.V., part of Royal IHC.

During this project, I have taken efforts to realize the results as they are presented within this report. However, this would not have been possible without the support of several strong individuals and organizations.
At first, I would like to extend my sincere thanks to all, who have supported me during the last milestone of my graduation.

I am highly indebted to Royal IHC Mining B.V. for their guidance and constant supervision, as well as for providing me the necessary information regarding the subject and also for their support in completing the project. In particular, I am grateful for the opportunity that Rick Lotman offered me to carry out this research and I would like to thank him for giving me the appropriate attention, feedback and time.

My thanks and appreciations also go to Maarten in't Veld and my other colleagues, who willingly helped me in developing the project with their abilities.

At the Delft University of Technology, I thank professor Cees van Rhee and Arno Talmon for their critical evaluation of my work, the possibility to discuss encountered difficulties, their advice and for their motivating feedback.

Last but not least, I take this opportunity to express my sense of gratitude towards Sabine, my parents and the rest of my family for their encouragement and support when things went down. You helped me in the completion of this project.

Xander de Boer
June 16th , 2015

Abstract

During the last years, developing economies such as China and India, have an increasing demand for heavy minerals because of their applications in urbanization and because of the growth in Gross Domestic Product and disposable incomes. The mining industry responds to this demand by developing new mines and by the innovation of new technologies.
In so called wet mines, the heavy minerals containing soil is excavated with dredgers. The dredged slurry is then pumped through a pipeline to the wet concentrator plant (WCP). In this processing facility, the valuable heavy minerals are extracted from the slurry by using separation spirals. The performance of spirals is related to the slurry feed and is adversely impacted by feed variability. Therefore, to work in the efficiency region of the spirals, the slurry flow and the slurry concentration must be as constant as possible.
Unfortunately, the production of the dredger fluctuates over time and, thus, cannot be coupled directly to the WCP. For this reason, a surge bin is placed between the dredger and WCP and functions as a large buffer tank to smoothen the production peaks of the dredger. Surge bins are typically conically shaped and vary in size depending on the number of dredgers that are connected to it. Surge bins do not only damp incoming concentrations, they also function as a separator of slimes and as a thickener.

To be able to design surge bins, it is of importance to get insight in how incoming concentrations are transformed in more damped out concentrations in the outflow. This leads to the primary objective of this thesis which is:

To develop a model which is able to simulate the sedimentation process within a surge bin and which can predict the volumetric concentration in the outflow as a result of the incoming concentration.

Therefore, the research as described in this thesis, focuses on the development of a dynamic 1.5D computer model in which the concentration at the outflow can be predicted as a result of the incoming concentration. The term 1.5D model implies that solid particles can travel only in vertical direct direction, assuming that gravitational forces are dominant. This would lead to a one-dimensional model. However, the conical shape plays an important role and must be implemented as well (1.5D).

At first, a bulk velocity is adopted within the surge bin as function of the inflow, outflow and jetflow. Subsequently, the hydraulic transport of solids is described by physical laws and equations. For the development of the 1.5D model, these equations are used in the advection-diffusion equation to describe the mathematical definition for the mixture flow in the surge bin. To determine the value of the diffusion coefficient, a function has been created which determines the coefficient as a function of the concentration gradient. The model, which is written in Matlab, is discretized in time with the explicit Forward Euler method and spatially discretized by making use of the Finite Volume Method.

An experiment on scale has been executed to gain information on the surge bin's functions. However, the primary goal was to validate the model. The experiment delivered good results and the buffer-function, damping-function and thickening-function are proven.
In addition, the calculated values from the model are compared with those measured with the experiment.
Based on the comparison between the results of the experiment and the model, it seems that the model introduces more damping and it needs significantly more time (20-40 seconds) to run out of sediment which is unfavorable. These effects can be the result of the applied numerical scheme. Nevertheless, it is concluded that the model gives good predictions because R squared (R^2) values are in the range of 0.76 up to 0.96 (these values indicate the correlation between the measured and calculated data). To make a better verdict on the applicability of the model, it is advised to gain prototype data. In addition, to reduce the numerical diffusion and to improve the accuracy of the model, other discretization methods should be applied.

Table of Contents

Nomenclature

Roman symbols

A	Cross-sectional area	$[m^2]$
D	Pipe diameter	$[m]$
Q	Volumetric flow	$[m^3/s]$
C_D	Drag coefficient	$[-]$
N	Number of fractions	$[-]$
v_m	Mean velocity	$[m/s]$
M	Mass	$[kg]$
V	Volume	$[m^3]$
$F_{gravity}$	Gravity force	$[kgm/s^2]$
$F_{buoyancy}$	Buoyancy force	$[kgm/s^2]$
F_{drag}	Drag force	$[kgm/s^2]$
v	Constant velocity	$[m/s]$
g	Gravitational acceleration	$[m/s^2]$
d	Particle diameter	$[m]$
C_D	Drag coefficient	$[-]$
v_s	Vertical settling velocity	$[m/s]$
Re_p	Particle Reynolds number	$[-]$
T	Temperature	[℃]
C_1	Ferguson & Church constant	$[-]$
C_2	Ferguson & Church constant	$[-]$
Stk	Stokes number	$[-]$
f_{wall}	Wall factor	$[-]$
v_{ts}	Terminal settling velocity	$[m/s]$
n	Richardson & Zaki exponent	$[-]$
v_{slip}	Slip velocity	$[m/s]$
v_h	Hindered settling velocity	$[m/s]$
$Q_{overflow}$	Overflow rate	$[m^3/s]$
Q_{inflow}	Inflow rate	$[m^3/s]$
$Q_{outflow}$	Outflow rate	$[m^3/s]$
Q_{jet}	Jetflow rate	$[m^3/s]$

F	Flux	$[-]$
t	Time	$[s]$
K	Constant in diffusion function	$[-]$
H^*	Dimensionless overflow rate	$[-]$
B	Width	$[m]$
L	Length	$[m]$
Fr	Dimensionless Froude number	$[-]$
C_v	Volumetric concentration	$[-]$

Greek symbols

ρ	Density	$[kg/m^3]$
ϕ	Volumetric fraction	$[-]$
ψ	Shape factor	$[-]$
ν	Kinematic viscosity	$[m^2/s]$
Δ	Specific density	$[-]$
μ	Dynamic viscosity	$[\mathrm{kg/ms}]$
κ	Diffusion coefficient	$[m^2/s]$

Subscripts

l	Liquid/water	$[-]$
s	Solids	$[-]$
m	Mixture	$[-]$
k	Fraction index	$[-]$
i	Position index	$[-]$

Superscript

n	Time index	$[-]$

List of Tables

List of Figures

Chapter 1

1. Introduction

During the last years, developing economies such as China and India, have an increasing demand for heavy minerals because of their applications in urbanization and because of the growth in Gross Domestic Product and disposable incomes. The mining industry responds to this demand by developing new mines and by the innovation of new technologies.

1.1 Heavy minerals

Mineral sands are sand deposits that contain minerals with a high specific gravity, also known as heavy minerals. Because of their higher specific gravity, heavy minerals tend to accumulate in placer deposits, which are accumulations of valuable minerals formed by gravity separation during sedimentary processes. Along coastlines, these placer deposits are often found because waves and currents deposit sand on the beaches. The backwash then carries the lighter minerals, such as quartz, back into the sea while the heavier minerals accumulate. In addition, onshore winds transport the lighter sediment inland, leading to higher concentrations of heavy minerals near the coastline (Heavy minerals, 2013). The deposits of heavy mineral sands generally consist of zircon, ilmenite, rutile and leucoxene.
Ilmenite, leucoxene and rutile are used as feedstock to produce titanium dioxide (TiO_2) which, on its turn, is used to produce pigment for coatings, plastics and other applications.
Zircon is used in the ceramics industry where it is milled into fine flour for tiles, sinks, bathtubs and so on. Furthermore, zircon is also used for refractory and abrasive applications and forms the most valuable heavy mineral in the mineral sands. (Moore, 2011) (Equity development, 2011) (TZMI, 2013)

1.2 The wet mining cycle

To excavate the onshore mineral sands, two main methods can be applied: dry excavating with the use of shovels and trucks, or dredge mining by the use of floating dredgers and pipelines. When large amounts of sediment need to be processed, such as mineral sands, dredge mining is used because the excavations costs per ton are lower (up to factor of 10).

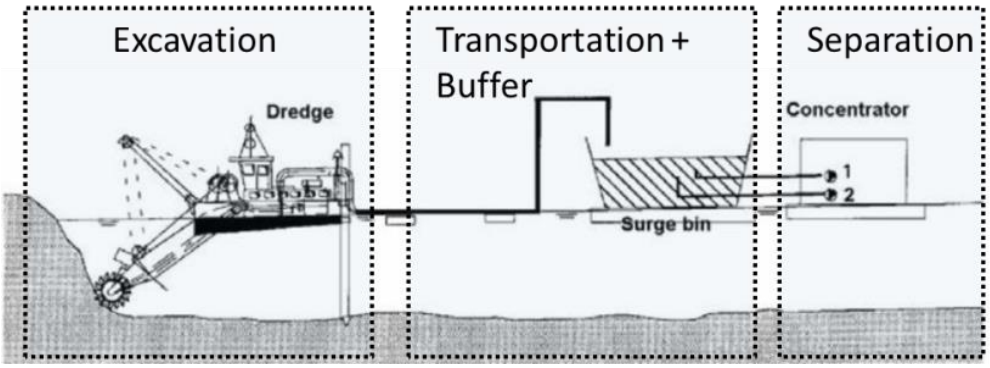

Figure 1-1 Dredge mining operation (Herchhorn, van Muijen, Ouwerkerk, Boor, Verkaik & Wit)

In Figure 1-1, the dredge mining cycle is divided into three processes: excavation, transportation (with buffering) and separation.

The excavation is typically done by bucket wheel dredgers or by cutter suction dredgers (CSD) but a combination of both types is also possible. The main difference between both types is that a bucket wheel dredge delivers a more constant production of solids while a CSD can reach higher but fluctuating productions in sandy soils. To transport the soil, water is needed to create a sand-water mixture (slurry) so it can be pumped to the desired location.

Once the soil is excavated, the slurry is pumped through a pipeline to the wet concentrator plant (WCP). In this processing facility, the valuable heavy minerals are extracted from the slurry by using separation spirals. These spirals can be described as centrifugal sluices that make use of the density properties of the minerals. When the slurry enters the spiral, the lighter particles (silica sand and clay) are thrown to the outer edge of the spiral helix while the higher density particles move along the inner helix of the spiral. The performance of spirals is related to the slurry feed and is adversely impacted by feed variability. Therefore, to work in the efficiency region of the spirals, the slurry flow and the slurry concentration must be as constant as possible (Mular, Halbe, & Barrat, 2002).

Unfortunately, the production of the dredger fluctuates over time and, thus, cannot be coupled directly to the WCP. For this reason, a surge bin is placed between the dredger and WCP and functions as a large buffer tank to smoothen the production peaks of the dredger. In addition it prevents the WCP from running out of sand if the CSD is has to move the spud poles.

Surge bins know their application typically in the heavy minerals industry, however, the application of surge bins to other mining operations is therefore not exempted.

1.3 Surge bin properties

As mentioned before, the surge bin is a buffer tank which collects the production of the dredger. However, it has more functions than only buffering.

Before the other functions are elaborated, the design of existing surge bins will be discussed. Figure 1-2 is a typical schematization of a surge bin as it is found in dredge mines. Right on top, a slurry flow with a fluctuating concentration enters the surge bin via a trommelscreen. This device filters boulders and other large obstacles out of the mixture. The surge bin has the typical form of a funnel and varies in size, depending on the amount of dredgers that are connected to it. At the bottom, fluidization jets are present to prevent hang up and to keep the sediment in suspension. Since the spirals in the WCP can handle relatively high mixture densities, the surge bin functions also as a thickener. By reducing the flow of the outlet, a net upward flux of water will occur and end up in the overflow, placed on top of the surge bin. A result of this volume balance is that a net upward flow is generated which leads to the last function of the surge bin: desliming. Slimes are very fine particles ($< 45\mu m$) which have a negative effect on the efficiency of the spirals (Chandrakala, Gajanan , & Mohan , 2006). Due to the upward flow in the surge bin, these slimes are not able to settle and, thus, flow along with the water into the overflow.
(Coastal & Environmental Services, 2002)

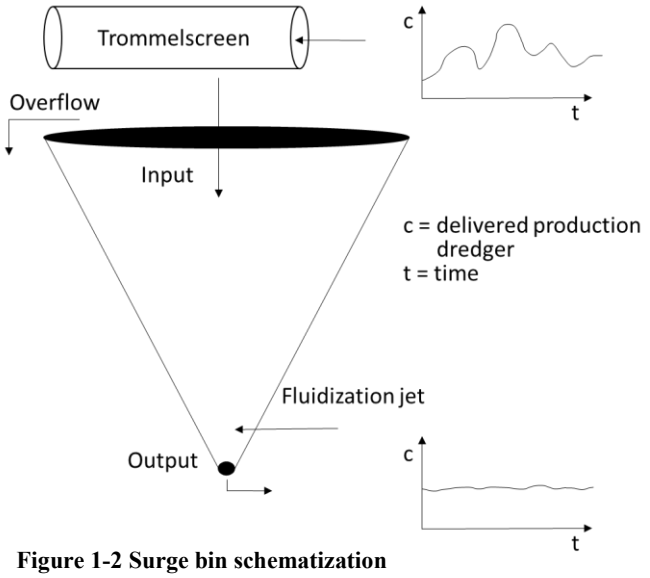

Figure 1-2 Surge bin schematization

Figure 1-3: Left: 2 CSD's connected to the surge bin and WCP; Right: top view of the surge bin

However, in spite of knowing the functionalities of the surge bin, very little information is present in terms of buffer capacities, overflow losses and the values of the jet and outflow. From personal communication with employees of Royal IHC, information became available based on their personal practical observations. Figure 1-3 shows an example of a surge bin located in the Moma mine in Mozambique. Here two CSDs can be seen which are connected to the surge bin and WCP via floating pipelines. The surge bin is placed behind the WCP and is not visible on the left picture. The photograph on the right shows the top of the surge bin

where slimes are floating over the edge into the overflow. The dimensions of the surge bin in Moma are about $19m$ in height and a diameter of $22m$, leading to an estimated volume of $2400m^3$ and an angle of 60°, relative to the horizontal. Similar surge bins are used in heavy minerals mine QMM in Madagascar (in't Veld, Surge bins at IHC sites, 2014). More photographs can be found in Appendix A

1.4 Problem definition

In order to transform the discontinuous production of the dredger into a more constant production, as is required by the concentration plant, the process of how the concentration profile in the buffer tank develops over time must be understood. If the sedimentation process is modeled, the concentration profile at the outflow of the surge bin can be determined and predictions can be made on how the surge bin transforms the incoming concentration signal. Subsequently, the dimensions of the surge bin could be optimized in such a way that it can buffer enough sediment to fill the time gap when a CSD delivers no sediment.

1.5 Thesis objective

In practice, optimizing the size of a surge bin will make it possible to reduce the production costs. However, the surge bin should be optimized in such a way that it still fulfills its functions. In this thesis, research is described aiming to understand processes that occur within the surge bin. Aspects such as buffering, thickening, separating and damping will be looked at. However, the primary objective is to develop a model which is able to simulate the sedimentation process within a surge bin and which can predict the volumetric concentration in the outflow as a result of the incoming concentration.
Subsequently, the model should be tested and be used to make prototype simulations. By adjusting the dimensions of the surge bin, an optimal volume should be derived in relation to feed parameters.

1.6 Report outline

Several steps are made to derive a satisfactory 1.5D model, to simulate the outgoing concentration of a surge bin. This report describes the essential steps that are taken in the derivation, calculation and validation of a 1.5D numerical model.

In chapter 2, a literature research is given based on the relevant physical phenomena for vertical hydraulic transport of solids. Subjects such as the settling and hindrance of the settling of particles are described.

In chapter 3, the derivation and implementation of the 1.5D model is given. First, several assumptions are described, including appropriate explanations and motivations. Next, the numerical model is elaborated: discretization methods, equations and boundary conditions are explained. In addition, a function is derived to deal with unexpected situations near the inlet and near the jet.
At last, to test the model, typical simulations have been carried out of which the results have been analyzed.

An experiment has been executed to validate the proper working of the numerical model. The entire test arrangement of the experiment is described in chapter 4. Here, the reader will find information on the applied

scaling laws, used instrumentation, working principles of the experiment and the methods the sensors are calibrated.

In chapter 5 the results of the experiment are first analyzed to make a verdict on the functions of the surge bin. Subsequently, a motivation is given on the determination of an introduced parameter K. Hereafter, the measured results of the experiment are compared with the calculated values of the numerical model. All of the datasets are placed in Appendix C.

The numerical model is used to make different true scale simulations, as reported in chapter 6. In these simulations, the size of the surge bin has been changed three times after which the results have been analyzed. After comparison of the results, a verdict has been made on which surge bin is best applicable.

Finally, the conclusions which can be drawn from the results of this report, are given in chapter 7. In addition, a list of recommendations for further development of the model is given.

Chapter 2

2. Physics of slurry flows

The sedimentation of solid particles in a surge bin can be compared with sedimentation models of hoppers and vertical transport models. In these models, the settling velocities of particles play an important role. These settling velocities are affected by many physical phenomena, therefore it is important to understand the underlying physics. A literature survey has been carried out on the physics of slurry flows which are described and discussed in this chapter.

2.1 General definitions

In the dredging industry, flows consist out of water and sediments such as sand, boulders, heavy minerals and so on. Because of the two occurring phases, fluid and solid, these flows are often referred to as two-phase flows or slurry flows. This report deals with both liquid and solid phases and, therefore, the subscripts *l* and *s* are introduced respectively to indicate which phase is considered. When multiple fractions of solids are considered, a certain fraction is indicated by the subscript *k*. In addition, when the two phases are described at the same time, subscript *m* is used.

2.1.1 MEAN VELOCITY

Solid particles occur in different sizes, shapes and densities. This variety in properties results in different settling velocities and will be discussed later in this chapter. In a slurry flow, the velocities of particles and the carrier fluid will be different. However, to make calculations with slurry flows, the bulk velocity is introduced:

$$v_m = \frac{Q_s + Q_l}{A} = \frac{\sum_{k=1}^{N} Q_{s,k} + Q_l}{A} = \frac{4Q_m}{\pi D^2} \tag{2.1}$$

In which v_m is the average bulk velocity in radial direction in a vertical pipe with diameter D. The bulk velocity, also called mean mixture velocity, is the ratio of the volumetric mixture flow Q_m divided by the cross-sectional area of the circular pipe. Q_m consists of the sum of liquid flow and solids flows (N fractions).

2.1.2 SOLID VOLUME FRACTION AND MIXTURE DENSITY

To indicate the part of a certain volume that is occupied by solids, the solid volume fraction ϕ_s is used.

$$\phi_s = \frac{V_s}{V_s + V_l} = \frac{\sum_{k=1}^{N} V_{s,k}}{\sum_{k=1}^{N} V_{s,k} + V_l} \tag{2.2}$$

Where V represents the volume of the solids and liquid. Now, by using a mass and volume balance, the mixture density can be derived. The mass and volume balances are given respectively by:

$$M_m = M_s + M_l = \sum_{k=1}^{N} M_{s,k} + M_l \tag{2.3}$$

$$V_m = V_s + V_l = \sum_{k=1}^{N} V_{s,k} + V_l \tag{2.4}$$

Where M represents the mass and V the volume. When the specific density of the fractions and fluids are known, the following relation can be derived:

$$\rho_m V_m = \rho_s V_s + \rho_l V_l = \sum_{k=1}^{N} (V_{s,k}\rho_{s,k}) + V_l\rho_l \tag{2.5}$$

In which ρ is the specific density of the sediment or liquid. Combining equations (2.5) and (2.2) leads to an expression for the mixture density.

$$\rho_m = (1 - \phi_s)\rho_l + \phi_s\rho_s \tag{2.6}$$

2.2 Settling velocity of sediments

The objective of this thesis is to describe how the volumetric concentration profile evaluates over time in the vertical direction. Therefore, settling velocities of particles in vertical direction are analyzed.

2.2.1 SETTLING VELOCITY OF A SINGLE PARTICLE

Very small particles, when submerged in water, have a mass small enough that they reach a terminal velocity before any turbulence develops. For larger particles, a separation wake can develop behind the falling particle. This wake results in turbulence and large pressure differences between the front and back of the particle. For some particles this effect can become so strong that viscous forces become small compared to pressure forces and turbulent drag dominates.
Assuming that a single particle settles in a stagnant fluid and all forces other than gravity, drag and buoyancy are neglected, the force balance can be written as:

$$F_{gravity} = F_{buoyancy} + F_{drag} \tag{2.7}$$

This force balance is visualized in Figure 2-1. In a fluid, the particle will settle because of gravity: $F_{gravity}$. The upward directed force F_{drag} is caused by the frictional drag of the surrounding fluid while the buoyancy force $F_{buoyancy}$ equals the magnitude of the weight of the fluid that is displaced by the particle.
The above described forces can be calculated by:

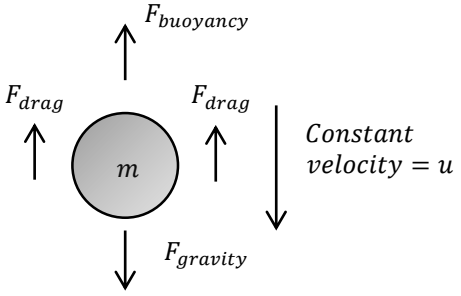

Figure 2-1: Forces on a settling particle

$$F_{gravity} = \rho_s g V \psi \tag{2.8}$$

$$F_{buoyancy} = \rho_w g V \psi \tag{2.9}$$

$$F_{drag} = C_D \frac{1}{2} \rho_w v_s^2 A \tag{2.10}$$

In equations (2.8) and (2.9), V is the volume of a particle and equals $V = \pi d^3/6$, g is the gravitational acceleration and ψ is the shape factor. The shape factor is a correction factor for the deviation of a non-spherical particle compared to a perfect sphere. For sand particles a shape factor value of 0.7 can be chosen. In equation (2.10), A is the area of the particle subjected to the resistance of the flow and is equal to $A = \frac{1}{4}\pi D^2$ and v_s is the vertical settling velocity of the particle. After substituting and rearranging the equations, the following formula for the settling velocity is obtained:

$$v_s = \sqrt{\frac{4g(\rho_s - \rho_w)d\psi}{3C_D\rho_w}} \tag{2.11}$$

Where d is the diameter of the particle and C_D is the drag coefficient. An empirical formula (Turton & Levenspiel, 1986) gives the relation between the drag coefficient and the particle Reynolds number:

$$C_D = \frac{24}{Re_p}\left(1 + 0.173 Re_p^{0.657}\right) + \frac{0.413}{1 + 16300 Re_p^{-1.09}} \tag{2.12}$$

The Reynolds particle number is defined as:

$$Re_p = \frac{v_s d}{\nu} \tag{2.13}$$

Where ν is the kinematic viscosity of the water in $[m^2/s]$ and can be calculated for water using the following relation:

$$\nu = \frac{40 \cdot 10^{-6}}{20 + T} \tag{2.14}$$

Where T is the temperature of the water in $°C$.
Looking at equations (2.11), (2.12) and (2.13), an iterative procedure is needed to calculate the settling velocity of a particle because the drag coefficient is a function of the particle Reynolds number (see Figure 2-2).

A more common way to calculate the settling velocity is to determine the regime of the flow. The drag coefficient is dependent of the regime of the particle which can be laminar, turbulent or transitional and is determined by the particle Reynolds number Re_p.

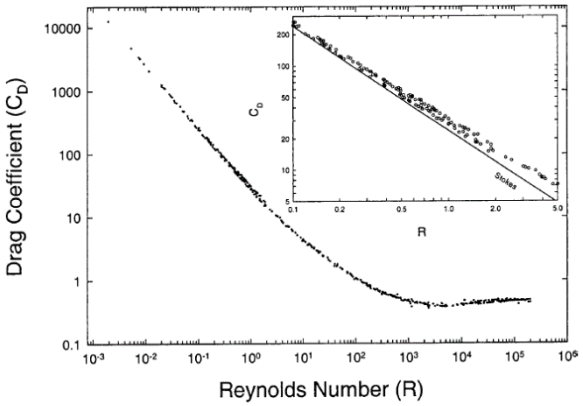

Figure 2-2 Relation between C_D and Re. (Brown & Lawler, 2003)

$$\begin{aligned} C_D &= 24/Re_p && Re_p \leq 1 \\ C_D &= \frac{24}{Re_p} + \frac{3}{\sqrt{Re_p}} + 0.34 && 1 < Re_p \leq 2000 \\ C_D &= 0.4 && Re_p > 2000 \end{aligned} \tag{2.15}$$

When $Re_p \leq 1$, the regime is called to be laminar because the particle moves through the fluid under streamlined conditions. For this regime, the Stokes settling velocity can be used:

$$v_s = \frac{\psi(\rho_s - \rho_w)gd^2}{18\nu\rho_w} = \frac{\psi\Delta g d^2}{18\nu} \tag{2.16}$$

Where Δ is the specific density of the particle and is defined as $\Delta = (\rho_s - \rho_w)/\rho_w$.

For $Re_p > 2000$, the flow around the particle is fully turbulent. Rittinger developed a settling formula for particles with diameter $d > 1mm$:

$$v_s = 1.8\sqrt{\Delta g d \psi} \tag{2.17}$$

In the transitional regime ($1 < Re_p \leq 2000$), Budryck derived the settling velocity for particles with $d > 0.1mm$ and $d < 1mm$:

$$v_s = 8.925\frac{(\sqrt{1 + 95(\rho_s - \rho_w)d^3} - 1)}{d} \tag{2.18}$$

In these equations, the diameter d of the particle is in $[mm]$, the densities ρ are in $[kg/m^3]$ and the settling velocity v_s is in $[mm/s]$.
The above presented settling formulas are plotted in Figure 2-3. Here, the black, thick line represents the combination of equations for the three different regions.

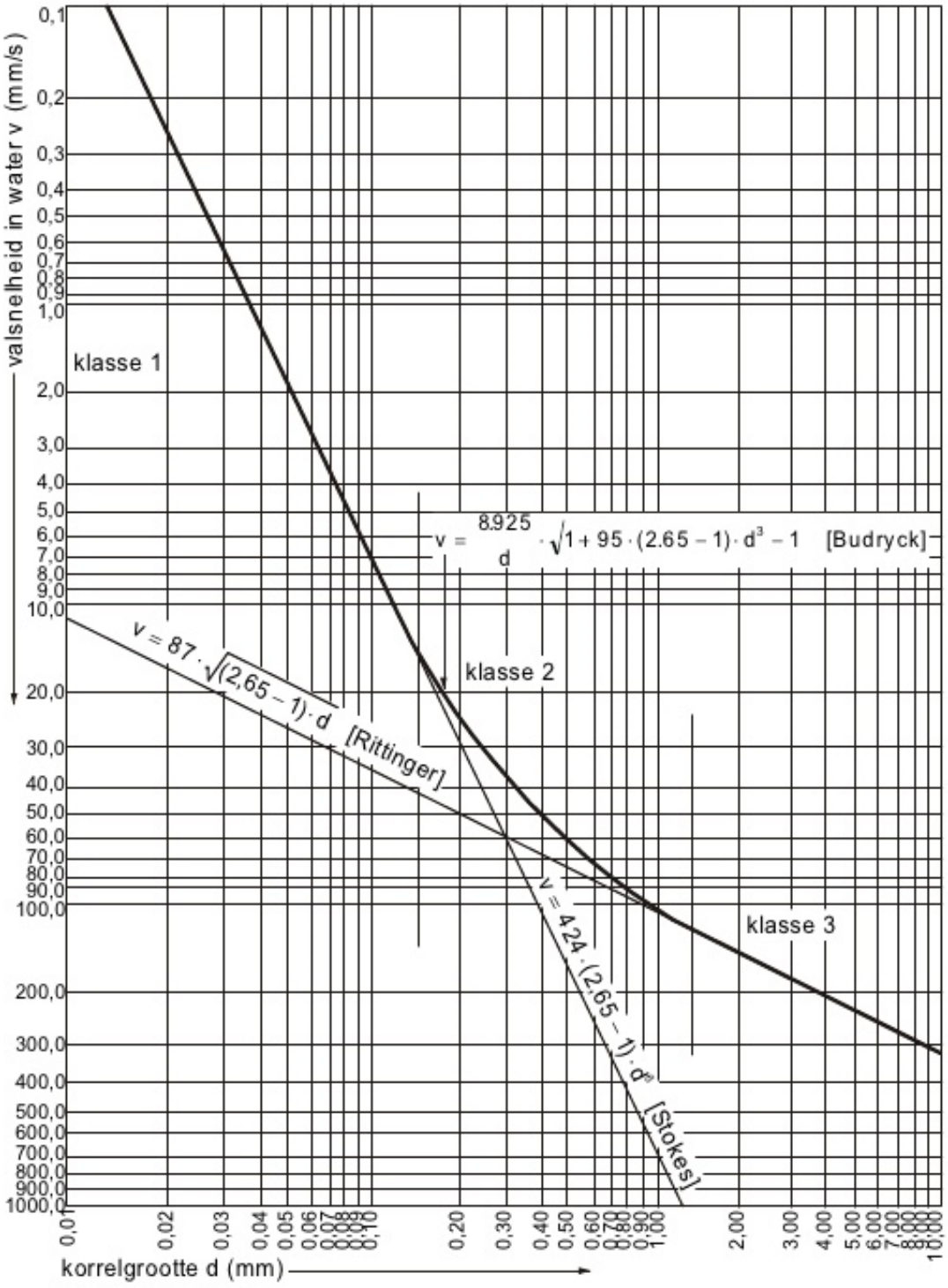

Figure 2-3 Terminal settling velocity of sand and water particles using Stokes, Budryck and Rittinger equations. Graph is taken from (Matoušek, 2004)

Another formula in the transitional regime is given by Ruby & Zanke. The dimensions of the settling velocity and particle diameter are $[m/s]$ and $[m]$ respectively.

$$v_s = \frac{10\nu}{d}\left(\sqrt{1+\frac{\Delta g d^3}{100\nu^2}}-1\right) \tag{2.19}$$

So, to solve equation (2.11), an iterative procedure is required because the drag coefficient is a function of the particle Reynolds number. For sake of simplicity the explicit equations of Stokes, Budryck and Rittinger can be used to determine the settling velocity without iteration.
An equation that can be applied to the entire range of sediment particles is given by the equation of Ferguson and Church (Ferguson & Church, 2004).

$$v_s = \frac{\Delta g d^2}{C_1\nu + \sqrt{0.75 C_2 \Delta g d^3}} \tag{2.20}$$

Where C_1 and C_2 are theoretical constants that take values of 18 and 0.4 respectively for smooth spheres. Depending on the shapes of the sediment, $C_2 \approx 1$ for natural grains with some variation in sphericity.
The advantage of this formula is that it is applicable for all grain sizes, including the transitional regime. Another advantage is that the formula includes the effects of specific densities and viscosity. Because of its simplicity, the equation of Ferguson and Church is used in the 1.5D computer model.

2.2.2 STOKES NUMBER

The terminal settling velocities, as described in the previous section, are not reached instantaneously but after a certain time and therefore it is important to analyze the behavior of grains in a fluid. To relate the particle response time to the flow field of the surrounding fluid, the dimensionless Stokes number is used. The Stokes number is defined as the ratio of the characteristic time scale of a particle to the characteristic time scale of the flow.

$$Stk = \frac{\tau_p}{\tau_f} = \frac{\tau_p u}{L} \tag{2.21}$$

In which τ_p and τ_f are the particle and hydrodynamic timescale respectively. The hydrodynamic timescale is subsequently defined as the ratio of a velocity u and length scale L.
When the Stokes number is large ($Stk \gg 1$), the behavior is dominated by mutual collisions of the particles and the grains are barely influenced by the fluctuations in the flow field. On the other hand, particles respond almost immediately to velocity fluctuations in the flow field when the Stokes number is small ($Stk \ll 1$) which means that the grains will follow the flow.

2.2.3 WALL EFFECT

Another phenomenon that has effect on the settling velocities of particles is the presence of the surrounding wall of a pipeline, or in this case the presence of the surge bin. When particles settle, the underlying fluid has to be displaced resulting in a flow in the opposite direction as a result of the volume balance.
The counter flux of the fluid can only flow through the free area available because it is bound by the wall. When the particle diameter approaches the diameter of the wall, the free area for the counter flow decreases. This decrease leads to a higher counter flow and makes it more difficult for the fluid to flow around the particle. As a result, the opposing motion of the water has a delaying effect on the settling velocity of the particle. The wall effect is described by the ratio of the settling velocity in a bounded fluid to the free settling velocity in an unbounded fluid. This ratio is called the wall factor.
An expression for the wall factor which covers the laminar, intermediate and turbulent regime has been derived by Di Felice (Di Felice, 1996).

$$f_{wall} = \frac{v_{tw}}{v_{ts}} = \left(\frac{1-\lambda}{1-0.33\lambda}\right)^{\phi_{wall}} \tag{2.22}$$

Here, f_{wall} is the wall factor, v_{tw} and v_{ts} are the terminal settling velocities in an unbounded and bounded fluid respectively and λ is the ratio between the grain diameter and the diameter of the pipe.
ϕ_{wall} is a function of the particle Reynolds number and is given by:

$$\frac{3.3-\phi_{wall}}{\phi_{wall}-0.85} = 0.1Re_p \tag{2.23}$$

For practical considerations, the wall effect is of importance when λ reaches values higher then 0.05 (Arsenijević, Grbavčić, Garić-Grulović, & Bošković-Vragolović, 2010).

2.3 Hindered Settling

So far, the settling behavior of a single particle in a fluid is described. Considering a real slurry mixture, the volumetric concentration of solids will be higher and the settling velocities are influenced as the grains interfere with each other. This effect is called hindered settling and is caused by the concentration of solids in the fluid.

2.3.1 EFFECT OF CONCENTRATION

At first, consider a mixture of which the particles are all having the same size and physical properties. To correct the terminal settling velocity for the influence of the volumetric concentration, it is multiplied with the so called hindered settling function.

$$v_h = f(\phi_s)v_{ts} \tag{2.24}$$

Here, v_h is the hindered settling velocity and $f(\phi_s)$ is the hindered settling function as a function of the volumetric concentration. A well-known empirical relation was proposed by Richardson & Zaki (1954) to describe the hindered settling function:

$$f(\phi_s) = (1 - \phi_s)^n \tag{2.25}$$

In this equation, Richardson & Zaki introduced an exponent n as a function of the particle Reynolds number and the diameter ratio of the particle and tube: d/D. The following relations were found:

$$\begin{aligned} &Re_p \leq 0.2 && n = 4.65 + 19.5\frac{d}{D} \\ &0{,}2 < Re_p \leq 1 && n = (4.35 + 17.5\frac{d}{D})Re_p^{-0.03} \\ &1 < Re_p \leq 200 && n = (4.45 + 18\frac{d}{D})Re_p^{-0.1} \\ &200 < Re_p \leq 500 && n = 4.45Re_p^{-0.1} \\ &500 < Re_p && n = 2.39 \end{aligned} \tag{2.26}$$

These values are obtained by experiments with concentrations $0.05 < \phi_s < 0.65$ and particle Reynolds numbers $0.000185 < Re_p < 7150$. It can be noted that the constant values are obtained for low and high Reynolds numbers. However, these values do not represent a smooth curve as can be seen in Figure 2-4.

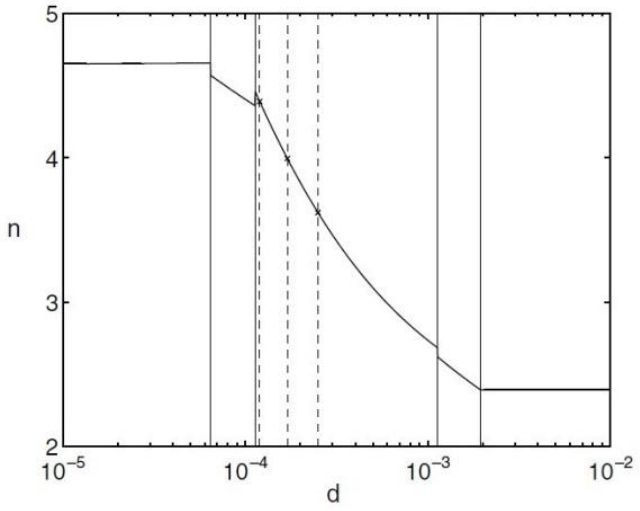

Figure 2-4 Hindrance exponent n as a function of particle diameter d (Basson, Berres, & Bürger, 2009)

However, a smoothened curve of the Richardson & Zaki curve is obtained when using the following relation:

$$n = \frac{a + bRe_p^{\alpha}}{1 + cRe_p^{\alpha}} \tag{2.27}$$

With values for the coefficients a, b, c and α presented in Table 2-1.

Table 2-1: Coefficients for hindered settling function

Authors	Re_p	Concentration	a	b	c	α
Garside & Al-Dibouni	$0.001 < Re_p < 3.10^4$	$0.04 < \phi_s < 0.55$	5.1	0.27	0.1	0.9
Rowe	$0.2 < Re_p < 10^3$	$0.04 < \phi_s < 0.55$	4.7	0.41	0.175	0.75
Di Felice	$0.01 < Re_p < 1.10^3$	$0 < \phi_s < 0.05$	6.5	0.3	0.1	0.74

The coefficients as derived by Garside and Rowe are used in the sedimentation model because of their application for high volumetric concentrations.

2.3.2 EFFECT OF PARTICLE SIZE DISTRIBUTION

The hindered settling relation as presented in equation (2.24**)** holds for single sized suspensions. To solve the equation for multiple fractions or poly-dispersed suspensions, another approach needs to be followed. In reality, very small particles can flow in the opposite direction because of the return flow of larger particles. A simple relation, which includes multiple fractions of sediment, can describe the settling velocity $v_{s,k}$ of a certain fraction k:

$$v_{s,k} = v_{ts,k}(1-\phi_s)^{n_k} \qquad \phi_s = \sum_{k=1}^{N} \phi_{s,k} \tag{2.28}$$

Here, n_k is corresponding with the particle Reynolds number of the relevant fraction. By using this equation, all particles would travel in the same direction and, thus, the effect that smaller particles might move in opposite direction is neglected.

As mentioned in chapter 1.3, fines play an important role and, thus, neglecting the return effect is not favorable. To incorporate this effect, a different approach must be used.

It is assumed that each particle settles with a so called slip velocity relative to the surrounding fluid velocity:

$$v_{h,k} = v_l - v_{slip,k} \tag{2.29}$$

In this equation v_{slip} is the slip velocity of a certain fraction and according to Mirza & Richardson (1979) it is calculated with:

$$v_{slip,k} = v_{ts,k}(1-\phi_s)^{n-1} \tag{2.30}$$

When considering a closed system, the volume balance of solids and water in vertical direction must hold. This means that the downward flow of sand must be compensated by the upward flow of the water. The formulae presented above are used for single fractions only. To calculate the settling velocities when *N* fractions are present in the mixture, the combined balance of all fractions must be satisfied:

$$\sum_{k=1}^{N} \phi_{s,k}\, v_{h,k} + (1-\phi_s) v_l = 0 \tag{2.31}$$

Here, the total volumetric transport of solids is given by the first term, while the second term describes the counter flow of the fluid. Now, an expression for the velocity of the fluid due to the transport of the particles (both upward and downward) is simply given by:

$$v_l = \sum_{j=1}^{N} \phi_{s,j} v_{h,j} \tag{2.32}$$

When equations (2.30) and (2.32) are substituted into (2.29), the final expression for the hindered settling velocity of a fraction k can be determined:

$$v_{s,k} = \sum_{j=1}^{N} \phi_{s,j} v_{h,j} - v_{slip,k} \tag{2.33}$$

Masliyah (1979) derived a similar expression as equation (2.33). The model is given by:

$$v_{s,k} - v_l = \frac{g d_k^2}{18 \mu_f} f(\alpha_t)(\rho_k - \rho_m) \tag{2.34}$$

This equation represents the generalized form of the slip velocity for the k^{th} fraction and is applicable in the low Reynolds number region.

Chapter 3

3. Model approach

This chapter elaborates on how the model's structure is dealt with. First, the occurring processes and other properties of the surge bin are described. Subsequently, an explanation is given on how these processes can be modelled and which assumptions should be made. At last, several simple model tests are carried out to test some first expectations.

3.1 Surge bin and its dominant processes

Chapter 1 already described the importance of the application of surge bins in wet mines. Basically, the surge bin must satisfy four functions: buffering, thickening, damping and separating.
The buffer function is proportional to the size. Assuming that a surge bin with a certain volume is filled with a sand water mixture and the CSD has zero production, it can provide the WCP with this mixture till the bin runs out of sediment. In fact, this period of time can be called the "idle time".
Thickening is a relative notion. If the delivered concentration of the dredger is high enough, no thickening is needed. However, from practice it is known that a dredger's average delivered concentration is lower than the required concentration from the WCP. To get a sense on the values that should be thought of, the spirals' optimal working range lies around the 45% of mass concentration (Henk van Muijen). This equals a volumetric concentration of about 23%. The thickening function in the surge bin can take place by reducing the flow of the outlet, relative to the flow of the inlet. A surplus of water will flow over the edge of the bin and, as a result, a higher concentration in the outflow is obtained. The surge bin is conically shaped so the sediment congregates at the bottom where it is sucked away by the discharge pump.
As mentioned above, a surplus of water flows over the edge because the inflow is higher than the outflow. In addition, jets are installed at the bottom of the bin to keep the sediment in suspensions and prevent bed forming. The amount of jet water can be added to the surplus of water reaching the overflow.

$$Q_{overflow} = Q_{inflow} + Q_{jet} - Q_{outflow} \tag{3.1}$$

Because of the surge bins' increasing cross-section area in upward direction, the velocity of the water will decrease significantly since it is proportional to the diameter D of the bin. As a result, particles with low settling velocities will follow the flow of the water and end up in the overflow. This function is called desliming or separating and can be regulated by adjusting the flows.
Last but not least, the surge bin must damp the incoming fluctuating production of the dredger. Typically, a CSD cannot deliver a constant mixture concentration for several reasons. For example, the production is different when the cutter is undercutting or overcutting, or, if the soil starts to breach, a higher and more continuous production can be delivered. In addition, when the CSD has to reposition the dredge ladder or the

spuds, only water is pumped in the surge bin and, thus, the delivered concentration is practically zero. Altogether, it can clearly be seen that the production is anything but constant.

3.2 1.5D Modelling

To derive a model that simulates the sedimentation process within a surge bin, several assumptions have to be made and numerous conditions must be dealt with. Nowadays, computer models are made which can solve very complex processes. However, it has been proven that relative simple models can give good predictions as well. E.g. in his thesis, van Rhee (2002) derived a one-dimensional model in vertical direction (1DV) which simulates the sedimentation process in a trailing suction hopper dredge. He concluded that his results from the 1DV model agreed closely to experimental results.

The decisions for the number of space variables forms an important step within the modelling process. The question is if one dimension will provide sufficiently accurate information about the behavior of the sedimentation process within the surge bin. It can be said that the decision for the number of space variables is in function with assumptions and the concerning physical behavior of the system. Here, it will be assumed that gravitational forces are dominant and, together with an assumed flow velocity within the surge bin, the sedimentation process can be described in vertical direction. Therefore, it is chosen to create a one-dimensional mathematical model for the simulation of the sedimentation process. This leads to a strongly simplified computer model.

Since the shape of the surge bin plays an important role for the thickening, buffering and overflow functions, it must be incorporated as a variable within the model. A 1D model makes use of a constant cross-section area. Here, the model is adapted in such a way that each segment can vary in size and volume. For example, a vertical pipeline can be modelled with a 1D model since the pipeline diameter is kept constant. A surge bin has a conical shape which has influence on the vertical mixture velocity as can be seen in Figure 3-2. In fact, the physical properties of the surge bin will also have an effect on the settling velocities because they are a function of the volumetric concentration at a certain position.

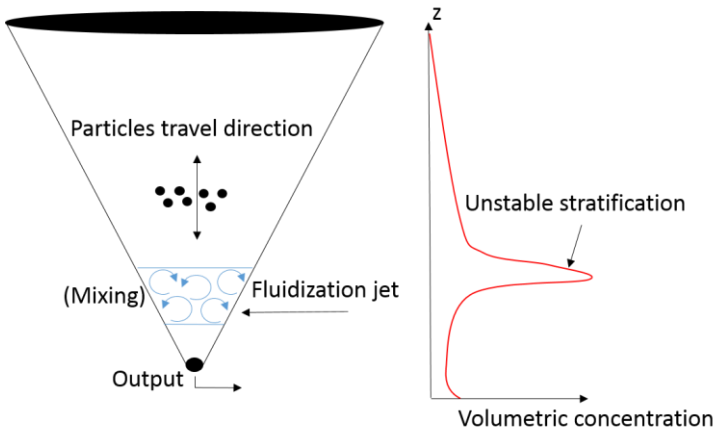

Figure 3-1: Particle travel direction and mixing of sediment (left), unstable stratification (right)

This way of modeling, allows sediment to travel only in a vertical direction, meaning that there is no transport in horizontal direction and thus 2D effects cannot be modeled. In fact, it is assumed that at each height, within the surge bin, the sediment is homogeneously distributed over the cross-sectional area.
Because sediment cannot travel in horizontal direction, mixing due to jets and turbulence has to be accounted for. Otherwise, unstable stratification will occur: e.g. when small particles reach the jet area, their settling

velocity becomes small relative to the surrounding fluid. This will lead to an increase in concentration above the jets (see Figure 3-1). However, in practice jets are present to keep the sediment in suspension and to mix the sediment with water. With a 2D or 3D model, these effects can be modelled, however, with a 1D model, this effect will be dealt with by increasing the diffusion coefficient. This will be demonstrated later in this chapter.

3.2.1 ASSUMPTIONS

It is assumed that the sediment influx is homogeneously distributed over the volume of the inlet zone (V_{inlet}) which can be seen in Figure 3-2.

Figure 3-2 Mixture velocity assumption within a surge bin

A second assumption is that the values of the inflow, outflow and jetflow are kept at a constant value which is also the case in practice. Doing so, a velocity profile of the surge bin is defined and assumed to be constant during a simulation. The velocity profile, as presented in Figure 3-2, is an example of how the mixture velocity is determined as a function of the flows and the cross section area. The diameter and the height of the surge bin can be adjusted within the program as well as all the flows. This leads to different velocity profiles and, thus, the mixture velocity, as shown in Figure 3-2, is used for illustration.

3.2.2 CONSERVATION OF MASS AND MOMENTUM

Mixture flows are governed by physical laws consisting of conservation of momentum, mass and energy. These conservational laws form the physical backbone of computer models.
At first, the continuity equation is given by:

$$\frac{\partial \rho}{\partial t} + \vec{\nabla}(\rho \vec{v}) = 0 \tag{3.2}$$

Where $\vec{\nabla}$ is the divergence operator and $\vec{v}$ is the velocity vector. When considering a Cartesian control volume with dimensions $\Delta x \Delta y \Delta z$ and working out the divergence operator, this can also be written as:

$$\frac{\partial \rho}{\partial t} = -\frac{\partial}{\partial x}(\rho v_x) - \frac{\partial}{\partial y}(\rho v_y) - \frac{\partial}{\partial z}(\rho v_z) \tag{3.3}$$

For an incompressible fluid, the density is constant and, thus, the temporal derivative of the density is zero and so the continuity equation reduces to the divergence free condition for the velocity:

$$\vec{\nabla} \cdot \vec{v} = 0 \tag{3.4}$$

Now, equation (3.2) can be written as:

$$0 = -\frac{\partial}{\partial x}(v_x) - \frac{\partial}{\partial y}(v_y) - \frac{\partial}{\partial z}(v_z) \tag{3.5}$$

This equation demonstrates that the inflow of mass is equal to the outflow of mass.

For a control volume, the conservation of momentum defines that the change in momentum is equal to the sum of external forces working on the control volume. These external forces consist out of surface and body forces. The surface forces are viscous stresses and the pressure, which are caused by the surrounding fluid. The body forces can be seen as forces which are generated by external fields and in this case only gravitational forces are considered.
Again, for an incompressible fluid, the so called Navier Stokes equation of motion can be written as:

$$\frac{\partial}{\partial t}(\rho \vec{v}) + \rho(\vec{\nabla} \cdot \vec{v})\vec{v} = -\nabla p + \rho \vec{g} + \mu \Delta \vec{v} \tag{3.6}$$

In this equation, the left hand side of the equation describes the acceleration of a volume of fluid (or inertial force). At the right hand side the three different contributions can be seen: the first term is the pressure gradient acting on the volume of the fluid, the second term is the gravitational force acting on the volume and the third term is the result from the viscous stresses with dynamic viscosity μ.

3.2.3 1D SEDIMENTATION

From the equations as presented in the previous section, the general conservative transport equation for the quantity U can be derived which has the following form:

$$\frac{\partial U}{\partial t} + \vec{\nabla} \cdot (\vec{v} U) = \vec{\Delta} \cdot \left(\kappa \vec{\Delta} U\right) + S_U \tag{3.7}$$

From equation (3.7), the one-dimensional transport equation for the volumetric concentration can be derived. The transport of sediment in vertical direction can now be written as:

$$\frac{\partial \phi_s}{\partial t} = -\frac{\partial}{\partial z}(v_s \phi_s) + \frac{\partial}{\partial z}\left(\kappa \frac{\partial \phi_s}{\partial z}\right) + \delta q_s \tag{3.8}$$

Where ϕ_s is the volumetric concentration, v_s is taken as the vertical velocity of a fraction and κ is the diffusion coefficient. The last term in the equation, δq_s, is a source term which is used to insert sediment in the system. Equation (3.8) can be solved for a whole particle size distribution which will be elaborated later in this thesis.

3.3 Numerical discretization

3.3.1 BASIC EQUATIONS OF THE MODEL

In chapter 3.2.3 the transport equation was shown for a single fraction. However, subchapter 2.3 showed that the particle size distribution has an effect on the settling velocities of the different fractions. Therefore, the advection diffusion equation will be solved for each fraction k separately and the equation can be written as:

$$\frac{\partial \phi_{s,k}}{\partial t} = -\frac{\partial}{\partial z}\left(v_{s,k} \phi_{s,k}\right) + \frac{\partial}{\partial z}\left(\kappa \frac{\partial \phi_{s,k}}{\partial z}\right) + \delta q_{s,k} \tag{3.9}$$

Where $v_{s,k}$ is the hindered settling velocity as described in eq. (2.33) in chapter 2. Equation (3.9) can be seen as the physical background behind the 1.5D model. The left hand side of this equation describes how the volumetric concentration of fraction k evaluates over time. The first term on the right hand side is the advection term which describes the movement of particles in vertical direction while the second term describes the random movement of particles due to turbulence. This second term is used to model the turbulence which is present near the jetzone and the inlet zone. It can be assumed that eddies and mixing occurs in these regions. As mentioned before, 2D effects cannot be modelled and therefore the mixing will be accounted for with this diffusion term.
In this chapter, the numerical methods to solve the different terms of the transport equation are discussed and elaborated.

3.3.2 FINITE VOLUME METHOD

In literature, many techniques are suggested for spatial discretization such as the Finite Difference Method (FDM), the Finite Volume Method (FVM) or the Finite Element Method (FEM). For a full and complete description of the different methods, the reader of this thesis is referred to (Hirsch, 2007) and (Versteeg & Malalasekera, 1995). In this report, a time level is indicated with superscript n, and the space position by the subscript i.

Here, use is made of the cell centered FVM which discretizes the computational domain into finite volumes. An advantage of this method is that it is conservative for the described property, in this case the volume fraction ϕ_s.
As mentioned previously, it is of importance to represent the conical shape of the surge bin. This is done by splitting up the cone in N number of segments or volumes.
For each of these segments the transport equation for each fraction can be solved, and the property ϕ_s can be transported from cell to cell. To make sure that conservativeness is met, the fluxes from one cell to the adjacent cell must be applied in a consistent way. In other words, the flux of ϕ_s leaving a cell, must be equal to the flux of ϕ_s that enters the adjacent cell.

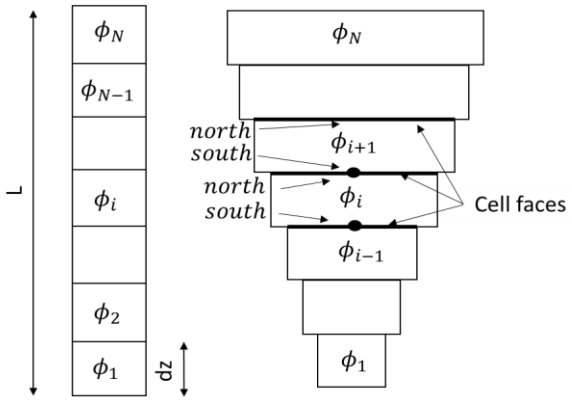

Figure 3-3: Surge bin discretization into finite volumes

To store the values of the variables, a cell centered method and a co-located grid is applied, meaning that the values of the variables are stored at the centers of the cells. The co-located grid has the advantage that boundary conditions are easier to implement compared to a staggered grid.
In Figure 3-3, a visualization is presented which shows how the conical shape is implemented.

3.3.3 TIME DISCRETIZATION

Numerically, schemes are often referred to as implicit or explicit methods. For explicit methods it is said that a computation for the unknown variables can directly be made from the available information. Contrary to that, for implicit methods, more variables are unknown at the same time step and, thus, extra iterative operations are required.
Each scheme has different properties in terms of accuracy, stability and error properties. A main advantage of an implicit scheme is that they are unconditional stable compared to explicit methods. Explicit methods are conditional stable, meaning that the time step and step size are restricted to keep a stable situation.
Here, use is made of the so called Euler Forward method, which is preferred above an implicit scheme because of its simplicity.
To deal with the stability, the Courant, Friedrich, Lewy (CFL) restrictions are defined:

$$\frac{|v_s|\Delta t}{\Delta x} \leq 1 \tag{3.10}$$

This restriction ensures that the variables in a cell are only influenced by its neighbor cells. The second restriction is given by

$$2\kappa \leq \frac{\Delta z^2}{\Delta t} \tag{3.11}$$

Here again, equation (3.11) ensures that the cells are only influenced by their neighboring cells. Equations (3.10) and (3.11) are in fact similar to each other, the difference is that equation (3.10) is only applicable on the advection term while equation (3.11) is only applicable on the diffusion term.

3.3.4 ADVECTION TERM

In this subchapter, the advection term of the transport equation will discretized. When the diffusion term is set to zero, the transport equation can be written as

$$\frac{\partial \phi_{s,k}}{\partial t} + \frac{\partial}{\partial z}\left(v_s \phi_{s,k}\right) = 0 \tag{3.12}$$

Now, for a certain cell i, the concentration at time step $n+1$ can be determined by setting up the balance of fluxes that go in and out of a cell. The change of concentration for a cell consists of different contributions. Consider the concentration ϕ_i in Figure 3-4. Then the change in concentration will consist out of the incoming concentration from the surrounding cells, minus the amount of sediment that leaves the cell.
In equation form, this can be written as:

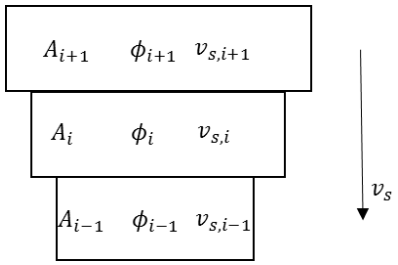

Figure 3-4: Advection through cells

$$\phi_{s,k,i}^{n+1} = \phi_{s,k,i}^{n} + \Delta t(F_{s,k,i+1}^{n} + F_{s,k,i-1}^{n} - F_{s,k,i}^{n}) \tag{3.13}$$

The equation above describes the change in volumetric concentration due to the fluxes that enter and leave the cell. Three fluxes (F) can be distinguished within the brackets. The first term is the flux of sediment that enters cell i and represents the amount of sediment that leaves cell $i+1$. The same holds for the second term, but then the flux comes from cell $i-1$. The last term is the amount of sand that leaves the cell itself. In general two methods are available to derive first order derivatives: upwind and central discretization. The advantage of central discretization is that it has a lower truncation error $O(\Delta z^2)$ compared to upwind discretization $O(\Delta z)$. Although the central discretization seems more accurate than the upwind scheme, the upwind scheme is applied because of stability reasons.
Applying the upwind method gives:

$$F_{s,k,i+1}^{n} = \begin{cases} \frac{A_{i+1}}{V} v_{s,k,i+1} \phi_{s,k,i+1} & if \quad v_{s,k,i+1} > 0 \\ 0 & if \quad v_{s,k,i+1} < 0 \end{cases} \tag{3.14}$$

For the second term:

$$F_{s,k,i-1}^{n} = \begin{cases} \frac{A_{i-1}}{V} v_{s,k,i-1} \phi_{s,k,i-1} & if \quad v_{s,k,i-1} < 0 \\ 0 & if \quad v_{s,k,i-1} > 0 \end{cases} \tag{3.15}$$

And, for the last term:

$$F_{s,k,i}^{n} = \frac{A_i}{V} v_{s,k,i} \phi_{s,k,i} \tag{3.16}$$

It can be noticed here that the fluxes go through the area of the cell where the flux comes from. However, a more convenient way of programming could have been applied, which uses the area of the north and south side of cell i (see Figure 3-3). This discretization can be found in Appendix A.

3.3.5 DIFFUSION TERM

Pure diffusion is obtained when the advection term is set to zero. Doing so, the transport equation can be written as:

$$\frac{\partial \phi_s}{\partial t} - \frac{\partial}{\partial z}\left(\kappa \frac{\partial \phi_s}{\partial z}\right) = 0 \tag{3.17}$$

Where κ is the diffusion coefficient with unity $[m^2/s]$. In the program, the diffusion coefficient is taken as a function of the concentration gradient and not as a constant. An elaboration on the diffusion coefficient is given in subchapter 0..

For the exact steps that have been carried out to apply the finite volume method for the one-dimensional steady state diffusion, the reader is referred to (Versteeg & Malalasekera, 1995).

However, a brief explanation on the discretization is given below. When the same discretized domain as presented in the previous chapter is considered (Figure 3-3), the fluxes through the north face and south face describe the change in concentration. In formula form this is written as:

$$\begin{aligned} \phi_{s,k,i}^{n+1} = \phi_{s,k,i}^{n} + \Delta t \Bigg[& \kappa_{north} \frac{\left(\phi_{s,k,i+1}^{n} - \phi_{s,k,i}^{n}\right)}{\Delta z} \frac{A_{north}}{V} \\ & - \kappa_{south} \frac{\left(\phi_{s,k,i}^{n} - \phi_{s,k,i-1}^{n}\right)}{\Delta z} \frac{A_{south}}{V} \Bigg] \end{aligned} \tag{3.18}$$

In this equation it can be clearly seen that first term between the brackets describes the flux through the north face of the cell while the second term describes the flux through the south face. In fact, for cell i, A_{north} equals A_i and A_{south} equals A_{i-1}. Furthermore, it can be seen that the direction of the flux is depending on the concentration gradient at the cell face.

3.3.6 SOURCE TERMS

So far, the transport of sediment by diffusion and advection has been explained. To bring sediment into the system, the source term $\delta q_{s,k}$ has to be defined. The source term of sediment for a certain fraction k is determined by the volumetric concentration at the inflow and the inlet zone of the surge bin.

$$\delta q_{s,k} = \frac{Q_{inflow} \phi_{s,k,in}}{V_{inlet}} \tag{3.19}$$

This source term is activated only at the inlet zone of the surge bin. Here, V_{inlet}, is the volume of the region where the sediment enters the surge bin and can consist of multiple cells. The value of $\phi_{s,k,in}$ follows from the particle size distribution and the total incoming concentration.

$$\phi_{s,k,in} = \alpha_k \phi_s \qquad \sum_{k=1}^{N} \alpha_k = 100\% \tag{3.20}$$

Where α_k is the percentage of a certain fraction in the particle size distribution.

3.3.7 BOTTOM AND BED BOUNDARY

At the bottom of the surge bin, sediment must be able to leave the surge bin where it ends up in the outflow. This amount of concentration is determined by the flux that leaves the bottom cell and, thus, leaves the surge bin. In, fact, this cell has the diameter of the discharge pipeline through which the mixture is sucked away. For simplicity, it is assumed that the flux that leaves the cell is dominated by advection and, thus, the second term in the brackets of equation (3.9) is set to 0. Furthermore, it is assumed that the velocity, with which the concentration leaves the bottom cell, equals the mixture velocity which is determined by $Q_{outflow}$. The concentration which leaves the bottom cell disappears from the system and, so, the bottom cannot function as a source. The fluxes that enter and leave the bottom cell are then written as:

$$\phi_{s,k,i}^{n+1} = \phi_{s,k,i}^{n} + \Delta t(F_{s,k,i+1}^{n} - F_{s,k,i}^{n}) \tag{3.21}$$

And

$$F_{s,k,i} = \frac{A_i}{V} v_m \phi_{s,k,i} \tag{3.22}$$

This equation is conditional true because sediment will only leave the bin if:

$$Q_{outflow} > 0 \tag{3.23}$$

It is possible that the volumetric concentration within a cell can increase until it reaches a maximum concentration. For loosely packed sand this value is approximately 0.5 to 0.6. When this value is reached, the fluxes into the cell are blocked. This function holds for every cell in the surge bin and, thus, a bed can be formed.

Remark:
For the validation of the model (chapter 5.4), the bottom cell was programmed in a different way. The height of the bottom cell (Δz) was chosen in such a way, that the condition in equation (3.10) was met. The value of v_s was determined by the ratio of $Q_{outflow}/A$, where A is the cross-sectional area of the discharge pipeline. This approach of programming gave no different results compared to the results if Δz was given the same value as the rest of the cells.

3.3.8 OVERFLOW BOUNDARY

At the top of the bin, a special condition has to be defined to simulate the overflow and where sediment can leave the system. Physically, this seems strange because sediment cannot flow through the water surface. However, because all models are a simplification, it must be assumed that the sediment which leaves the top

of the bin ends up in the overflow. With this assumption, the amount of sediment which leaves the cell at the top of the bin is given by:

$$F_{overflow,k} = \frac{A_i}{V} v_{s,k,i} \phi_{s,k,i} \tag{3.24}$$

This equation is only conditional true, because sediment can only end up in the overflow when there is a net upward flow and if the settling velocity is directed upward (and thus negative). So, sediment can only end up in the overflow if:

$$v_{s,k,i} < 0 \quad \& \quad Q_{inflow} + Q_{jet} - Q_{outflow} > 0 \tag{3.25}$$

3.4 Matlab program and typical simulation results

The above described information is programmed in Matlab to predict the concentration profiles within the surge bin. From the previous subchapters it became clear that the concentration has influence on the settling velocities for the different fractions and on the diffusion coefficient. Therefore, it is necessary to calculate these values for each time step and each for each cell. The complete transport equation which is solved is given by:

[redacted] (3.26)

3.4.1 VARIABLES OF THE PROGRAM

To run the program and to implement results, one should know the basic principles of how the program works. The process of how sediment is transported through the surge bin is already elaborated. However, it should be noticed that different variables have to be made up. The program, including a manual, can be found on the USB stick which is an accessory to this report.
The most important variables such as the simulation time, inflow, outflow, jetflow, surge bin dimensions, particle size distribution and the incoming concentration are put in via the graphical user interface (GUI). However, the user must be aware that values such as the Ferguson & Church coefficients, temperature, diffusion factor, time steps and so on, are defined in the code behind the GUI. Nevertheless, these values can easily be adapted just by changing their values within the Matlab code.

3.4.2 GRAPHICAL USER INTERFACE

The 1.5D model continuously determines the vertical volumetric concentration profile of the surge bin as a result of the incoming concentration. In addition, the amount of sediment that leaves the surge bin, via the overflow and via the outflow, is monitored. To present all this information, a Graphical User Interface is

created where all this information is visualized. At the end of a simulation, data files are generated and stored for further analysis. The GUI is made by Maarten in't Veld and is presented in Figure 3-5. The different visuals are described below the picture.

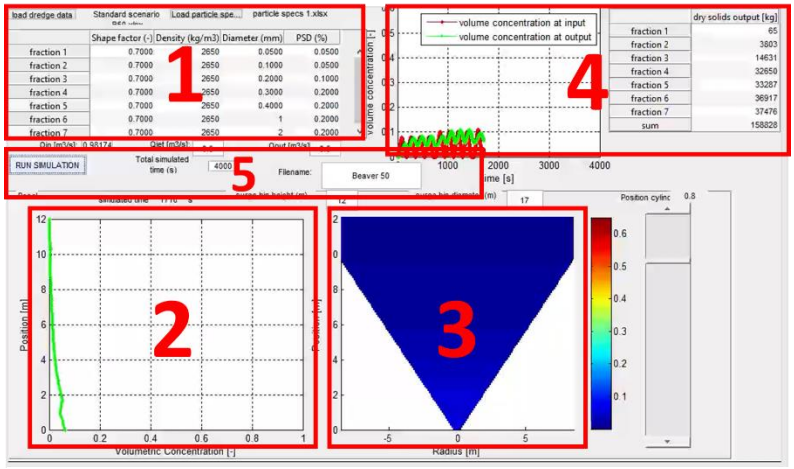

Figure 3-5 Illustration of Graphical User Interface of 1.5D model

1. Screen 1 shows the values of the particle size distribution, the sediment density, shape factor and the particle diameters. At the top, two buttons can be seen which enable the user to enter the particle specifications and to load an incoming concentration profile. The particle size distribution can easily be adapted by changing the values within the Excel file which is attached in the folder.
2. This screen shows the vertical volumetric concentration profile of the surge bin. On the vertical axis the height of the surge bin can be seen while the horizontal axis shows the volumetric concentration.
3. To interpret the values from screen 2, the values are translated into colors and a visualization of the surge bin has been made.
4. Shows the volumetric concentration signal which enters and leaves the surge bin. The horizontal axis shows the elapsed time and the vertical axis represents the volumetric concentration.
5. Here, the variables such as simulation time, inflow, outflow, jetflow, and the surge bin dimensions can be filled in.

3.4.3 MODEL TEST AND EXPECTATIONS

Until now, a wide variety of formulas and equations have been elected and the applied programming methods have been elaborated. The resulting program describes the development of the volume concentration of multiple fractions in time, inside a surge bin with variable dimensions and adjustable flows. Before any prototype test with the program is carried out, several simulations are made to check whether the predicted functions of the surge bin are met, the way they are described in chapter 1.

Before the model tests are carried out, several general parameters and fictive surge bin characteristics are assumed. The chosen values are presented in Table 3-1.

Table 3-1: Assumed parameters for model test

Water density	$1000\ kg/m^3$
Solids density	$2650\ kg/m^3$
Diffusion coefficient	$5 \cdot 10^{-5} m^2/s$
C1 Ferguson Church	$18\ [-]$
C2 Ferguson Church	$1\ [-]$
Height surge bin	$10m$
Diameter top surge bin	$8m$
Volume surge bin	$250m^3$
Number of grid points	$50[-]$
Time step	$0.01s$

For the hindered settling function, the Richardson & Zaki exponent is determined according to Garside. The values as present above are used in all of the simulations of this chapter. Here, for the first simulations, the diffusion coefficient is given a low value of $5 \cdot 10^{-5} m^2/s$ because this value can be taken as the self-diffusion coefficient and means that barely any mixing is simulated in the surge bin.

Thickening

As mentioned before, it is expected that due to the difference between inflow and outflow, a higher concentration will be measured in the outflow. To check the thickening function of the program, a constant volumetric concentration of 30% enters the surge bin for a period of 20 seconds.
First, the values of inflow and outflow are kept constant at $1.5 m^3/s$, to see how the block function moves through the surge bin and to set a reference point. Subsequently, the value of the outflow is reduced to $1 m^3/s$ to see whether this leads to the expected increased concentration at the outflow. For both situations the jet is set to $0 m^3/s$.

The particles for both simulations have an identical diameter of 2mm and a shape factor of 0.7, leading to a settling velocity of $196 mm/s$ according to the Ferguson & Church formula.
The result is plotted in Figure 3-6 which shows the incoming concentration in green and the different concentration profiles predicted at the outflow in blue and red.

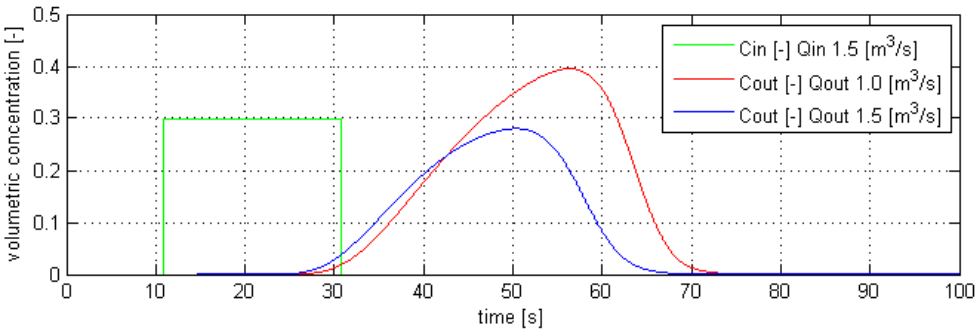

Figure 3-6: Results of thickening simulation, incoming concentration = 30%

When analyzing the blue line in Figure 3-6, it can be seen that the block signal is damped out slightly asymmetrically. This is the effect of the hindered settling which causes the first particles to travel directly to

the outflow without any hindrance, while the particles at the back are influenced by the return flow. Furthermore, the maximum concentration is slightly lower than the incoming concentration.
Now, when analyzing the red line where the outflow is reduced, it can be seen that the volumetric concentration has increased to a value of 40%. This means that the thickening function can be met when the outflow is reduced. Compared to the blue line, a difference can be observed when the first particles reach the outflow. In fact, the red curve is slightly shifted to the right. This effect is the result of the reduced outflow which determines the mixture velocity below the inlet zone and, thus, influences the time for particles to reach the outflow. The time needed in this case for the particles to reach the output is about 20 seconds.

Note: It is a mistake to think that more material is introduced for the red graph because of its larger curve. It must be realized that the mass balance still holds because:

$$\int_0^t Q_{inflow}(t)c_{in}(t)\rho_s dt = \int_0^t Q_{outflow}(t)c_{out}(t)\rho_s dt \tag{3.27}$$

Or plotted in a graph:

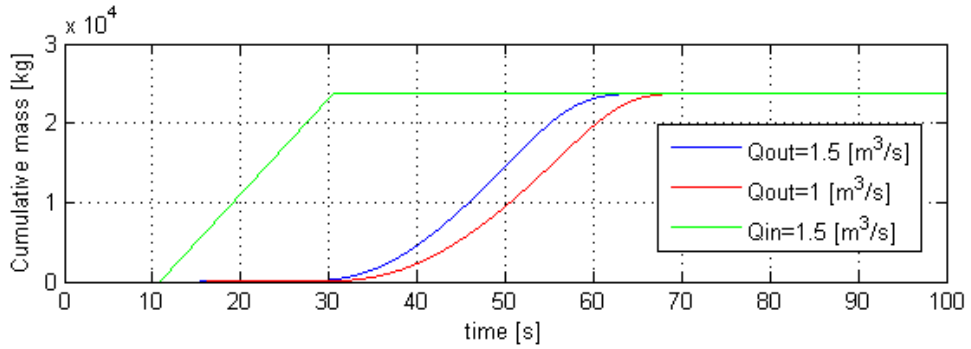

Figure 3-7: Mass balance: cumulative masses at inflow and outflow

The graph clearly shows now that no extra sediment is introduced for the red curve. It can also be seen that the amount of sediment calculated at the outflow for both situations, equals the amount of sediment calculated at the inflow.
A simulation has been made to look at the effect on the results when the number of grid points is increased.

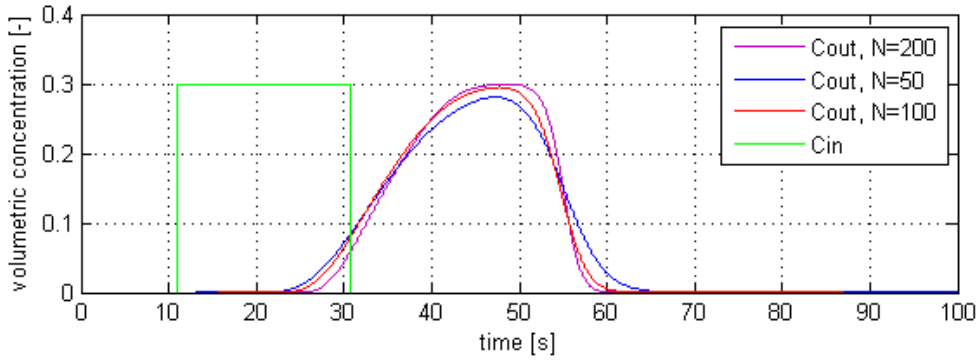

Figure 3-8: incoming concentration = 30%, effect of number of grid points

Figure 3-8 shows the results of three identical simulations with $Q_{in} = Q_{out} = 1.5m^3/s$ and an incoming concentration of 30% for a period of 20 seconds. The only difference is the applied number of grid points. The difference between purple and red ($N = 200$ and $N = 100$ respectively) is barely noticeable as the lines are almost overlapping each other. When the results of the purple and blue line are compared ($N = 200$ and $N = 50$ respectively), it can be noticed that a little more numerical damping is introduced. However, the difference is not significantly large. Therefore, the number of grid points is taken 50 what results in a grid size of $0.2m$.

Now, compared to Figure 3-6, the same test is done but now with a lower incoming concentration of 20% of which the results can be seen in Figure 3-9. No significant differences can be distinguished, apart from the values measured in the output which are logically lower.

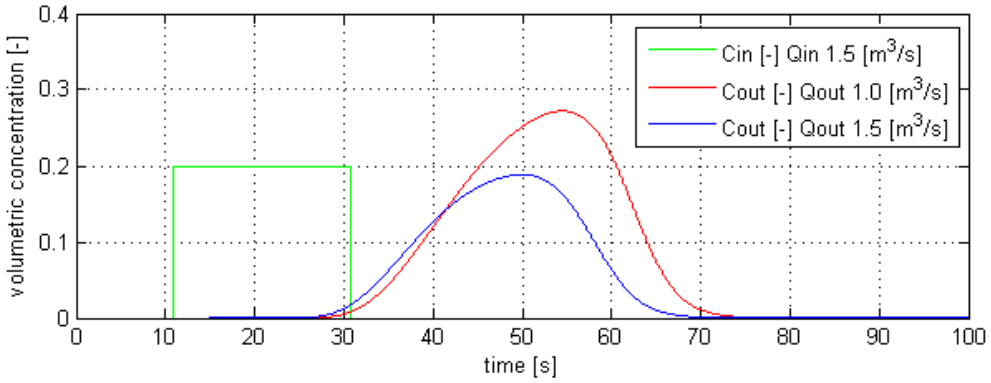

Figure 3-9: Results of thickening simulation, incoming concentration = 20%

Damping & buffering

As already concluded in the simulations above, some damping of the incoming signal occurred. A second simulation has been carried out to take a better look at the damping effect. In this simulation, the incoming concentration profile consist of two block functions placed after each other. The period between the two signals is first taken at 20 seconds. The values of the inflow and outflow are taken equal to get a better view on the damping.

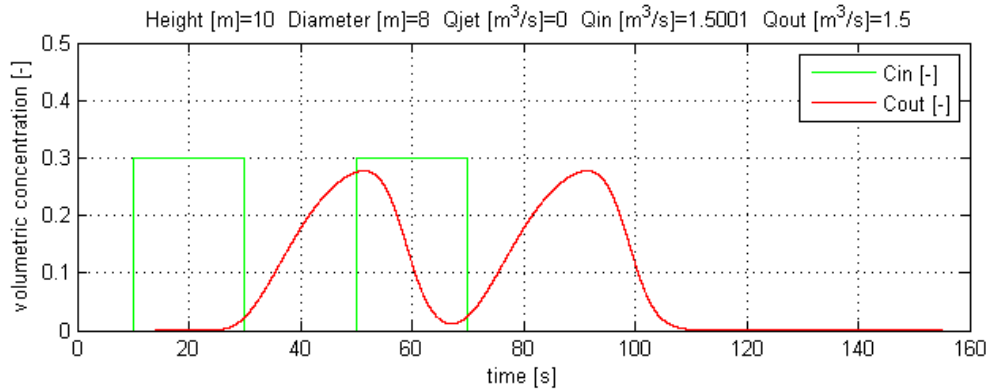

Figure 3-10: Results of two incoming pulses of 30% and 20 seconds in-between

Here, the two incoming signals can be seen in green with the corresponding reaction in red. It is worth noting that the first and the second peak overlap each other in the middle, meaning that the outflow has not run out of sediment. This means that the first batch has not disappeared yet, while the second batch already started reaching the outflow. Now, the block signals will be activated with a 10 seconds interval time.

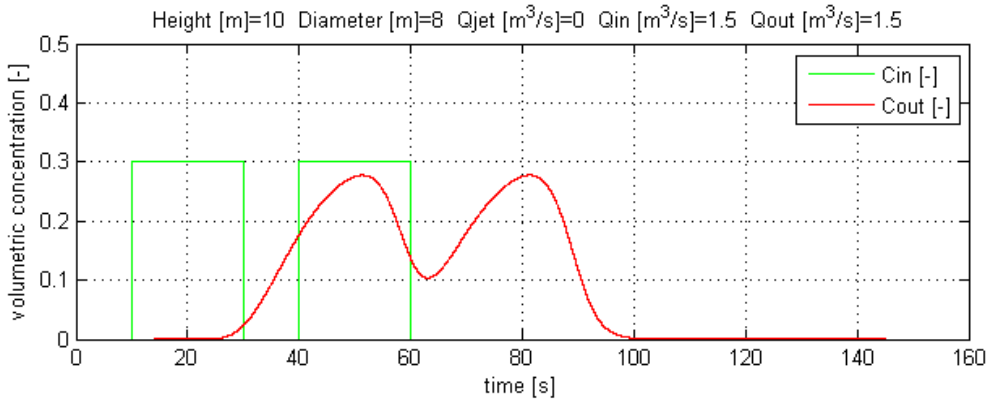

Figure 3-11: Results of two incoming pulses of 30% and 10 seconds in-between

In Figure 3-11 the damping effect can clearly be seen. The block signals are reduced to a damped function with a reduced amplitude of 28% and a minimum value of 10%. Also, the first effect of buffering can be distinguished because the outflow keeps delivering a certain concentration compared to the zero incoming concentration.

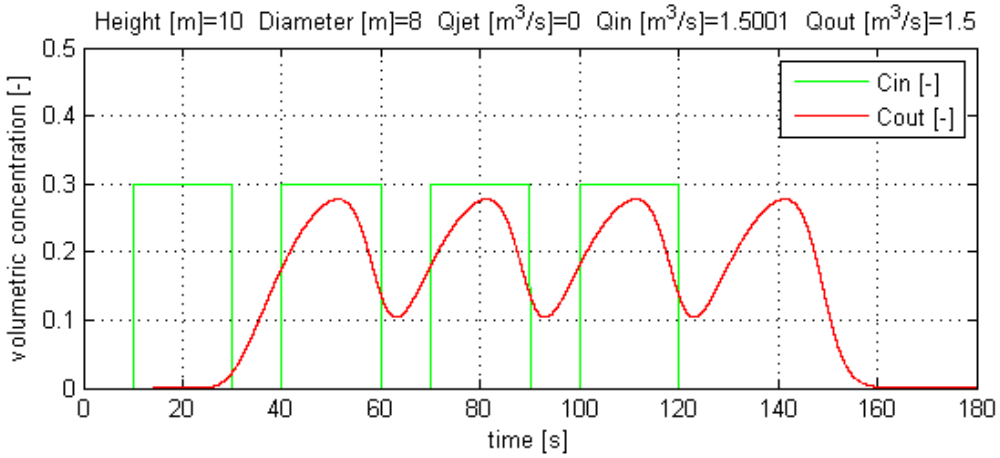

Figure 3-12: Results of four incoming pulses of 30% and 10 seconds in-between

When the time between two block signals is in this case reduced to zero, a long constant incoming profile is created. This means that the surge bin is fed by a continuous amount of sand and, thus, no wiggles in the outflow should appear. This is visualized in Figure 3-13. Here a steady situation is reached meaning that the amount of sand which enters the surge bin is equal to the amount of sand leaving the bin.

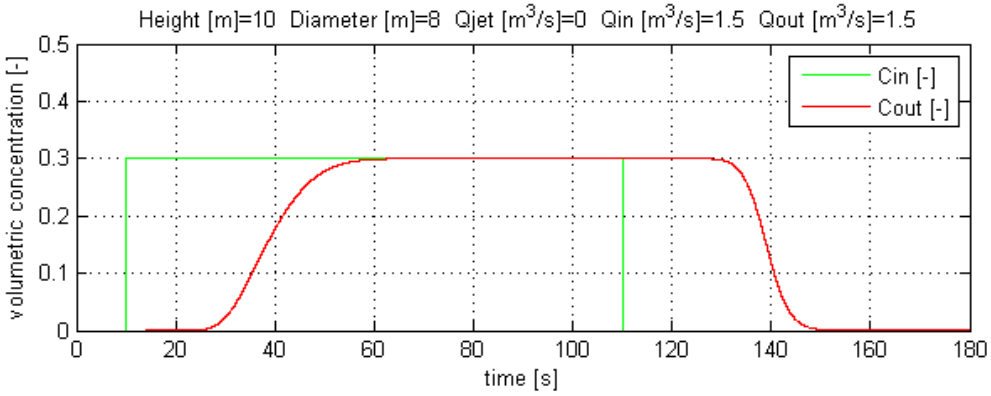

Figure 3-13: Results of 100 seconds during pulse of 30%

Now, the thickening function could also be checked over a longer period by reducing the outflow in the above simulation.

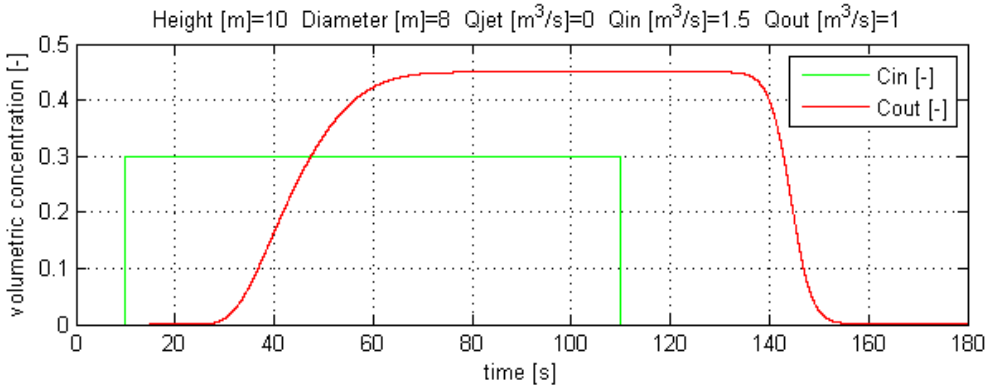

Figure 3-14: Results of 100 seconds during pulse of 30% with reduced outflow

Indeed, a steady state situation has been achieved again and due do the reduced outflow, the concentration has increased as expected.

Separating

In the above situations, only a single grain size has been used. As described in chapter 2, the velocity of the particles is relative to the mixture velocity. This means that small particles can flow upward if they are small enough. To check the overflow function of the model, a different PSD is introduced. The PSD consists out of two fractions, which are even distributed (both 50% of the total volume). The second particle diameter is chosen in such a way that the terminal settling velocity is lower than the upward mixture velocity on top of the bin. Here, the upward mixture velocity is dependent of the ratio of Q_{inflow}, $Q_{outflow}$ and Q_{jet}. In Table 3-2, an overview of the used values for the different parameters is given, as well as the terminal settling velocities of both fractions.

Table 3-2: Assumed parameters for separating

Q_{inflow}	$1.5\ m^3/s$
$Q_{outflow}$	$0.6\ m^3/s$
Q_{jet}	$1.0\ m^3/s$
$v_{mixture,top}$	$37\ mm/s$
$v_{s,50\mu m}$	$2\ mm/s$
$v_{s,2mm}$	$196\ mm/s$
Number of grid points	$50[-]$
Time step	$0.01s$

Again, a simulation has been made with an incoming volumetric concentration of 30% for 20 seconds. The masses that have passed the overflow and outflow, have been measured till the surge bin ran out of sediment. The calculated concentration at the overflow and at the outflow have been plotted in the Figure 3-15.

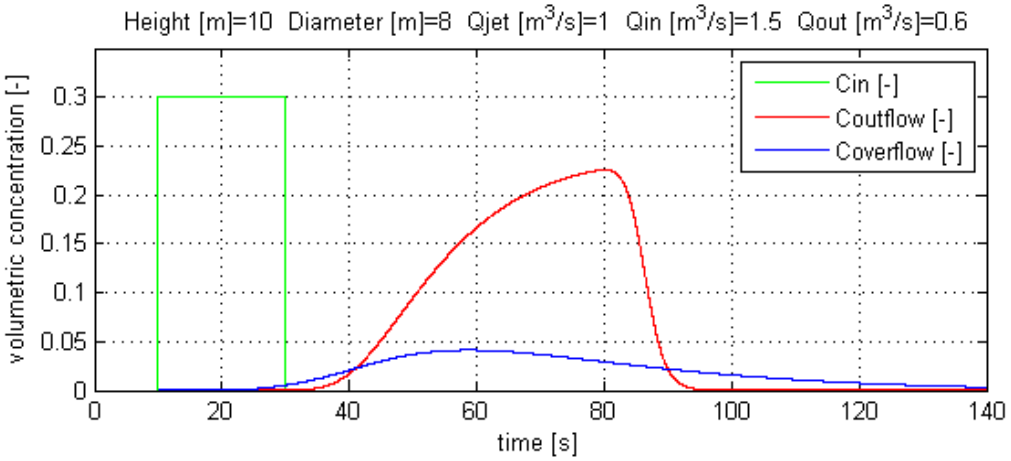

Figure 3-15: Results of separating simulation: sediment in overflow and outflow

Here, it can be seen that sediment transport took place through both the outflow and overflow. However, this graph gives no information on the distribution of the two fractions. Therefore, to see where the fractions have ended up, the masses of both fractions have been calculated at the inflow and overflow.
This information is given in Table 3-3.

Table 3-3: Separating results: mass calculated in overflow and outflow

	Fraction 1: $2mm$	Fraction 2: $0.05mm$
Inflow		
Percentage in PSD	50%	50%
Mass in	$11925kg$	$11925kg$
Mass calculated at outflow	$11925kg$	$0kg$
Mass calculated at overflow	$0kg$	$11925kg$

Now it can be seen clearly that all the fine $0.05mm$ sediment has ended up in the overflow, while the heavier $2mm$ particles travelled to the outflow. In this case, it means that the blue line corresponds with the smallest fraction that ends up in the overflow and the red line represents the sediment leaving the outflow. When the

graph is further analyzed, it can be said that the small sediments needs more time to leave the surge bin. This is the result of the low upward mixture velocity at the top of the surge bin. However, it can be concluded that separation of the fine particles indeed took place.

Buffering

Before a random simulation is made, a little more attention is paid to the buffer function. In the damping simulations it became clear that the incoming concentration profiles were damped out. However, this was for a single fraction only. Now, if two fractions would be used with different settling velocities, it can be expected that the buffer function might increase due to the lower settling velocities of the smaller particles. Here again, the PSD consists out of two fractions (2mm and 0.5mm), which are evenly distributed (both 50% of the total volume).

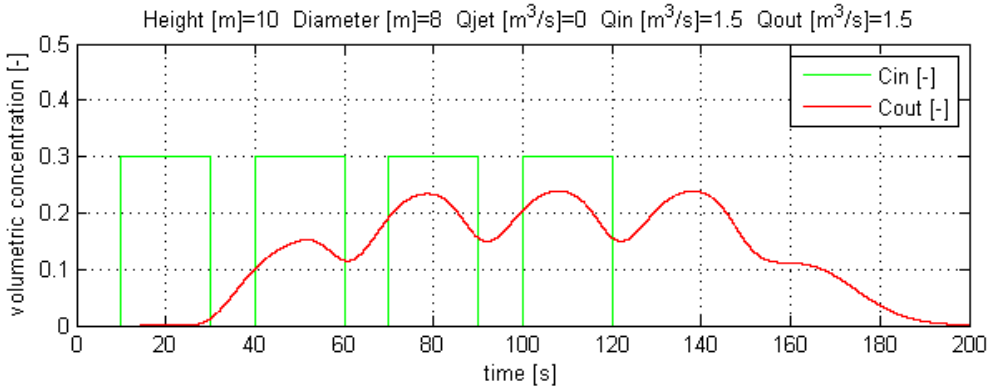

Figure 3-16: Results of buffer simulation, four incoming pulses of 20 seconds

Compared to Figure 3-12: , several differences can be observed. At first, the maximum reached volumetric concentration reaches a value of 22% which is lower than the 28% from Figure 3-12: . A different effect is the calculated values of the peaks at 50 seconds and 165 seconds. The peak value at 50 seconds can be explained by the amount of 2mm particles which traveled faster to the outflow than the smaller ones. The peak at 80 seconds consists of the delayed 0.5mm particles of the first block signal and the 2mm particles of the second block signal. Lastly, the value of the concentration at 160 seconds is the result of the 0.5mm fraction which still has to leave the bin. Now, comparing the times to run out of sediment in Figure 3-12 and Figure 3-16, a difference of about 30seconds of buffering can be observed.

Important remark

A circumstantially occurring effect is that the settling velocity of a grain (especially the fines) reduces when it approaches the jet area. When the settling velocity is higher than the upward flow, it keeps falling down. However, when the settling velocity equals the upward mixture velocity it will stop settling and will “float”. This effect will lead to an increase in concentration, relative to the concentration below. In addition, when large amounts of sand enter the bin at the inlet zone in a short period of time, the concentration increases significantly compared to the concentrations below.

In the example given at the separation function, the small sediment was chosen in such a way that its settling velocity was small enough to end up in the overflow. Now, looking back at the graph as presented in Figure 3-2, one can notice that the mixture velocity just above the jet is defined by the values of Q_{jet} and $Q_{outflow}$. This means that when the settling velocity of the sediment equals the upward velocity of the water, the sediment will stay floating in a "dead" zone. As a result, an increase in concentration will appear at this height because the sediment cannot penetrate through the jet layer. To illustrate this effect, a simulation is made which is visualized in Figure 3-17. Here the development of the concentration is plotted as a function of the height.

Table 3-4: Assumed parameters for simulation jet layer

Q_{in}	$1.4m^3/s$
Q_{out}	$1.0m^3/s$
Q_{jet}	$1.1m^3/s$
Diameter sand	$0.5mm$

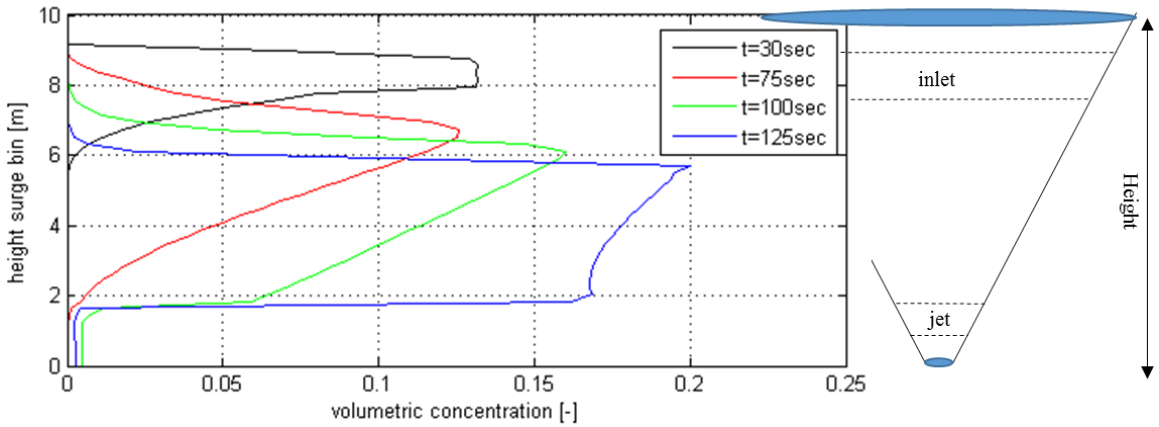

Figure 3-17: Development of a layer above the jet

The used values for the flows and diameter are given in Table 3-4.

In this graph, the development of the sedimentation process of a certain amount of sand is plotted at four time intervals. The black line shows the concentration at the inlet which starts to settle toward the outflow. Next, the development of the concentration is plotted after 75 seconds and shows that the first particles start to reach the jet zone. Here, the upward velocity of the water starts to reach the settling velocity of the sediment and, thus, the particles will start to float. This process becomes even clearer when the green line is analyzed, which shows the volumetric concentration after 100 seconds. Lastly, the blue line (125 seconds) shows that particles are still settling and the concentration above the jet zone is increasing.

Here, once more, the reader should not think that the amount of sediment has increased during the sedimentation process. This plot shows the development of the volumetric concentration in time, which is relative to the volume of the position in the bin. In other words, a low volumetric value at the top of the bin, can lead to a high volumetric concentration near the outlet of the bin.

An increase in concentration as shown above, is not only occurring above the jet. Also when large amounts of small particles are put in the surge bin in a very short period of time, the volumetric concentration at that zone increases drastically. Particles do need some time to travel away from the inlet zone and when their velocity is low, they do not have the time to leave the inlet zone while sediment continuous to flow in. This effect becomes clearer in Figure 3-18.

Table 3-5: Assumed parameters for simulation inlet zone

Q_{in}	$3m^3/s$
Q_{out}	$1.4m^3/s$
Q_{jet}	$0m^3/s$
Diameter sand	$0.1mm$

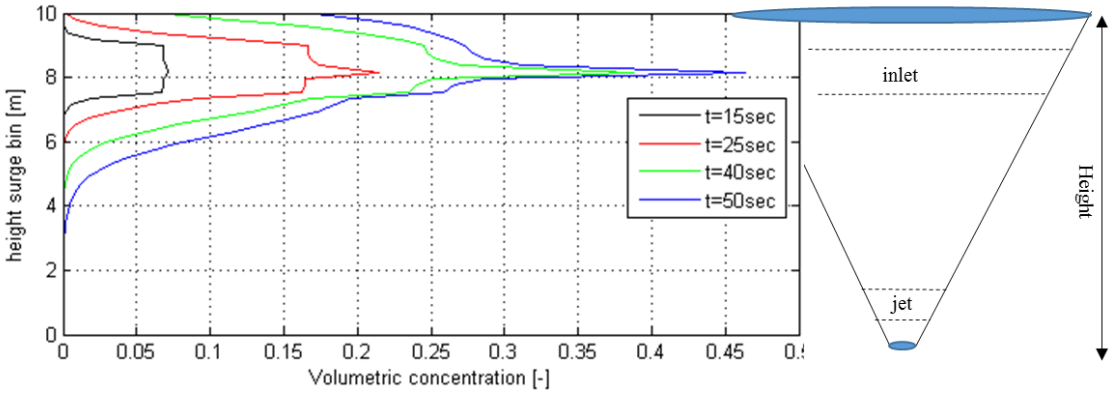

Figure 3-18: Development of a layer near the inlet

In this simulation, a volumetric concentration of 40% keeps entering the surge bin continuously. For the flows and the used sediment, the values in Table 3-5: are used.

This simulation clearly shows that the volumetric concentration at the inlet increases in time enormously. The black line shows that the concentration starts to increase due to the incoming sediment. However, because fine sediment is used, is does not have the time to travel to the outflow or overflow. 10 seconds later, a significant increase can be observed and the sediment also starts to move to the overflow and the outflow. It can also be noticed that a peak value starts to develop. This is due to the same effect as the one which is described at the "dead zone" above the jet: the settling velocity of the sediment equals the upward velocity of the water at that position.

3.4.4 DIFFUSION COEFFICIENT

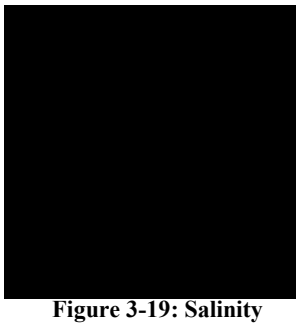

Figure 3-19: Salinity gradient in ocean layers

Figure 3-20: Function for diffusion coeffcient

3.4.5 CONCLUSION

From the simulations that have been carried out it can be concluded that the model already satisfies several expectations. From the simulations it can be concluded that:

- The surge bin works as a thickener when the outflow is reduced.
- The surge bin works as a damper.
- The surge bin works as a buffer.
- The surge bin works as a separator if the upward flow velocity is high enough, relative to the slimes.
- Unstable stratification occurs due to sediment that floats above the jet.
- Unstable stratification occurs when sediment enters the surge bin too fast.

Chapter 4

4. Experimental setup

4.1 Introduction

The 1.5D model describes the movement of particles in the vertical direction and, thus, neglects the fluxes in horizontal direction. However, assuming that the vertical fluxes are dominant, the 1.5D model might give good predictions about how the concentration profiles evaluate in time. By performing an experiment on scale, which simulates a true scale surge bin, concentration values can be measured and compared with values from the computer program. When the values of the experiment and the model are comparable, it can be concluded that the assumptions and working principles of the program are assumed to be correct. In addition, occurring processes and functions of the surge bin such as buffering, thickening and damping can be investigated. However, it must be realized that the emphasis of the experiment lays on the validation of the numerical model.
In this chapter the experiment setup is explained, and, where necessary, schematically illustrated. In addition, a video has been made where the experiment is in operation and an explanation is given on how data is gathered. This video can be seen on the USB supplied with this thesis. The functions of all the valves, data loggers, flows, jets and so on are shown and elaborated as well.

4.2 Research questions and experiment requirements

If an experiment would be executed, it must deliver values which can validate the program. Therefore, it is necessary that information will be measured or generated which satisfies the produced research questions. The questions on which information should be given are listed as follows:

- How does the volumetric concentration evaluate as a function of height and time?
- How is the surge bin fulfilling its functions:
    - Thickening
    - Buffering
    - Damping
    - Separating
- How much and which sediment ends up in the overflow?

With these questions in mind, the requirements of the experiment setup are determined as follows:

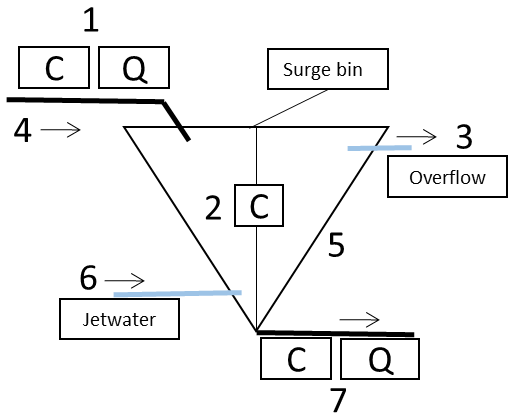

Figure 4-1: Overview requirements experiment

In Figure 4-1, C and Q represent concentration sensors and flow sensors respectively. Furthermore, the numbers refer to the following processes:

1. The concentration and flow must be measured before the mixture enters the surge bin.
2. The concentration in the surge bin must be measured over the height.
3. An overflow must collect the overflowing sediment and water.
4. The mixture that enters the surge bin must have a constant flow, but, the volumetric concentration of sediments must fluctuate (to simulate the production of a dredger).
5. It is preferable to use a funnel shaped sedimentation tank.
6. Water jets must be present to generate a positive upward flow and to keep the sediment in suspension.
7. The concentration and flow must be measured at the surge bin's outlet.

4.3 Scaling laws

Test models and prototypes are designed to be similar in geometrical, kinematical and dynamical points of view. Kinematic similarity implies that the ratios of velocities and accelerations between the prototype and the model are equal.
The dimensions of the experiment will be smaller than the full scale dimensions and, to keep the exact geometry, the experiments have to be performed on a non-distorted scale.

$$E(S) = \frac{S_{model}}{S_{prototype}} \tag{4.1}$$

In which $E(S)$ is the scale function and S is any quantity of measurement which describes the surge bin. To keep the exact geometry, the scale ratio $E(S)$ must be constant, where S represents the length, radius and height of the surge bin:

$$E(Length) = E(height) = E(diameter) \tag{4.2}$$

The flows in the surge bin are governed by the balance of inertial forces and gravitational forces. This balance is given by the ratio of these forces and is called the Froude number.

$$Fr = \frac{U}{\sqrt{g \cdot L_c}} \tag{4.3}$$

In which Fr is the dimensionless Froude number, U is the velocity, and g and L_c are the gravity acceleration and characteristic length respectively. When a full scale model is scaled, Froude number similarity must be maintained:

$$E(Fr) = \frac{E(Fr_{model})}{E\left(Fr_{prototype}\right)} = 1 \tag{4.4}$$

Another dimensionless parameter is the overflow parameter H^* and can be seen as the settling efficiency for a certain grain size. This parameter is given by:

$$H^* = \frac{Q}{BLw_s} \tag{4.5}$$

In which B and L represent the width and length of a TSHD's hopper, w_s is the settling velocity and Q the discharge into the basin. The dimensionless overflow parameter should be equal for both full scale and experimental scale models. In case of the surge bin, the values of L and B are replaced by the cross sectional area on top of the bin. Now, when comparing the volume flows of a surge bin and a TSHD, a difference volume balance is observed due to the presence of an outflow and jets. Therefore, in this thesis, H^* is taken as the ratio of the velocities halfway the surge bin.

Several values for the flows and for the particles need to be determined for the experiment (see Table 4-1). From reference projects, barely any information is available. Some prototype surge bins are connected to multiple dredgers, while others are only fed by just one. It also occurs that surge bins are not equipped with jets at the bottom or that they have an overflow. Nevertheless, for an order of magnitude, a prototype in Madagascar is taken.

From a reference project in QMM Madagascar, several values of dimensions and flows are assumed (in't Veld, Surge bins at IHC sites, 2014). From a practical point of view, use is made of an available buffer tank which has a different geometry compared to prototype surge bins which means that the scaling law as presented in (4.2) is not pursued. The buffer tank used can be seen Figure B-7 (Appendix B), including its dimensions. All the available data is gathered in the table below.

Table 4-1: Dimensions of prototype surge bin and experiment surge bin

Prototype QMM		Scaled buffer tank	
Height [m]	19	Height [m]	1.08
Diameter top [m]	22	Diameter top [m]	0.7
Volume $[m^3]$	2400	Volume $[m^3]$	0.34
Q_{inflow} $[m^3/s]$	3	Q_{inflow} $[m^3/s]$	To determine
$Q_{outflow}$ $[m^3/s]$	2	$Q_{outflow}$ $[m^3/s]$	To determine
d_{50} [mm]	0.4	d_{50}[mm]	To determine

The d_{50} of the prototype sediment is taken from a local S-curve of the location, see Figure 6-1. Furthermore, for the following calculations, it is assumed that the flow of the jet is set to zero for simplicity. The following calculations have been made subsequently:

For Froude scaling, the characteristic lengths and the velocities are unknown. For the calculation the characteristic length is taken as the height of the prototype surge bin and the model. For the velocity of the prototype surge bin, the value of the settling velocities are taken from the d_{50} of the sediment ($= 0.056 m/s$). From equation (4.3) and (4.4) follows:

$$\frac{U_{prototype}}{\sqrt{g \cdot L_{c,prototype}}} = \frac{U_{model}}{\sqrt{g \cdot L_{c,model}}} \tag{4.6}$$

Filling in the values from the table and rewriting, the value for U_{model} must equal $0.012 m/s$. This should subsequently be the velocity of the d_{50} used in the experiment. This corresponds with particles with a diameter of $130 \mu m$. Sand supplying company Filcom delivered samples of three different types of sand. These samples have been sieved and the PSD can be seen in Figure B-1 in Appendix B.
Looking at the particle distribution of these types of sand, the AF-100 type comes close. However, because a significant part of this gradation is smaller than $100 \mu m$, this type of sediment is not chosen due to cohesive effects that might occur. Therefore, the M34 sand is used which has a d_{50} of approximately $150 \mu m$. The corresponding settling velocity of the d_{50} of this sediment, according to equation (2.20) is $0.0149\ m/s$ which comes close to the $0.012 m/s$.

Now, the values of the inflow and outflow have to be determined. This is done by using the dimensionless overflow parameter H^*.
Just like Froude Scaling, similarity must be achieved, but now in the dimensionless hopper parameter:

$$\frac{Q_{prototype}}{A_{prototype} w_{s,prototype}} = \frac{Q_{model}}{A_{model} w_{s,model}} \tag{4.7}$$

The dimensionless hopper parameter tells something about the settling efficiency. This means that it can be seen as a ratio of the settling velocity of the grains and the flow in the surge bin. That in mind, the average flow within the surge bin is taken. This is the flow halfway in the surge bin and must give a good indication of how the ratio of the sediment settling velocity over the average flow is. The values used for $A_{prototype}$ of the prototype surge bin is then determined by the cross-sectional area halfway the surge bin. The flow which occurs at this spot is determined by $Q_{outflow}$. For the model, Q_{model} can now be determined since the area halfway the bin is known, and the settling velocity is determined by the Froude scaling.
Filling in the values leads to Q_m which obtains a value of 2 l/s and is, thus, the outflow of the model. Now the same ratio of $Q_{inflow}/Q_{outflow}$ is taken from the prototype model which leads to an inflow of $3\ l/s$ in the experiment.

4.4 Test arrangement

The resulting test arrangement consists of a closed 50mm circuit of which a schematized overview is presented on the next page. The circuit is created in such a way that volume balances are kept constant which provides the great advantage that long time simulations can be made without interrupting the simulation. Secondly, the sediment in the experiment can always be collected in a mixture reservoir. This brings two advantages: the first is that no extra efforts have to be put in the shoveling of sand and, secondly, the user can always create a system where only water is circulating.
In the overview, the slurry circuit can be seen of which the flow direction is indicated by arrows. Also, the positions of the measuring instruments are visualized, as well as the different buffer tanks.
The pipeline segments used, are made from transparent uPVC which makes it easy to keep an eye on what is happening inside the pipes, especially when high density mixtures are pumped through the system.

Instrumentation used
In the experiment, different types of sensors and other instruments are placed to generate, log and store data. Before any explanation is given on the working principles of the experiment, the used sensors and instrumentation will be elaborated.

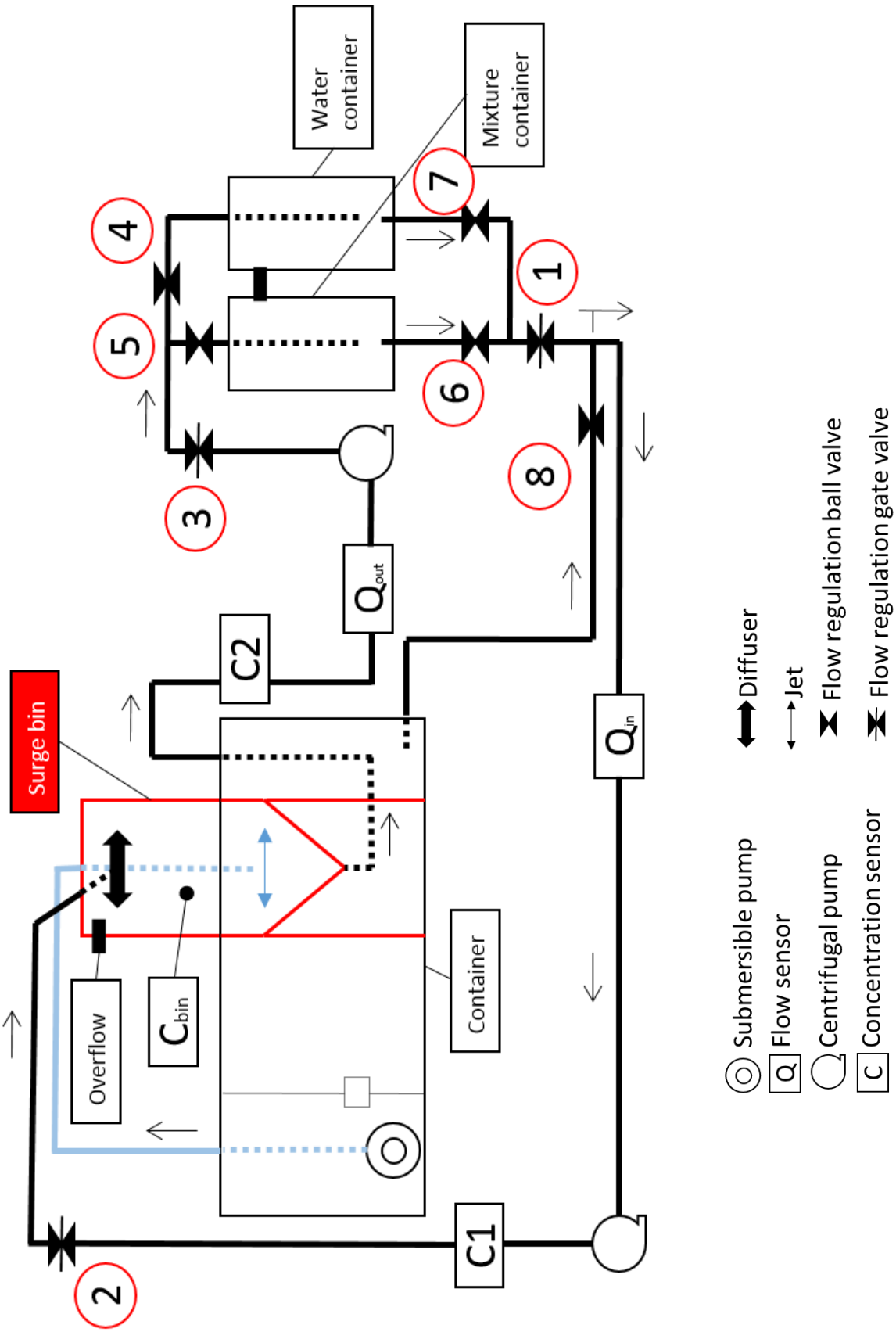

Figure 4-2: Experimental setup, schematization

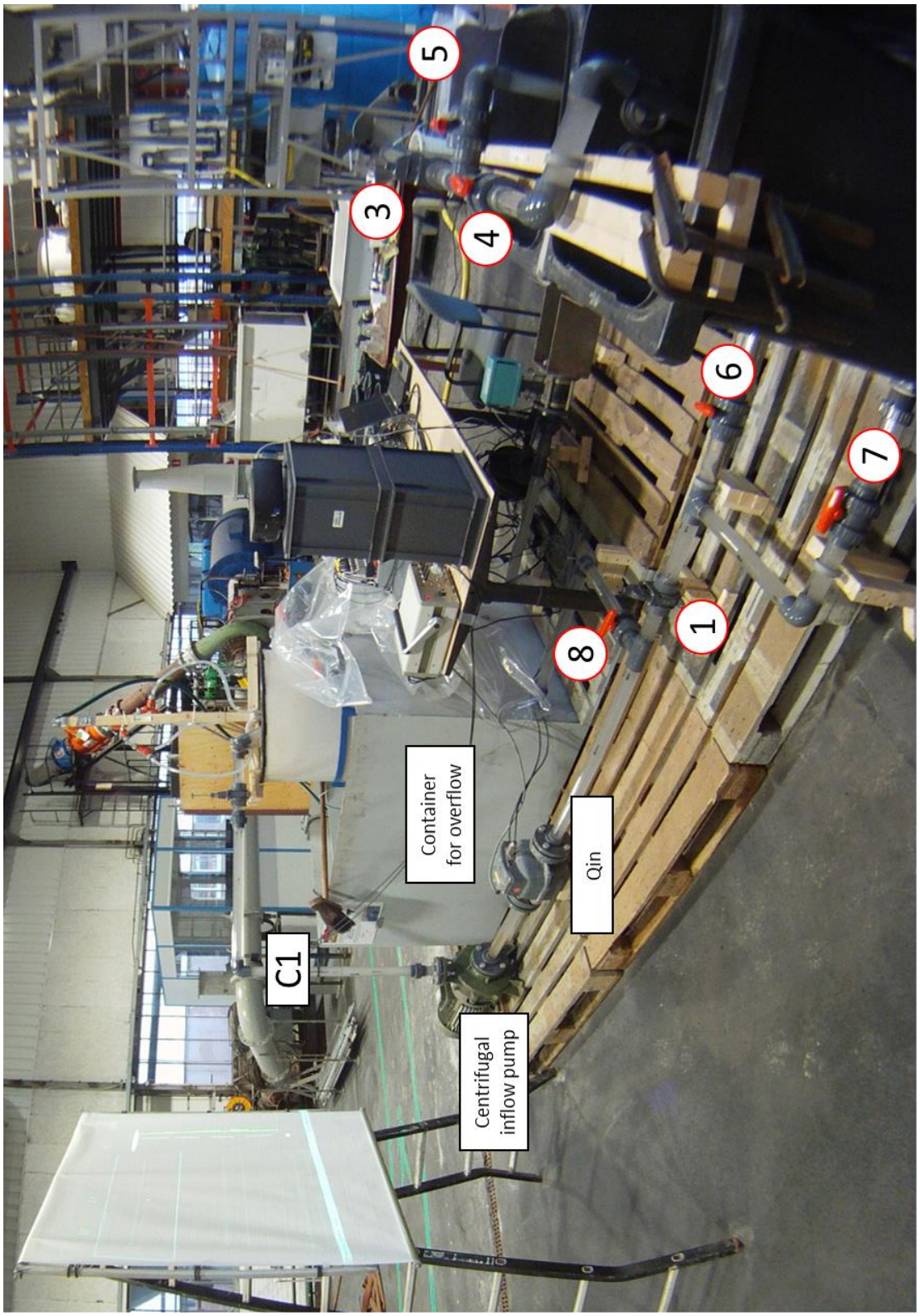

Figure 4-3: Experimental setup: picture in the MTI laboratory

In this section, the instrumentation is listed which is used to satisfy the experiment requirements, as they are defined in chapter 4.2. The abbreviation as used in the schematization is given between brackets.

- Inflow surge bin: Foxboro flow sensor (Q_{in})
- Concentration inflow: conductivity concentration measurement ($C1$)
- Outflow surge bin: Flowtech variomag flow sensor (Q_{out})
- Concentration outflow: conductivity concentration measurement ($C2$)
- Concentration within surge bin: conductivity concentration measurement (C_{bin})

The electric conductivity sensors are installed in the pipelines by the research institute Deltares. A sensor consists of two titanium screws which are drilled through the wall of the pipe, so the tips are surrounded by the mixture inside. Fundamentally, the electrical conductivity of the sand-water mixture between the two screws is measured. Since sand is non-conductive, the concentration can be determined from the measured conductivity. However, the measuring method is sensitive to temperature variations and mineral content of the carrier fluid, and, thus, these deviations have to be compensated for. This will be elaborated in the calibration chapter of this thesis. To be sure that the electrical current goes through the inner side of the pipe, the screws are sealed with a special silicon layer. For backup and more precision, two couples of screws are placed at the same height in the pipe as can be seen in Figure 4-4. At the top of this photograph, the second pair of screws can be seen (which are placed at the opposite side of the pipeline).

Figure 4-4: Electric conductivity sensors

To measure the concentration profile within the surge bin, the same technique as described above is applied. Only here, electric conductivity probes are used which consist of multiple sensors placed in a row. These probes are placed in a fixed position in the surge bin, so each sensor could measure the concentration at a specific height inside the bin. A more detailed overview of the position of the probes can be seen in Figure 4-6.

Figure 4-5: Electric conductivity probes

All the wires from the electric conductivity sensors are subsequently connected to a GCM (Geleidendheids Concentratie Meter) which amplifies the measured signals. On its turn the GCM is connected to a data logging device which logs the signals and stores them on the PC.

The flow sensors used, make use of electromagnetic induction of which the exact working principle is beyond the scope of this thesis. However, a brief explanation of the working principle is that in the sensor, a magnetic field is created and channeled into the fluid which is flowing through the pipe. The flow of the conductive liquid through the magnetic field will generate a voltage signal which is sensed by conductive sensors placed inside. When the fluid moves faster, a higher voltage is generated which can be translated to the mixture

velocity. Because the diameter of the pipe is known, the flow rate can be determined as a result. Contrary to the concentration sensors, the flow sensors are directly connected to the data logging device.

For the position of the flow and concentration sensors, a minimal distance from bends and pumps has to be respected. This distance is taken at 5 times the internal diameter of the pipeline (personal communication with A. Talmon). Furthermore, the pipelines in which the concentration is measured, are placed in a vertical

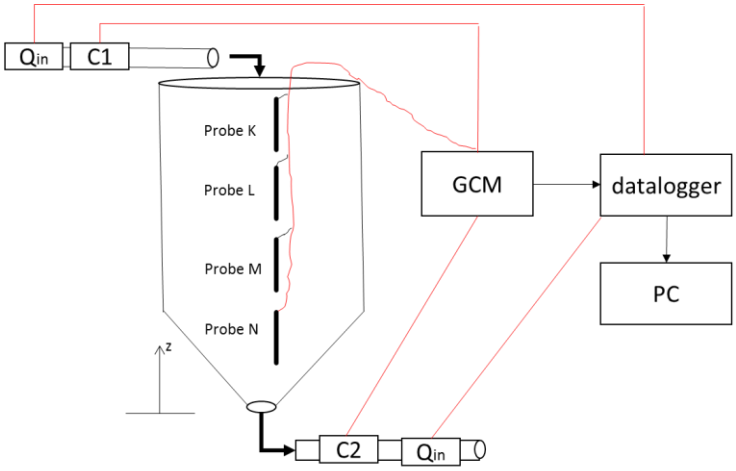

Figure 4-6: Positions of electric conductivity probes in surge bin

direction because it can be assumed that the mixture is then more or less equally distributed over the pipeline's cross-section. If it would be placed in a horizontal direction, different concentration values could be measured along the pipeline's cross-section due to the settling of particles inside the pipe.

On the PC, use is made of Dewesoft data acquisition software, which is able to visualize and store all the collected signals from the flow and concentration sensors. While running the experiment, the user can continuously monitor what is happening. This is of great importance, because when high density mixtures are pumped through the system, the pipes might get blocked and, thus, the user can anticipate immediately to avoid these situations.

Pumps and diffuser used

Because the buffer tank has an in- and outflow, the need for two pumps is essential. The flows are driven by two Saer centrifugal pumps which are able to pump slurry mixtures. To obtain the correct inflow and outflow values for the experiment, the revolutions of the impeller are controlled separately by two control devices. In addition, gate valves are placed to fine-tune the flows in place. Jet water is pumped into the surge bin by using a simple submersible pump which is placed in separate compartment. This is done to only pump fresh water and to avoid the jets to get congested.

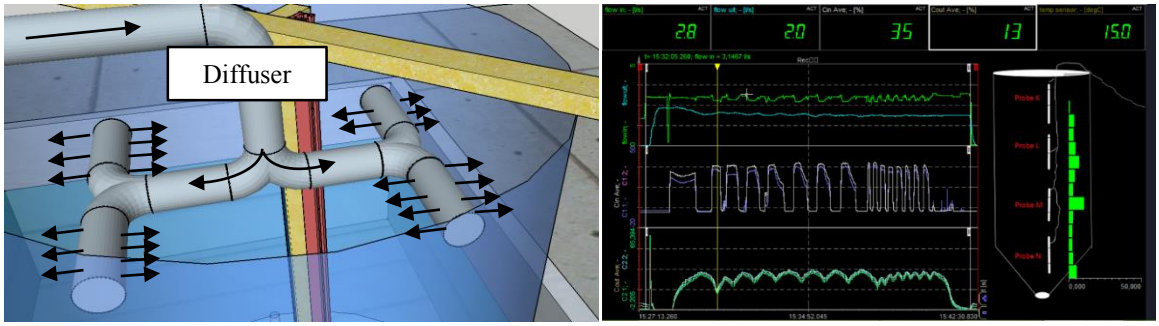

Figure 4-7: Impression of diffuser (left) and Interface of Dewesoft (right)

Special attention should be given on the diffuser which is placed in the surge bin. One of the assumptions in the 1.5D model is that the incoming concentration is distributed homogeneously over the cross-section of the surge bin. Therefore, it is of upmost importance to imitate this process in the experiment. A special diffuser is constructed which distributes the incoming flow over different tubes (see Figure 4-7). In these tubes, small holes are drilled in a horizontal way, so the mixture is sprayed out across the whole area of the bin.

Working principles

Till here, an overview of the experiment has been given, including a short description of the most important instruments and parts. Below, a step-by-step description is given on how the complete setup works. The water levels of the starting position are as follows: the mixture tank, water tank and the surge bin are filled till the overflow.

1. Steady state:

The first step of the experiment is to generate a steady state flow of water in the system. This steady state is achieved by turning all the pumps on and by opening valves 1, 2, 3, 4 and 7. To make sure that the inflow and the outflow of the surge bin are equal, the flows can be regulated with gate valves 2 and 3. Also, the flow of the jet pump can be turned on or off.
Now, when the outflow of the surge bin is smaller than the inflow, water will flow over the edge of the surge bin and is collected in the surrounding container. As a result, the water container will slowly run out of water. This situation can be solved by opening 8 and closing 7. Water running out of the container is then flowing back into the system.

2. Generating homogeneous mixtures:

When the steady state situation of step 1 is obtained and the inflow and outflow of the surge bin are equal, it is time to start sending sediment through the system. To do this, the sand in the mixture container must be fluidized so a sand-water mixture is generated. By closing 4 and opening 5, water is pumped in the sand container and, subsequently, the sand is brought in suspension. Because 6 is still closed, clear water flows from the top of the mixture container into the water container and again a steady state situation is achieved.

3. Creating fluctuating mixtures:

Now, the setup is ready to use. At the moment, only water is pumped through the system and sand is in suspension in the water container. If 6 is opened and 7 is closed, the mixture starts flowing from the mixture container into the surge bin. After a short period of time the sand settles in the bin and is pumped back into the mixture container. Again, a steady state situation is achieved. The outflow of the surge bin can be reduced by closing gate valve 3 a little bit. As a result, water start to flow over the edge of the surge bin. To keep the volume balances intact, the overflow water can enter the system again by slowly opening valve 8.
To simulate the production of a CSD, a fluctuating mixture have to be created. This can simply be done by switching valves 7 and 6.

4. Collecting sediment:

To finish a test batch, it is favorable to collect all the sediment back into the mixture container and, subsequently, have all the pipelines filled with water. This is done by closing 6, opening 7 and by reducing the outflow significantly by closing 3. All the sediment is now collected in the mixture container and, because the flow is reduced, the sediment has the time to settle and water can flow via the overflow to the water container. Once the surge bin is empty, 5 can be closed and 3 and 4 can be opened again.

5. Volume balances and finishing the experiment:

By executing all the previous steps, a steady state situation is obtained again. Now, the levels of water in all the containers can be brought back to their initial level. Simply by closing 7 and opening 8 all the water levels can be brought to the desired level. Once these levels are reached, 3 and 2 can be closed and the pumps can be turned off.

Calibration
Now, the instrumentation used and the working principles are elaborated, an explanation on the calibration of the electric conductivity sensors will be given because it forms an important part of the experiment, including the interpretation of the generated data. As mentioned before, the electric conductivity sensors are sensitive to the amount of dissolved ions in the water and to temperature variations. The experimental setup is regrettably not designed to do instant calibration tests. In other words, it is not possible to calibrate the sensors with the experiment itself. For this reason, a separate calibration loop has been designed in which the sensors are placed. A schematic overview of the loop is given in Figure 4-8 and this separate loop brings several advantages:

- Pipeline sensors can be calibrated at the same time.
- The values of the flow sensors should deliver the same values.
- Because of its small volume, the temperature will increase significantly fast due to the presence of the pump. As a result the effect of the temperature on the conductivity could be measured.

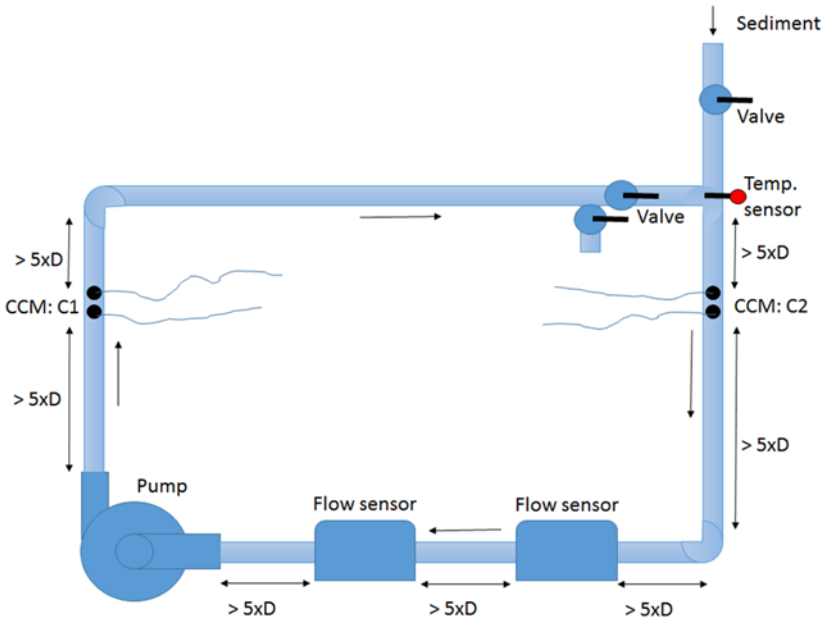

Figure 4-8: Schematization of the calibration loop

The calibration loop has been used twice, once before the experiment, and once after. The steps that are followed to calibrate the concentration sensors are:

1. Calibration loop is filled with process water from the experiment.
2. A certain amount of dry sand is added. The amount of sand corresponds with a volumetric concentration. In total, seven calibrations tests are executed: 0%, 5%, 10%, 15%, 20%, 25% and 35% of volumetric concentrations.
3. The mixture is pumped through the loop with average flow velocity of $3m/s$ to achieve a homogeneous mixture. This velocity is two times the limit deposit velocity of the d_{50} (see Appendix B).
4. The conductivity and the temperature are logged for a broad temperature range.
5. After logging, the process water (with increased ions because of the added sand) is collected.
6. The conductivity of the "new" process water is measured and can be compared to the original process water.
7. Step 1 is repeated with another amount of sand.

The amount of sand for a certain volumetric concentration is determined with the following formula:

$$Amount\ of\ sand\ = C_v * V_{testloop} * \rho_{sand} \tag{4.8}$$

Where:

- Amount of sand is in [kg]
- $V_{testloop}$ is the volume of the calibration loop and is equal to 11.3 liters
- ρ_{sand} is the density of sand =2.65 kg/dm^3
- C_v is the volumetric concentration: 0%, 5%, 10%, 15%, 20%, 25% and 35%

The underlying thoughts behind step 6 is that the amount of ions in the process water will increase because dry sand is added. Subsequently, extra ions will dissolve in the water which will affect the conductivity. When the conductivity of the water is measured, it can be compared with the original conductivity of the process water.
With the gathered data, a function for each sensor can be derived which determines the volumetric concentration as a function of the measured millivolts and the temperature. For the proceeded steps which are followed to determine these functions, the reader is referred to Appendix B, where a detailed explanation is given (as well on the deviations). An example of the functions of one of the sensors is given:

$$C_v = -1.464 \cdot 10^{-4}(mV + (14 - Temp) * 206.69) \; + \; 1{,}016 \tag{4.9}$$

Where C_v is the volumetric concentration, mV are the measured millivolts and $Temp$ is the temperature of the fluid in degrees Celcius.

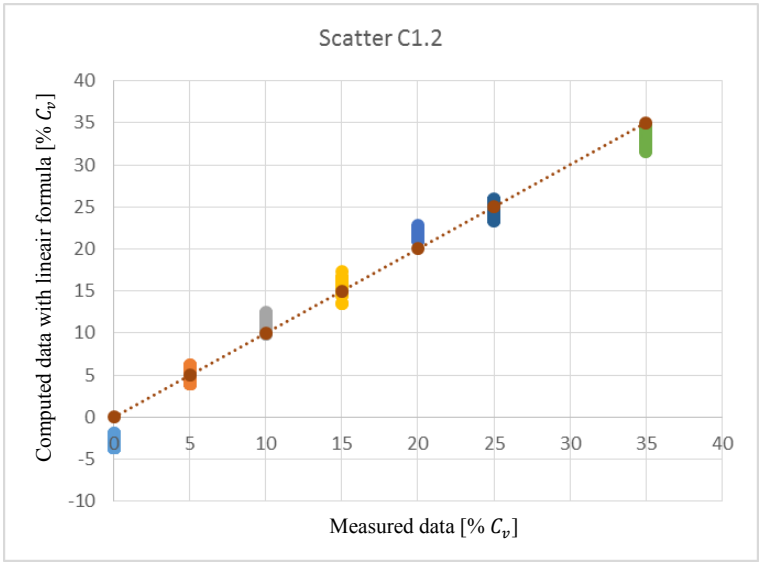

Figure 4-9: Scatterplot of measured data and calculated data with the derived formula

The scatter plot shows how the raw data from the calibration test is now translated into volumetric concentration. It should be interpreted the following way: on the x-axis the theoretical volumetric concentration can be seen: this is the exact value of the concentration. On the y-axis, the results are plotted from the formula that solves the raw data. It can be concluded that apart from some deviations, the formula results in a good fit.

Chapter 5

5. Experimental results and model validation

In this chapter, the results which were measured during the execution of the experiment are discussed. First, an overview will be given on the different testing situations that are created, including a description and motivation. Subsequently, the gathered information will be analyzed in two parts: first the general expectations of the surge bin will be discussed, including several remarks on the experiment itself. Thereafter, the accuracy and predictions of the 1.5D model are tested.

5.1 Experiment scenarios

To get the maximum amount of information out of the experiment, a test plan is made to test different scenarios. Here, a scenario is characterized by different values for the inflow, outflow and jetflow. In total, six test scenarios, each with 7 batches are executed. A batch is on its turn characterized by the concentration profile that enters the surge bin. A description of these scenarios and batches are given below.

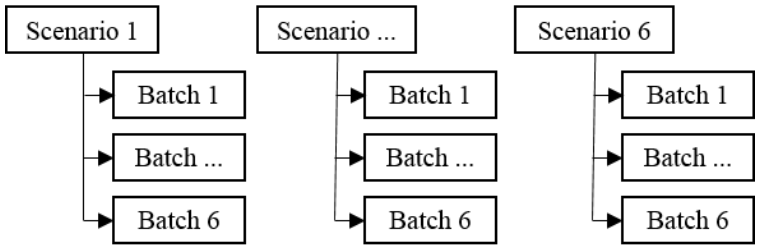

Figure 5-1: Schematization of experiment scenarios and batches

Scenarios:
In the experiment the flows can be regulated with gate and ball valves. Because the settling velocity of the grain sand is relative to the surrounding flow of the water, different values for the inflow outflow and jet water flow are determined. Doing so, different values for the settling efficiency parameter H^* are obtained. For the experiment, B and L are replaced by the cross-section halfway of the surge bin and Q is determined halfway the surge bin as $Q = Q_{jet} - Q_{outflow}$. Furthermore, w_s is taken as the settling velocity of the d_{50} of the sediment ($150\mu m$) which equals $14.9mm/s$ according to equation (2.20).
In addition, the ratio between $Q_{outflow}$ and Q_{inflow} have been varied. In Table 5-1, six different scenarios are presented with the corresponding flows.

Table 5-1: Six scenarios with their corresponding flows

Scenario	Q_{inflow} [l/s]	$Q_{outflow}$ [l/s]	Q_{jet} [l/s]	H^* [-]	Ratio [-] $Q_{inflow}/Q_{outflow}$
1	3	1.9	0.35	0.27	1.58
2	4	2.4	0.35	0.35	1.67
3	2.25	1.43	0.26	0.20	1.58
4	3	1.5	0.35	0.20	2.00
5	3	1.9	0	0.33	1.58
6	3	2.65	0.35	0.40	1.13

Compared to scenario 1, scenario 3 and 5 have a lower and higher H^* respectively, but the ratio $Q_{inflow}/Q_{outflow}$ is kept constant. Scenario 6 has the same Q_{jet} and Q_{inflow} as scenario 1, however, the outflow has increased to change the ratio of $Q_{inflow}/Q_{outflow}$. The same is done for scenario 4, the values for Q_{jet} and Q_{inflow} are kept constant, but now the outflow is reduced.
In addition to these scenarios, a different scenario has been executed where the value of the jet changed over time.

5.2 Experiment batches

Each scenario is defined by constant values for the flows as presented in Table 5-1. For each scenario, six batches, are defined. The purpose of the batches is to gain information on the different functions of the surge bin such as thickening, buffering, and damping.
The six batches are visualized in the diagrams below and the purpose of each batch is given respectively.

Batch 1

Batch 1 ensures that a constant volumetric concentration is entering the surge bin for a certain period of time. The purpose here is to see the increase of concentration in the outflow and, thus, prove that the surge bin indeed functions as a thickener. Furthermore, information on the buffer function of the surge bin can be gathered. The batch is finished after an equilibrium in the outflow is reached. The value of the incoming volumetric concentration lays around 15%.

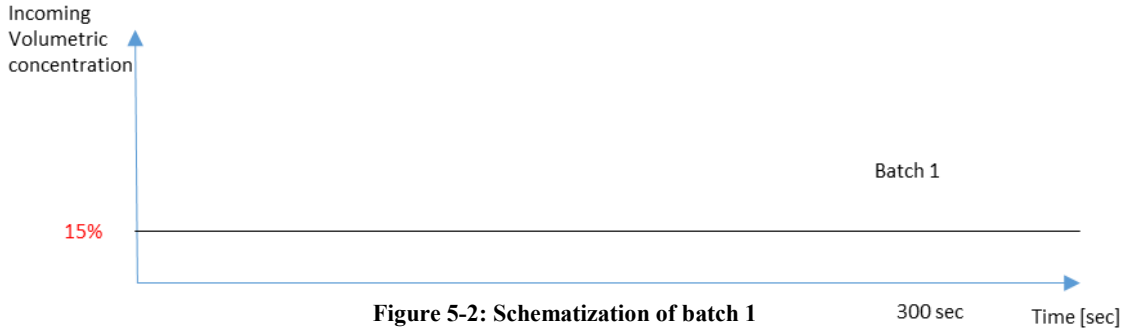

Figure 5-2: Schematization of batch 1

Batch 2

The second batch is comparable to batch 1, however the incoming concentration is slightly higher. The incoming volumetric concentration has increased to a value of about 20%. Doing so, the results of the outgoing concentration can be compared to those of batch 1. If again a steady situation arises, the batch will be ended. It can be expected that if a steady state situation has formed, the outgoing concentration will be higher compared to the final steady state value of batch 1.

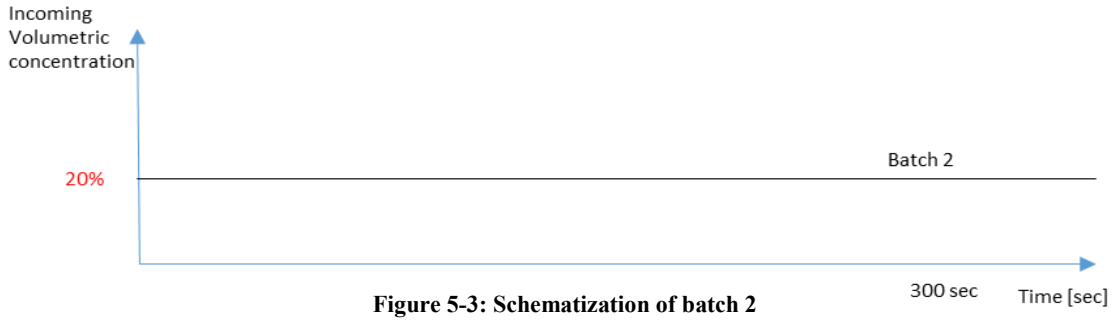

Figure 5-3: Schematization of batch 2

Batch 3

One of the properties of the surge bin is to damp fluctuating incoming concentration signals. In batch 3, pulses with a very high volumetric concentration of about 35% are generated. The purpose is to look at the response of outgoing mixture. When executing this batch, the time between two succeeding pulses will be changed several times.

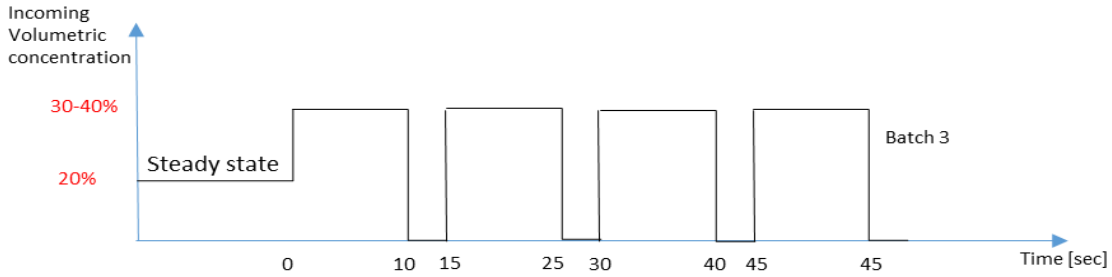

Figure 5-4: Schematization of batch 3

Batch 4

For the fourth batch, a fluctuating incoming concentration will be created around a certain value. This situation is comparable to batch 3, but the intensity of the pulses is significantly lower. The results will be compared to the situation of batch 1 and 3 and, again, the effect of the pulses in the output of surge bin will

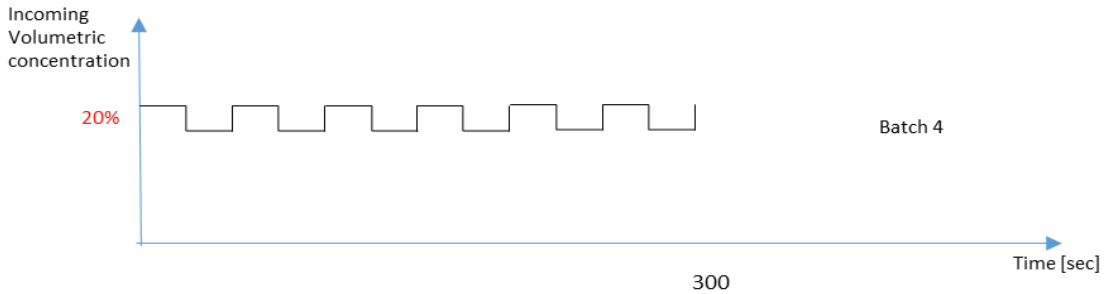

Figure 5-5: Schematization of batch 4

be analyzed. It can be expected that the outgoing concentration will be a combination of the results of batch 1 and batch 3.

Batch 5

With batch 5, a large amount of sand is inserted in the surge bin. In fact, the attempt is to try to fill the surge bin as much as possible. This is done by opening the valve of the mixture container till it is empty, and so the maximum amount of sand is pumped into the bin. Doing so, the time needed by the surge bin to empty itself can be checked. This experiment is strongly dependent on the available amount of sand in the mixture tank and requires extra attention during the execution because a higher risk of sanded pipelines will occur.

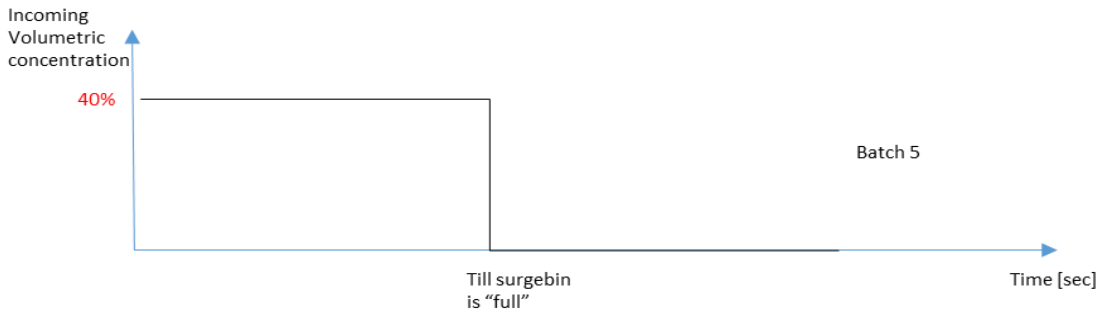

Figure 5-6: Schematization of batch 5

Batch 6

Fundamentally, the delivered concentration profiles from a CSD will not have the profiles as presented above, but will consist more out of a random combination of them. Therefore, the last batch simulates a total random incoming signal. This total random concentration profile will function as a final test to compare the results of the 1.5Dmodel with the results measured with the experiment.

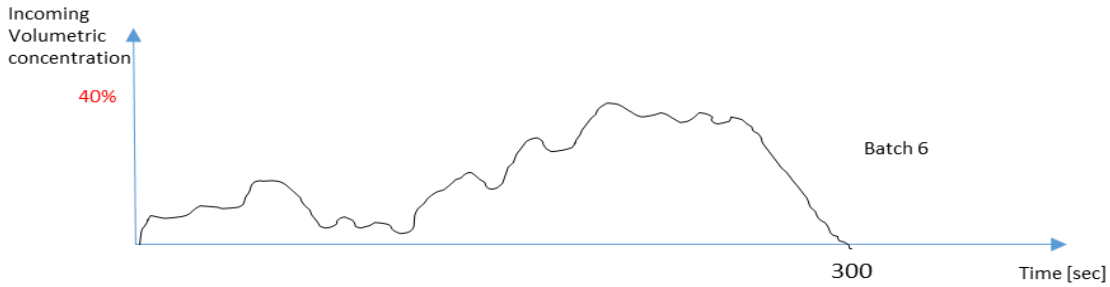

Figure 5-7: Schematization of batch 6

Batch 7

For completion, a final batch is executed where the jet is turned on and off at certain time intervals. Doing so, the effect of the jet at the outflow can be seen.

5.3 Experimental results

In this subchapter the results measured from the experiment are presented and analyzed.

5.3.1 GENERAL OBSERVATIONS

All batches and scenarios as described above, have been carried out with high attention and precision with regards to the experimental setup as described in chapter 4. When impurities during the data logging were experienced or noticed (air bubbles, flow problems), the batch was performed again. Despite the attention paid, the flows of scenario 1 (batch 1 and 2) have a small deviation relative to the planned value. Batch 4 was more difficult to create than expected.
From a practical point of view, scenarios 2 and 4 could not be executed due to unforeseen circumstances. For example, the inflow of scenario 2 was too high leading to a lot of turbulence in the surge bin. This resulted in large amounts of sand flowing over the edge of the surge bin. Also, it became too difficult to generate the concentration profiles because the mixture tank ran quickly out of sediment. In scenario 4, the outflow was too low which resulted in sanded pipelines and a blocked diffuser in the mixture container. Because of these reasons, no information could be gathered for these scenarios.
To collect the sediment which would end up in the overflow, a special hole for the overflow was created. However, this part of the experiment did not work out well because its capacity was too low. This lead to water flowing over the edge of the tank and, thus, the sediment ending up in the overflow could not be collected and examined. Despite that, the overflow was continuously and visually inspected during the tests. Apart from scenario 2, the amount of sediment that floated over the edge was barely noticeable. Especially compared to the incoming amounts of sand it can be assumed that the sediment ending up in the overflow was nihil.
Apart from these unforeseen circumstances, the experiment worked out well. The different incoming concentration signals (batches), were carried out as good as possible. Only small deviations occurred but the achieved results are conform expectations.
The equations for the sensors, as described in 4.4, are programmed in Dewesoft and, subsequently, the logged data (with a frequency of $100Hz$) is exported to Excel files.
All graphs are placed in Appendix C but the results will be discussed in this chapter, apart from batch 7 with the fluctuating jet. A brief analysis of this batch can also be found in Appendix C.

5.3.2 SURGE BIN FUNCTIONS

Thickener
Batch 1 and 2 ensure that the surge bin is filled with a constant mixture density. The concentration at the outflow has been monitored till it reached a constant value. The graphs themselves can be found in Appendix C. However, the graph of batch 1.1 is presented below.

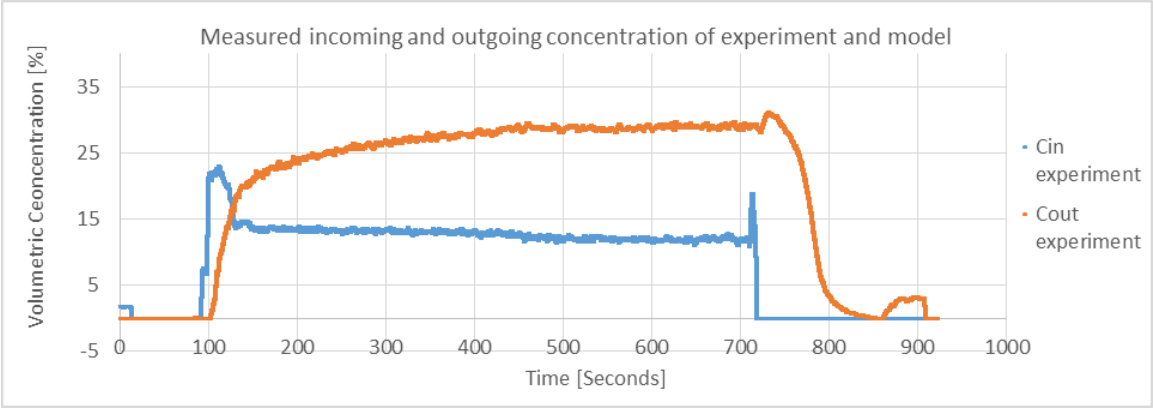

Figure 5-8: Thickening: measured increased concentration in the outflow compared to the inflow

In Table 5-2, all the results are presented for the different batches. The value of C_{in} is the average concentration that entered the surge bin, while C_{out} is the constant concentration reached after certain period of time.

Table 5-2: Results of batch 1 and 2

Scenario	Batch	C_{in} [%]	C_{out} [%]	C_{out}/C_{in} [-]	$C_{out} - C_{in}$ [%]	$Q_{inflow}/Q_{outflow}$ [-]
1	1	13	27	2,1	14	1.88
	2	17	30	1,8	13	1.67
3	1	14	24	1,7	10	1.50
	2	17	26	1,5	9	1.50
5	1	13	22	1,7	9	1.61
	2	18	28	1,6	10	1.61
6	1	13	15	1,2	2	1.20
	2	17	19	1,1	2	1.20

It can be noticed that for each scenario an increase of outgoing concentration, relative to the incoming concentration, took place. This confirms that the surge bin indeed functions as a thickener. A remark should be made that the rate of thickening is somehow related to ratio of $Q_{inflow}/Q_{outflow}$. For example, if scenario 6 is compared to scenario 1, 3 and 5, a significant difference can be distinguished in the ratio of C_{out}/C_{in}. If batch 1 and 2 of each scenario are compared mutually, it can be seen that an increase in the incoming concentration leads to a higher concentration at the output. However, the relative difference of $C_{out} - C_{in}$ stays more or less equal.

These observations are not surprising, because if a steady state situation occurs the rate of $Q_{inflow}/Q_{outflow}$ should equal the rate of C_{out}/C_{in}. This can be seen in the dimensionless graph below where the ratios of the flows and concentrations are plotted against each other. If a perfect steady state is achieved, a batch should lay on the dotted line. The numbers near the triangles represent the scenario number and batch number.

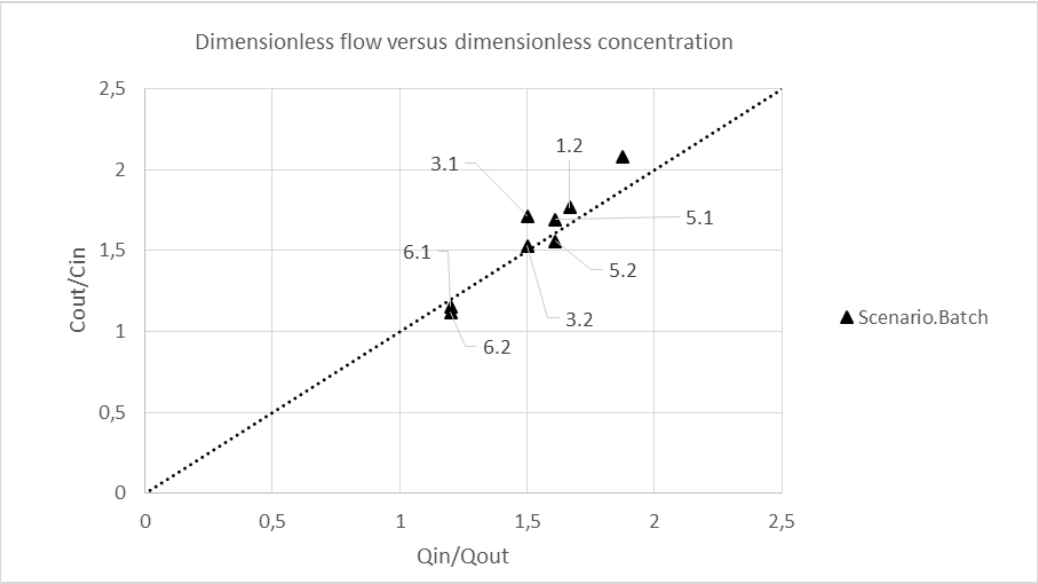

Figure 5-9: Dimensionless flow vs dimensionless concentration

The plot shows that the ratios are approaching the dotted line really well, which means that a steady state situation was achieved. The small deviations in the batch of 1.1 can be declared by calibration deviations due to the applied formula as shown in equation (4.9).
The attempt to make a verdict on the change in H^* did not work out. The reason is that the calculated values of H^* are chosen too close to each other. If other sediment would be used, H^* could be changed significantly. E.g. if sediment with a $d_{50} = 400\mu m$ would be used, the value of H^* would change with a factor 3.5.

Buffering

One of the most important functions of the surge bin is that it must function as a buffer tank. This means that it can be filled for a certain period of time and, subsequently, it must be able to deliver a concentration for a longer period of time. In order to check whether this function is met, the filling time is compared to the time it needs to empty itself: the idle time. The idle time can thus be seen as the time wherein the surge bin processes all the incoming sediment. However, looking at Figure 5-10, the idle time is chosen in such a way that the outgoing concentration is slightly higher than zero (about 1%). By doing this, a conservative value is obtained for the idle time.

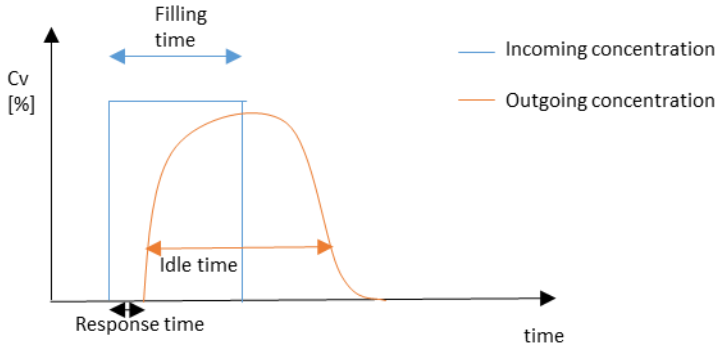

Figure 5-10: Vizualisation of the defined times

In Table 5-3, the results of batch 5 are gathered. In this table the values of the filling time and idle time are presented. A first look at these values clearly shows that the idle time is significantly longer than the filling time which means it indeed functions as a buffer for a certain period of time. The buffer time is the difference in time between the filling time and the idle time.

Table 5-3: Results of batch 5

Scenario	Batch	Filling time [s]	Idle time [s]	Buffer time [s]	Response time [s]
1	5	90	158	68	9
3	5	96	143	47	10
5	5	120	184	64	9
6	5	51	105	54	7

During the experiment it was for practical reasons not possible to really fill the surge bin. If this could have been accomplished, the maximum buffer time could have been determined. Also, for scenario 6, the outflow lead to an overflow problem in the mixture tank which lead to a shorter filling time compared to the other scenarios. The buffer time is, logically, relative to the amount of sediment present in the surge bin. However, with this experiment the function of buffering is proven because for each test the idle time is significantly longer than the filling time.
The response time in the table is the "reaction" time, the time needed for the incoming concentration to reach the outflow. So, to prevent the outflow from running out of sediment, sediment must enter the bin within the buffer time minus the response time.

Damping

In practice, the separation plant is sensitive to fluctuating productions and, therefore, it is favorable to damp out the oscillating production profile of the CSD. To test this behavior, an oscillating concentration signal was sent into the surge bin with very high amplitudes (up to 35% C_v). An example is given in the graph below.

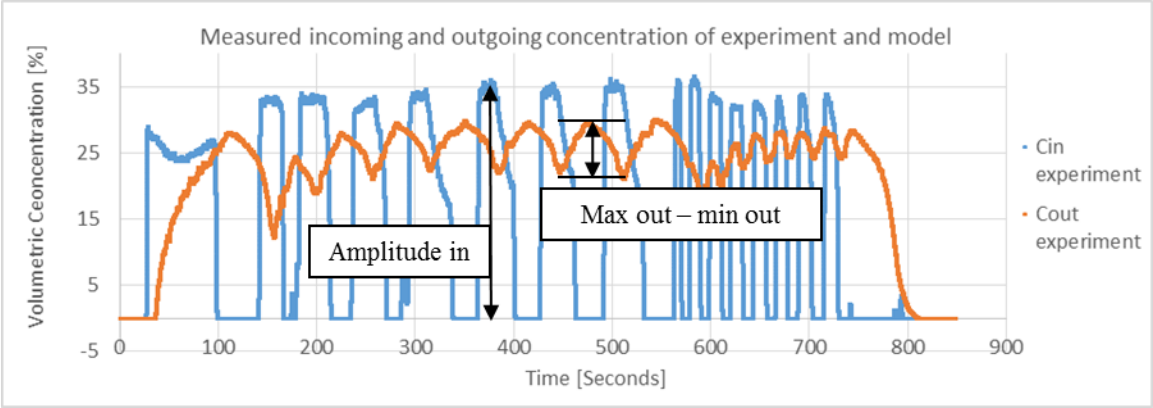

Figure 5-11: Damping: Incoming signal (blue) is significantly damped (orange)

In fact, the buffer time as described in the previous chapter returns in these profiles. When the surge bin is fed fast enough (short interval), the output will not run out of sediment and the fluctuation in the output reduces. Table 5-4, shows the values of the incoming concentration profile and the corresponding amplitude in the output.

Table 5-4: Results batch 3

Batch	Amplitude in [% C_v]	Amplitude out: maximum [% C_v]	Amplitude out minimum [% C_v]	Difference [% C_v] (maximum - minimum)
1.3	35	30	22	8
3.3	34	27	20	7
5.3	35	30	25	5
6.3	24	17	13	4

Here, the amplitude of the incoming signal can be seen, as well as the amplitude which occurs in the outgoing profile. Looking at the second and the last column, the reduction of the amplitude can be seen and it can be concluded firmly that the surge bin functions as a damper.

When all the datasets signals are compared to the concentration measured at the outflow the following conclusions can be made:

- The amplitude of the signals is significantly reduced.
- The frequency of the pulses can be seen in the concentration profile of the outflow.
- A higher frequency of the pulses leads to less deviation in the profile of the outflow.

5.4 Validation of the 1.5D model

In this subchapter, the results of the 1.5D model are elaborated. This elaboration is split up into two parts. First, the model results are compared with available experimental results from sedimentation tests in a

cylinder (benchmark). Subsequently, the datasets which are gathered with the surge bin experiment are compared with the predictions of the 1.5D model.

5.4.1 BENCHMARK

Tests have been carried out with a sedimentation column to measure volume concentration at different heights, see (Klerk & Kranenburg, 1998) and (Rhee C. v., 2011). The tests were carried out in a cylindrical tube with a height of $1.4m$ and an inner diameter of $0.28m$ where a sand mixture was brought in suspension after which it could deposit. Within this cylinder, 12 conductivity sensors were installed which could measure the concentration at different heights.
To get a first impression on the proper working of the program, the results of the model will be compared with those of experimental data from one experiment. To simulate the formation of a bed, the fluxes into a cell are blocked if the concentration reaches a value above $0.55\ C_v$. The used values for the particle size distribution are given in Table 5-5.

Table 5-5: Particle Size Distribution benchmark

Particle diameter [mm]	Volume fraction [%]
0.765	2
0.98	4
1.15	15
1.37	22
1.63	29
1.94	20
2.31	6
3.02	2

Figure 5-12: Sedimentation column with rotating frame. Figure is taken from (Rhee C. v., 2002)

Furthermore, the following parameter values have been used:

- Initial concentration: 32%
- Maximum concentration: 55%
- $\Delta t = 0.002\ [s]$
- Number of grid points $N = 100$
- Simulation time $t = 200\ [s]$
- Hindered settling coefficient n is determined according to the values of Garside

In the graphs given below, the concentration profiles from the experiment and 1.5D model are plotted. On the vertical axis, the height of the sedimentation column is given, the horizontal axis is the volumetric concentration. The graphs show the concentration at $t = 50\ [s]$, $t = 100\ [s]$, $t = 150\ [s]$ and $t = 200\ [s]$:

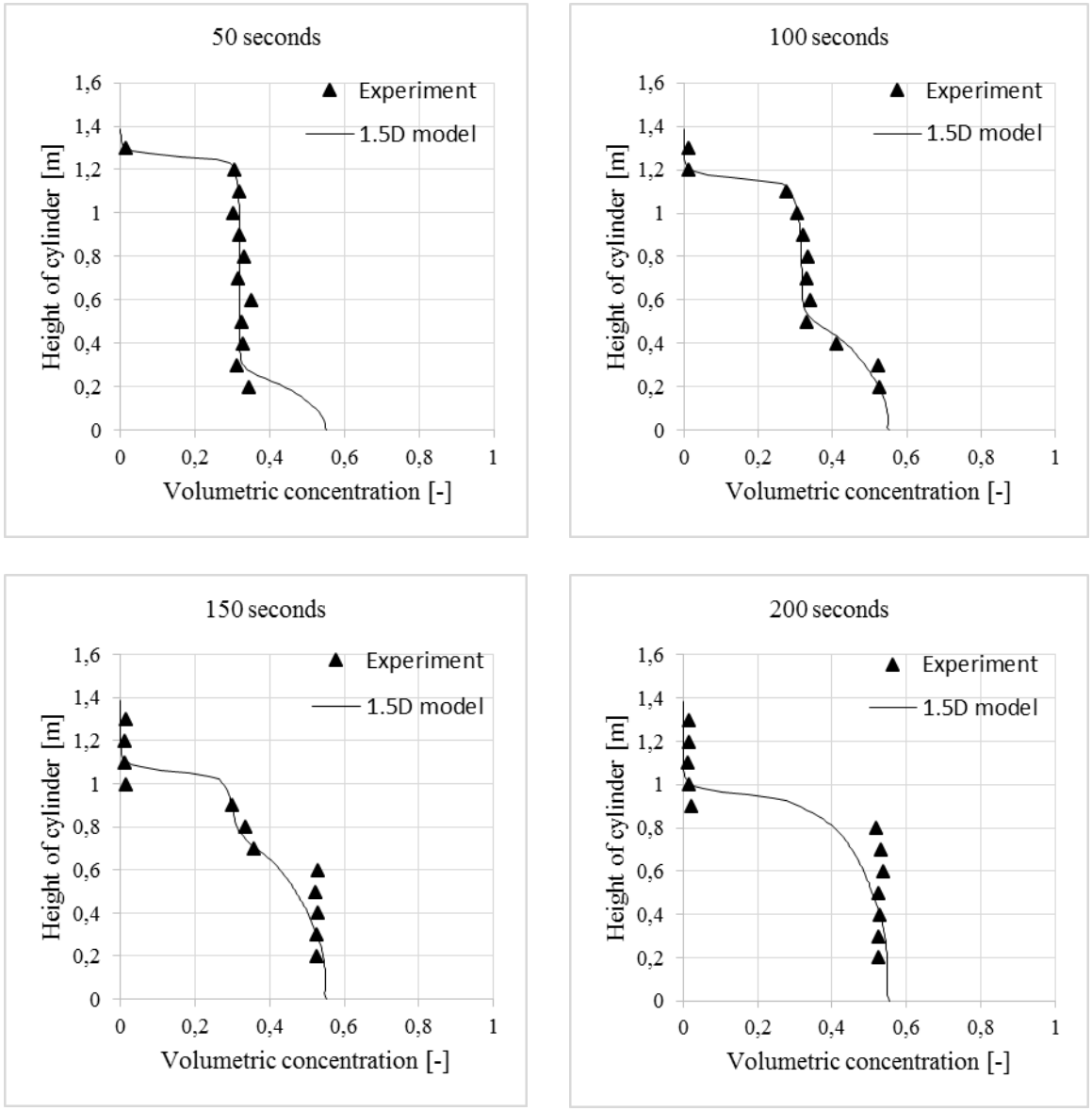

Figure 5-13: Benchmark: calculated and measured concentrations at t=50[s], t=100[s], t=150[s] and t=200[s]

It can be seen that the model fits the data well. The last two graphs show that the concentration profile from the model is very smooth. This can be the effect of the upwind method which is used for the advection term within the model which causes numerical damping.

With the agreements between calculated and measured results, it can be concluded that the sedimentation part of the program delivers good predictions.

5.4.2 DETERMINING DIFFUSION COEFFICIENT

In chapter 0 a description has been given on the function for the diffusion coefficient:

[redacted] (5.1)

Here, K is a factor which still has to be given a certain value. To do this, a complete random dataset is generated with the experiment. The measured incoming volumetric concentration of the dataset is subsequently used as the incoming concentration for the computer model. A visualization of this process is given in Figure 5-14.

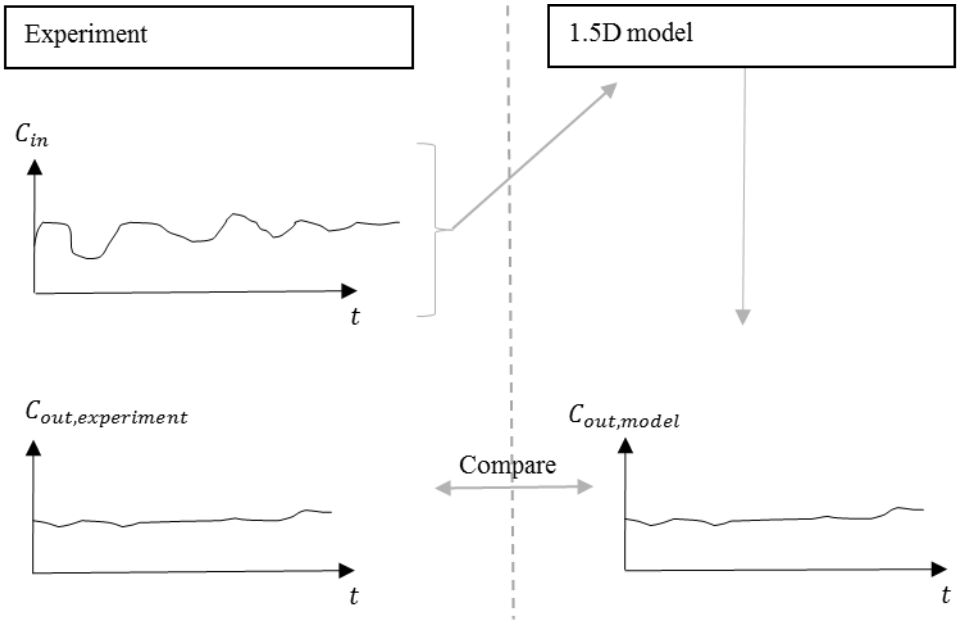

Figure 5-14: Schematization of the validation process

In the 1.5D model, five different values [redacted] This resulted in five different datasets which are each compared with the measured data. As a measure how well the calculated data fits the measured data, use is made of the R squared value. The R squared value is an indication of how well data points are fitting a curve. In this case: how well does the computed curve fit the measured curve? The R squared value can be calculated using the Pearson Correlation which is a correlation between two random variables (for more information see Appendix C) and is given by the following formula:

$$R(X,Y) = \frac{\sum_{i=1}^{n}(x_i - \bar{x})(y_i - \bar{y})}{\sqrt{\sum_{i=1}^{n}(x_i - \bar{x})^2 \sum_{i=1}^{n}(y_i - \bar{y})^2}} \quad (5.2)$$

Where $\bar{x}$ and $\bar{y}$ are the average values of the datasets. The R squared value can now be determined as $R^2(X,Y)$. The values for R squared have a range between 0 and 1 and $R^2 = 1$ indicates that the computed data fits the measured data perfectly.

First, the R squared value of the outgoing concentration profiles are compared to the measured data. This resulted in the following graph:

Figure 5-15: Results of different values of K (N=20 & $\Delta t = 0.01s$)

In this graph, the blue line represents the random generated incoming concentration, measured at the inlet of the surge bin while the orange line is the concentration, measured at the outflow. The four other plots, are the concentration profiles as they are calculated with the 1.5D model, each with a different value for K. It can be noticed that with an increasing K, the calculated concentration profile will fit the measured data better. [redacted]

In Table 5-6, the values of R squared are presented and give a correlation between the measured and the calculated data.

Table 5-6: R squared values for different values of K, see Figure 5-15

K	[redacted]	[redacted]	[redacted]	[redacted]	[redacted]
R^2	[redacted]	[redacted]	[redacted]	[redacted]	[redacted]

[redacted] a good fit starts to occur. However, no significant increase can be distinguished after [redacted].

Table 5-7: R squared values for different values of K, see Figure 5-16

[redacted]	[redacted]	[redacted]	[redacted]	[redacted]
[redacted]	[redacted]	[redacted]	[redacted]	[redacted]
[redacted]	[redacted]	[redacted]	[redacted]	[redacted]
[redacted]	[redacted]	[redacted]	[redacted]	[redacted]
[redacted]	[redacted]	[redacted]	[redacted]	[redacted]
[redacted]	[redacted]	[redacted]	[redacted]	[redacted]
[redacted]	[redacted]	[redacted]	[redacted]	[redacted]
[redacted]	[redacted]	[redacted]	[redacted]	[redacted]
[redacted]	[redacted]	[redacted]	[redacted]	[redacted]
[redacted]	[redacted]	[redacted]	[redacted]	[redacted]
[redacted]	[redacted]	[redacted]	[redacted]	[redacted]
[redacted]	[redacted]	[redacted]	[redacted]	[redacted]
[redacted]	[redacted]	[redacted]	[redacted]	[redacted]
[redacted]	[redacted]	[redacted]	[redacted]	[redacted]
[redacted]	[redacted]	[redacted]	[redacted]	[redacted]
[redacted]	[redacted]	[redacted]	[redacted]	[redacted]
[redacted]	[redacted]	[redacted]	[redacted]	[redacted]

[redacted]

[redacted]

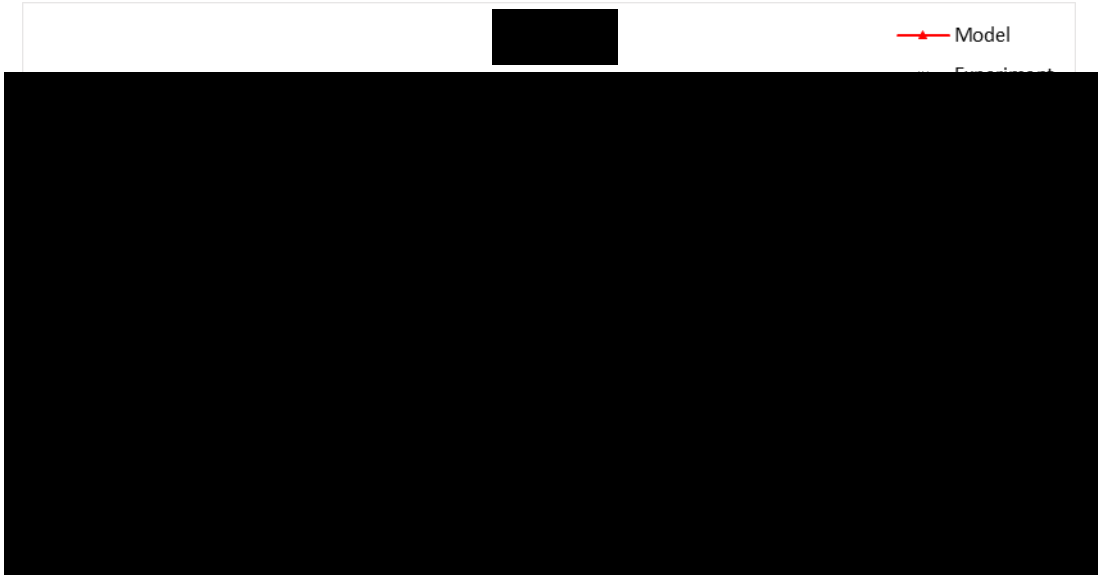

Figure 5-16: Measured and calculated concentration in surge bin at different time moments

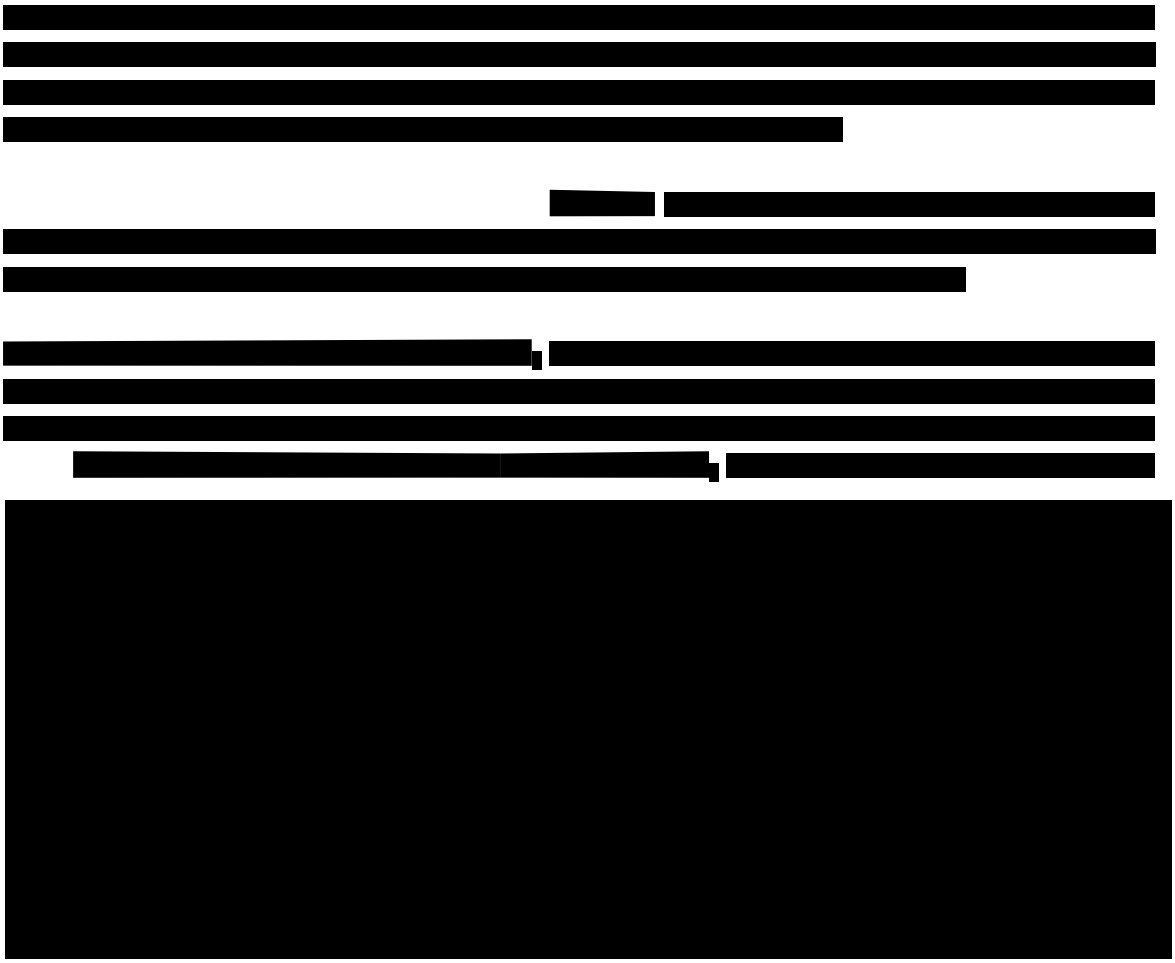

Figure 5-17: Results of different values of k_z (N=20, $\Delta t = 0.01s$)

in Figure 5-17 k_z and are indicated with the black, red and yellow line respectively.

Table 5-8: R squared values for different values of k_z

k_z $[m^2/s]$			
R^2 [-]			

k_z

Note: A second simulation with a different incoming concentration has been executed. This simulation is This simulation is presented in the figure below:

Figure 5-18: Second simulation: Results of different values for K

Table 5-9: R squared values for different values of K, see figure Figure 5-18

K					
R^2					

5.4.3 COMPARISON OF TEST RESULTS WITH 1.5D MODEL RESULTS

All of the datasets which are generated with the experiment have been simulated with the 1.5D model. The results of the measured outflow concentration have been compared with those from the model. For each simulation, an overview is made in which the results are presented and where statistical values are given. The statistical results and other observations will be discussed here. However, for the complete overview of the results (graphs), the reader is referred to Appendix C.
First, a brief explanation is given on the created graphs and deviations.

1. General information of the experiment is given such as water temperature, average flows, batch and scenario numbers.
2. Is the plotted data of the experiment. The blue line represents the concentration at the outflow while the orange line represent the concentration at the inflow. The orange line is used as an input signal for the 1.5D model.
3. Shows the computed concentration at the outflow of the model (blue line) and the measured data from the experiment.
4. Gives the error between the computed and measured data. This graph is obtained if the blue line is subtracted from the orange line in number 3). From this graph, the maximum deviation is determined.
5. Shows a summary of the calculated statistics.

All the statistical results from the batches are gathered in Table 5-11. The results as presented in this table will be discussed in this paragraph.
For all of the simulation, $N = 20$ and $\Delta t = 0.01s$.

Figure 5-19: Example of dataset. All datasets can be found in Appendix C

Batch 1 & 2

Looking at the batches 1 and 2 from all the scenarios, the measured data (orange line) is consequently a few percentages higher than the values from the model (blue line). Because a steady state solution was reached during the experiments, and knowing that the model is mass conservative, it is plausible that the steady state value of the model is correct. Supposing that this assumption is true, the deviation of the measured value

could be explained by the deviation introduced by the linear calibration formulas: the standard deviation of the experiment and generated data lays around the 2 and 3 % C_v while the average standard deviation from the calibration lays around 2% C_v. However, it can be said that the predicted values from the model approach the measured data very well because the R squared values are varying from 0.83 up to 0.97.
A noteworthy difference is that the 1.5D model needs significantly more time before it runs out of sediment, varying from 15 seconds up to 30 seconds. The steepness of the slope at the end is less abrupt than the slope from the experiment which leads to the maximum deviations.

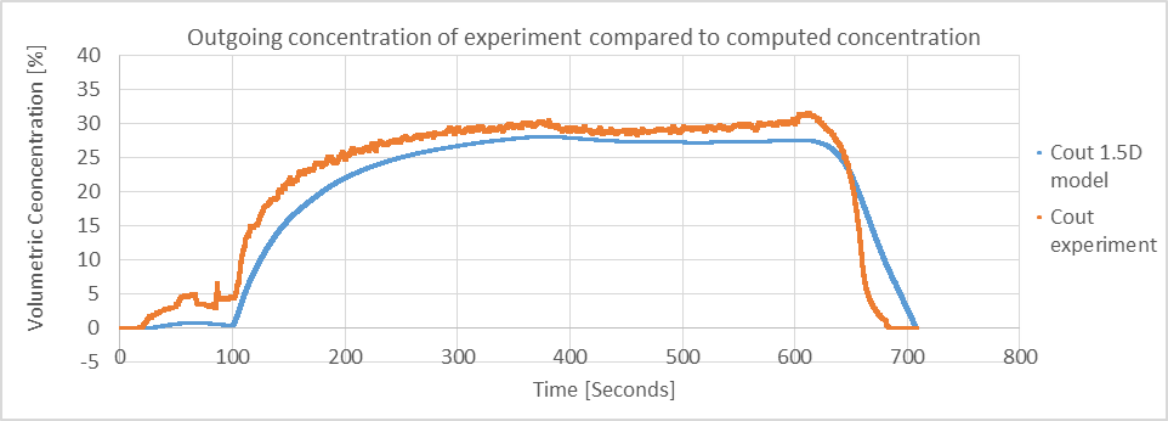

Figure 5-20: Example of the results of measured and calculated data of batch 1 and 2

Batch 3 & 4

Again, the predicted values from the model approach the measured dataset surprisingly well. The calculated data have the same trend and shape compared to the measured concentration. Nevertheless, the model has a higher damping. The peaks from the pulses can be recognized in the model results as well as their frequency. The starting points of the periods of both graphs coincide as well.
Looking at the statistical values, the standard deviation varies around the 3% C_v. However, this deviation does not say anything about the damping.

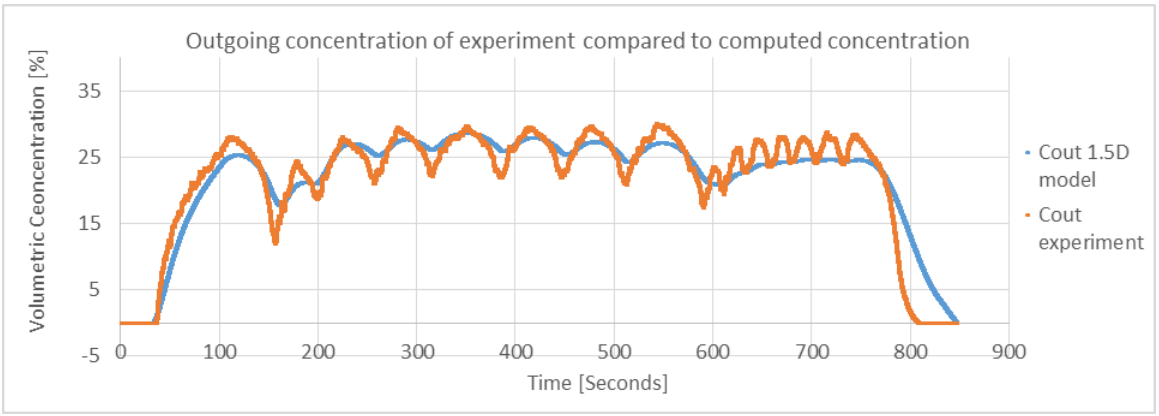

Figure 5-21: Example of the results of measured and calculated data of batch 3

For all the test executed, the difference between the model and the measured data lays around 5% C_v what can be assumed acceptable.

Batch 5

From the analyses of the previous batches it became clear that the model reacts less intense on the pulses compared to the measured data. When batch 5 is analyzed this behavior can be ascertained again. The computer model needs consequently needs more time to empty itself. This was already noticed during the analyses of batch 1.

In Table 5-10, the difference in the measured and calculated idle times are shown.

The last column is the ratio of the idle time from the model over the idle time of the experiment. Here, it becomes clear that the extra time needed to run down is in the order of 20-30% percent.

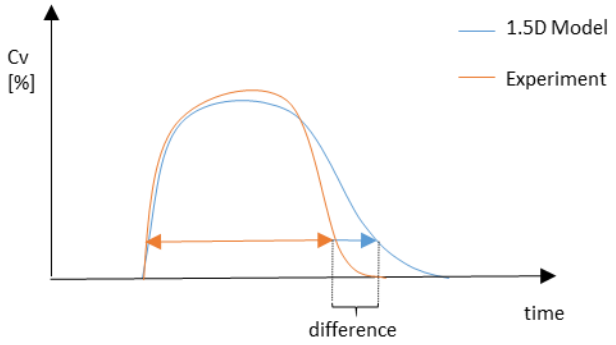

Figure 5-22: Example of delay by the calculated data

Table 5-10: Results of batch 5

Scenario	Batch	Idle time measured [s]	Idle time model [s]	Difference [s]	Ratio [-]
1	5	158	187	29	1.18
3	5	143	185	42	1.29
5	5	184	210	26	1.14
6	5	95	116	21	1.22

An explanation of this delay could be the result of the following possibilities:

- Numerical solving method used in the program which causes damping.
- During the experiment, the sediment was maybe given an initial velocity due to the diffuser which makes the sediment go faster to the outflow Figure 4-7. In the model, it is assumed that sediment is homogeneously released at the inlet zone.
- In the model it is assumed that the sediment settles relative to the mixture velocity and that for the whole area of the bin this mixture velocity is equal. It might be concluded that this assumption is not really correct because the sediment in the experiment settles significantly faster which can be the result of an eddy which occurred during the experiment: see Figure 5-23.

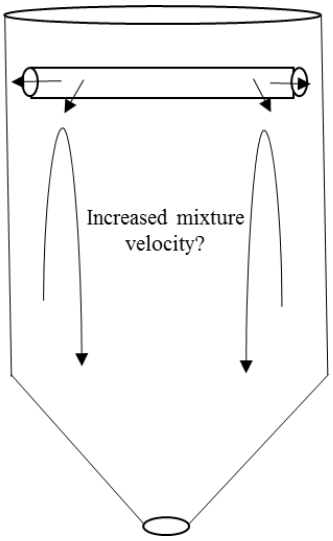

Figure 5-23: Possible formation of an eddy during the experiment

Due to this delay the R squared value decreases which can be seen in Table 5-11. The range of values lays in between 0.76 and 0.89 which is lower compared to all the other batches. When the graphs are compared with their corresponding maximum deviation values, it can be concluded these maximum deviations are a result of the delay caused by the model.
In addition, a second conclusion is that for all batches the program needs more time to run out of sediment.

Batch 6

The last batch is in fact a combination of all the above presented batches. In fact, batch number 6 forms a good test, to check whether the model gives good predictions since the input signal is totally random.
The previous batches gave a good illustration where the program deviated relative to specific input signals. However, in practice it will be more likely that a combination of these signals will take place. The random signal in fact is a combination of the previous batches.
When analyzing the graphs, it can be concluded that the predicted values have the same trend as the measured data. Remarkably, but not very surprisingly, the extra damping and the delay of the model can be seen back in the graphs. Despite of these effects, the R squared values are all above 0.83 and the standard deviation lays around the 4% C_v. Yet again, relative large maximum deviations are measured, but it can be concluded that these are the result of the slower response of the model.

Table 5-11: Overview of the statistical results from all batches and scenarios

Batch	Scenario	Maximum Deviation [% C_v]	Standard Deviation [% C_v]	R^2 [-]
1	1	7.7	2.7	0.97
	3	10.5	3.8	0.83
	5	6.4	2.2	0.93
	6	6.4	1.9	0.9
2	1	11.6	3.1	0.92
	3	9.9	3.3	0.91
	5	13.0	2.9	0.93
	6	7.1	2.4	0.90
3	1	11.6	3.0	0.89
	3	12.2	3.9	0.85
	5	10.2	2.6	0.94
	6	8.6	2.4	0.89
4	1	11.1	2.9	0.96
	3	8.4	3.2	0.84
	5	9.2	2.0	0.94
	6	6.2	2.0	0.8
5	1	12.9	4.7	0.84
	3	15.1	5.7	0.82
	5	15.9	4.6	0.89
	6	9.6	4.7	0.76
6	1	14.0	3.9	0.83
	3	14.2	4.2	0.9
	5	16.7	4.1	0.84
	6	7.4	3.1	0.84

5.5 Conclusion and remarks

Remarks

- Scenarios 2 and 4 could not be executed due to unforeseen circumstances
- Measuring the overflowing concentration did not work out well. Therefore no verdict can be made on the overflow function of the surge bin. However, the overflow is visually inspected during the execution of the tests.

Experimental conclusions

- The variations in the flows and H^* were not large enough to make verdicts based on these parameters. For this purpose, experiments with different types of sediment should be executed.
- For batches 1 and 2, a buffer time varying from 47 to 68 seconds was measured meaning that the surge bin indeed functions as a buffer tank.
- Heavy fluctuating incoming concentration profiles are damped significantly. E.g. incoming concentrations varying from 0-35% were reduced to outgoing concentration fluctuating from 22% to 30%. When the interval between two consecutive pulses reduces, the fluctuation in the outflow reduces as well. The frequency of the pulses can be seen in the outgoing concentration profile.
- When the outflow of the surge bin is reduced compared to the inflow higher concentrations in the outflow are measured. Thus, the thickening function of the surge bin is thereby proven.

Model conclusions

- With the agreements between calculated and measured results from the benchmark, it can be concluded that the sedimentation part of the program gives good predictions. However, it can be noticed that numerical damping is present in the model.
- [redacted] to determine the diffusion coefficient. Higher values do not lead to better results while lower values do. This value is taken in the validation of the model.
- The model results are compared with the measured data (for 24 datasets). The R squared values vary from 0.76 up to 0.96, meaning that good predictions can be made.
- For each dataset, the model responds slower compared to the experiment. Measured peak values are lower compared to calculated peak values which might be the result of damping introduced by the model. The variations lay around 5% volumetric concentration.
- For each dataset, the model needs more time to run out of sediment compared to the experimental data. Looking at the data of batch 5 this in the order of 20-40 seconds. This is not favorable because it is an important design criterion. However, it is of importance to investigate why the model is slower.

Chapter 6

6. Application of the model on a prototype case

6.1 Introduction

In chapter 5, it was shown that the 1.5D model approached the measured values from the experiment well if [redacted] same value for K. In the simulation, the effect on a random incoming concentration profile will be tested. This incoming concentration signal is generated by a computer model of Royal IHC which simulates the production of the CSD (in't Veld, 2015).
Subsequently, the same simulation will be made with two smaller surge bins. These two smaller surge bins will be called "Medium" and "Small".

In the simulation, the PSD of Table 6-1 is used. This PSD is derived from the S-curves as plotted in Figure 6-1 which shows a typical distribution of the sediment in the QMM mines. However, it can be seen that there are two fractions with the same particle diameter, but with a different density. The underlying thought is that the heavier particles (heavy minerals and, thus, the valuables) need to flow to the outflow and not to the overflow. At the end of a simulation, the amount of sediment which gets lost in the overflow can be determined.

Table 6-1: PSD used for the protype simulation

Particle diameter [mm]	Volume fraction [%]	Density $[kg/m^3]$
0.05	5	4500
0.05	5	2650
0.2	10	2650
0.3	20	2650
0.4	20	2650
1	20	2650
2	20	2650

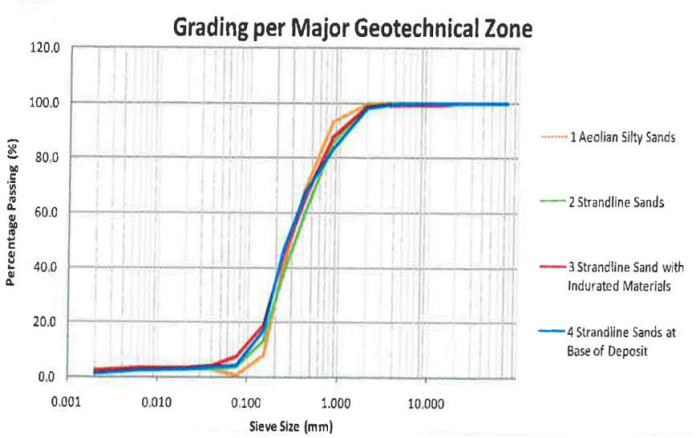

Figure 6-1: Particle size distribution of QMM Madagascar (Boshoff, 2011)

For the dimensions of the surge bins, the following values will be used:

Table 6-2: Dimensions and flows for different surge bins

	Prototype QMM	Medium	Small
Height $[m]$	19	14	10
Diameter top $[m]$	22	16	11.5
Slope [°]	60	60	60
Volume $[m^3]$	2400	1000	380
Q_{in} $[m^3/s]$	3	3	3
Q_{out} $[m^3/s]$	2	2	2
Q_{jet} $[m^3/s]$	0.6	0.6	0.6
Number of grid points [-]	95	70	50
Time step [s]	0.02	0.02	0.02

Since no information is available on the amount of jet water which is added, a value of $0.6m^3/s$ will be assumed (=20% of inflow). In the prototype surge bin, this leads to a net upward flow of $4mm/s$ at the overflow. Particles with a diameter of $50\mu m$ have a settling velocity of $2mm/s$, and thus, can move with the flow into the overflow.

In practice, it appears that the surge bin is fed by multiple dredgers. It even occurs that surge bins are fed with dry sand by backhoes. Here, it is assumed that the surge bin is only fed by 1 dredger, which is able to deliver the incoming concentration as presented in Figure 6-4.
The dimensions of the height of the smaller surge bin "Medium" is taken 25% smaller than the prototype surge bin while "Small" is taken 50% smaller.

6.2 Prototype simulations

First, a simulation will be made to determine the idle time of the surge bin. Here, it is assumed that the surge bin is filled from the bottom of the bin up to the inlet with a mixture of 20% volumetric concentration.

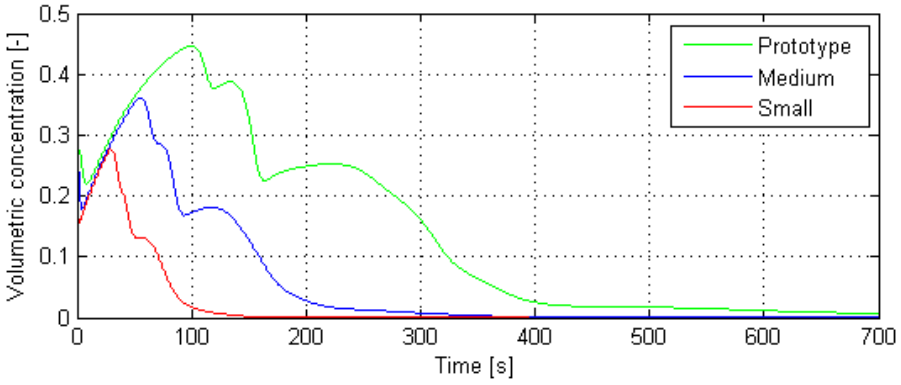

Figure 6-2: Results of the idle times for three different surge bins

Subsequently, no sediment enters the surge bin to let the surge bin run out of sediment. The results are plotted in Figure 6-2. The goal of this simulation is as follows: assume that it is possible to fill the surge bin till this situation is met, then the dredger has the time to replace its anchors within the idle time.

At first, it can be noticed that the concentration calculated at the outflow is not constant. This is the effect of the particle size distribution. The larger particles will travel faster than the lighter ones which leads to peak values in the concentration profile.
An analyzes of the results shows clearly that the prototype surge bin has a significant longer idle time. If the values at about 3-4% C_v are compared with each other, it can be said that the prototype has 400 seconds of buffer time, compared to 100 and 200 seconds of "Small" and "Medium" respectively.
This is not surprising because the buffer capacity of the prototype surge bin is larger than the two smaller ones and, thus, more sediment can be stored.

Now, an incoming concentration profile is generated to simulate the discontinuous production of a CSD, see the left graph in Figure 6-4. The tooth shape is the result of the dredger swinging from left to the right which leads to low production in the corners. Also a difference in the height of the tooth shapes can be distinguished, this is due to the different layers the CSD is cutting. This can best be seen at $t = 1800\ sec$ where the cutter is cleaning up the spill. Spillage is the material that is cut but no sucked up by the dredged pump. After cleaning up the spill, the CSD needs time to replace its spud poles after which it can start all over again. After a certain amount of repositionings the spuds, the CSD needs to relocate the anchors after which the cycle is finished. Relocation of the anchors cannot be seen in the production graph.

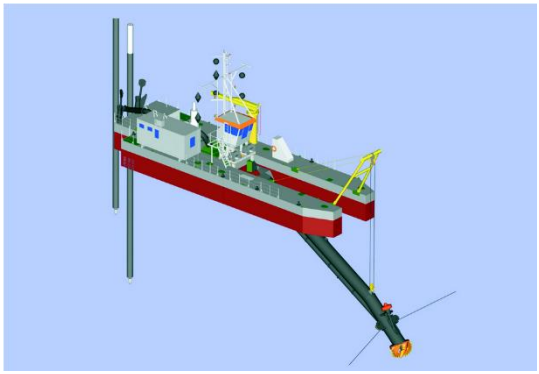

Figure 6-3: Cutter Suction Dredger

The graph on the right in Figure 6-4, shows the outgoing volumetric concentration of the prototype surge bin and the two smaller ones (Medium and Small) in green, blue and red respectively. After an analyses of these three graphs, the following conclusions can be made:

- The three graphs have the same trends, only small deviations can be noticed.
- The dredging of the spill can clearly be seen in the three graphs.
- During the dredging of the spill, the outgoing concentration from the prototype surge bin is slightly higher than Medium and Small.
- Surge bin Small, almost ran out of sediment due to the replacement of the spud poles. However, the difference compared to the other two surge bins is not large.
- The damping is of the same order of magnitude for the three surge bins; no significant differences can be distinguished.

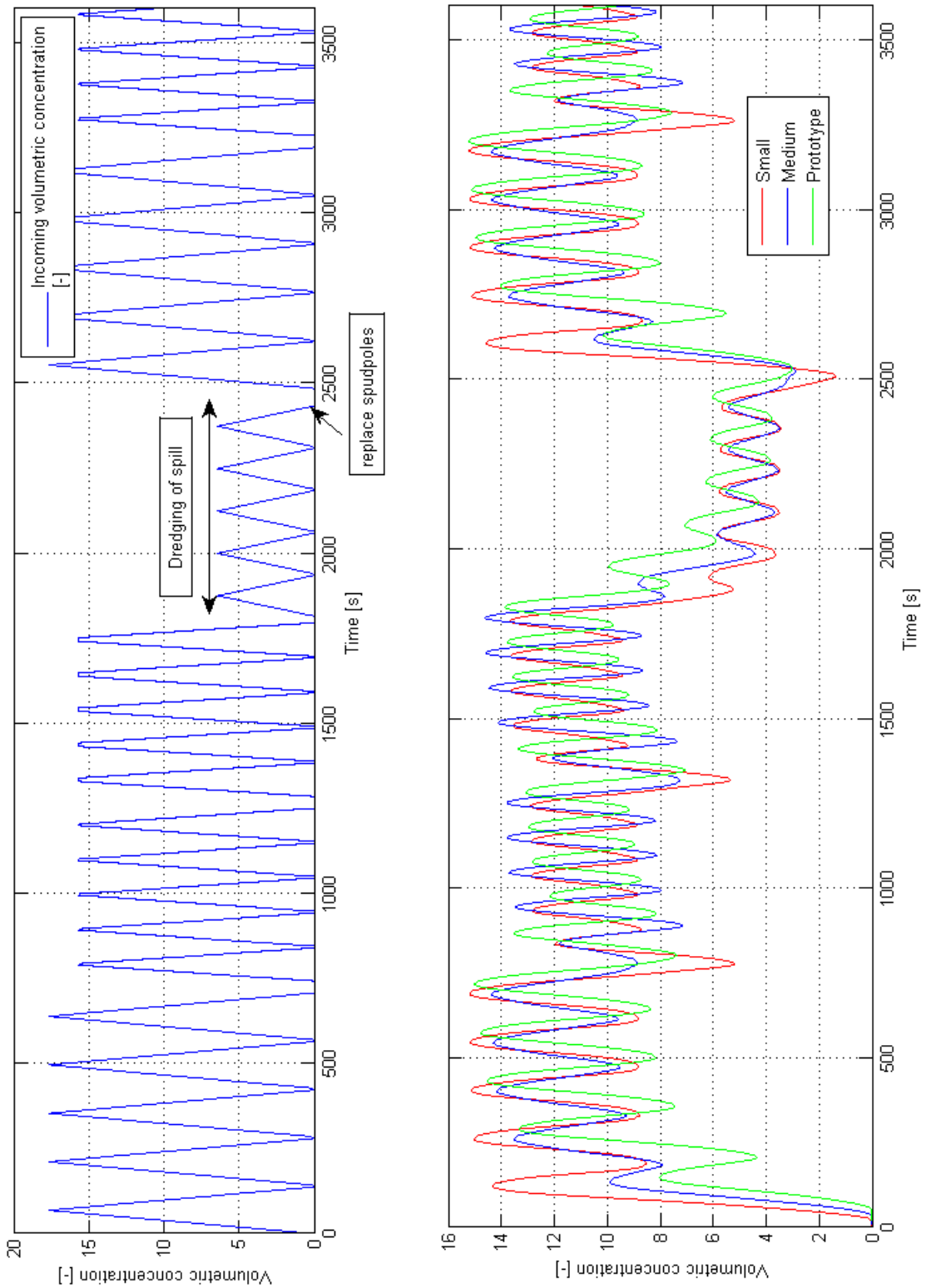

Figure 6-4: Left: Incoming concentration simulating a CSD, Right: Calculated concentration in output of three types of surge bins

From these first analyses, it can be concluded that surge bin Small is very suitable for this situation. However, looking at Table 6-3, the overflow losses of the heavy minerals and slimes can be seen. Here, it becomes clear that surge bin Small, loses up to 53% of the incoming heavy minerals.
Surge bin Medium has a low recovery rate as well, since 40% of the valuables end up in the overflow. On the other hand, it seems that the prototype surge bin works well with only 8% of lost material. It must be noticed that the amount of slimes in the overflow has reduced as well which is not favorable.

Table 6-3: Results of calculated overflow losses of heavy minerals and slimes for three types of surge bins

	Small		**Medium**		**Prototype**	
	Heavy minerals	Slimes	Heavy minerals	Slimes	Heavy minerals	Slimes
Total dry solids in [kg]	170870	100620	170870	100620	170870	100620
Dry solids in overflow [kg]	90448	56057	67737	49037	12920	31435
% Lost	**53%**	56%	**40%**	49%	**8%**	31%

Remark
In practice, the losses of heavy minerals will be lower because here it is assumed that all the heavy minerals have the same diameter as the slimes. When exact PSDs of the dredge locations can be obtained, better predictions of the losses can be made.

6.3 Conclusion

The responses of the three surge bins on the incoming concentration are comparable. Some deviations can be noticed but no significant differences are present. None of the bins has ran out of sediment when the CSD replaced the spud poles, however, surge bin Small almost did. From this point of view, it can be concluded that surge bin Small fulfills all the surge bins' functions and, thus, is favorable in terms of costs (less material). However, looking at the overflow losses, only the prototype surge bin is efficient. Surge bin Small and Medium lose almost half of the valuable heavy minerals due to the high mixture velocity. It can be assumed that efficiency is decisive for a client, especially in the longer term. Therefore, from these simulations the advice would be that the prototype surge bin is the best option.

It is recommended to make more simulations with more specific information such as a more detailed particle size distribution. And, it can be seen that the concentration in the outflow is strongly dependent on the delivered concentration from the CSD. Therefore, more different simulations should be made.

Chapter 7

7. Conclusions and recommendations

This final chapter will provide an overview of the conclusions which can be drawn from the obtained results from experiment and the model. After that, recommendations are given for further improvement of the model.

7.1 Conclusion

A numerical model has been programmed in Matlab which is used to determine volumetric concentration profiles in the outflow of the surge bin, related to certain incoming concentration profiles. The model is called 1.5D because the applied physics are modelled in one dimensions, but the segments can vary in size and volume, meaning that the shape of the surge bin can be implemented.
Sediment propagates through the surge bin, relative to an assumed mixture velocity which is dependent of the inflow, jetflow and outflow. It is assumed that gravitational forces are dominant and, together with the assumed flow velocity within the surge bin, the sedimentation process can be described in vertical direction. Use is made of the Ferguson & Church formula to calculate the terminal settling velocity (Ferguson & Church, 2004) which is subsequently used to determine the hindered settling velocity.

Simple simulations have been carried out first to check its functionality and to look at typical simulation results. Here, it was shown that the surge bin works as a thickener, a damper and a buffer. If the upward flow in the surge bin is high enough, the surge bin also works as a separator because fine particles will end up in the overflow.
Near the inlet- and jet zone of the surge bin, situations could occur that solid particles kept floating because their settling velocity was equal to the upward flow velocity. This led to an increase in volumetric concentration near these zones. This effect was dealt with by introducing a function for the diffusion coefficient.

Experiments have been carried out to examine the surge bin's functions and to validate the 1.5D model. The following conclusions regarding the experiment can be made:

- Heavy fluctuating incoming concentration profiles are damped significantly. E.g. incoming concentrations varying from 0-35% were reduced to outgoing concentration fluctuating from 22% to 30%. When the interval between two consecutive pulses reduces, the fluctuation in the outflow reduces as well.
- The buffer function is proven, because the periods when no sand was inserted, were mitigated by the surge bin. Also, a longer idle time was measured compared to the filling time of the bin.
- The frequency of the pulses can be seen in the outgoing concentration profile.

- When the outflow of the surge bin is reduced compared to the inflow, higher concentrations in the outflow are measured and, thus, the surge bin works as a thickener.
- The variations in the flows and H^* were not large enough to make verdicts based on these parameters.
- Measuring the overflowing concentration did not work out well. Therefore, no verdict can is made on the overflow function of the surge bin.

The following conclusions regarding the validation of the model can be made:

- [redacted]
  Higher values did not lead to better results while lower values do. This value is taken in the validation of the model and furthermore also in the prototype simulations.
- The model results are compared with the measured data (for 24 datasets). R squared values vary from 0.76 up to 0.96, meaning that good predictions can be made.
- For each dataset, the model responds slower compared to the experiment. Measured peak values are lower compared to calculated peak values which might be the result of damping introduced by the model. The variations lay around 5% volumetric concentration.
- For each dataset, the model needs more time to run out of sediment compared to the experimental data. It even appears that this delay is in the order of 20-40 seconds. This is not favorable because it is an important design criterion.

From the prototype simulations, the following conclusions can be made:

In the future, the model can be used to predict the outgoing concentration profiles of a surge bin related to the incoming concentration. From the true scale simulation it appeared that the prototype surge bin QMM has been designed in the correct way because of its efficiency in winning heavy minerals. Smaller surge bins damp out the incoming concentration really well. However, they lose too much valuable heavy minerals in the overflow.

Although an attempt has been made to approach the reality as closely as possible, numerical diffusion is introduced due to the numerical representation of the transport equation. In addition, numerous assumptions have been made and physical phenomena have been simplified or neglected to enable programming. For these reasons, careful use of the 1.5D model is required and critical assessment is recommended.

7.2 Recommendations

Principally, the aim of the numerical 1.5D model is to simulate a truthful representation of reality. To improve the accuracy of the model and to extend the reliability and usability, a list of recommendations for future research is given:

- More information on prototype surge bins should be gathered:
  - Typical values of the concentration measured in the surge bin's outflow and inflow.

    - Values of the amount of jet water which is added.
    - Overflow losses.
- Values should be gathered on the acceptable deviations for the separation plant.
- Prototype measurements (data) should be compared with the calculated results from the model.
- To improve the accuracy of the model, other discretization methods should be applied to reduce the numerical diffusion.
- More research on the determination of K is advisable. Could K be scaled?
- Other approaches to determine the diffusion coefficient should be looked at. One should think of the Prandtl Mixing Length approach.
- Expand the model with a fluctuating jet, or a jet with regulation.
- Expand the model to two dimensions (2D) or three dimensions (3D) to incorporate the "plunging" of the incoming concentration and to see the effect of the jet (mixing).

Recommendations for future experimental tests:

- Implement conical shape of the surge bin.
- Experiment with tests where the inflow equals the outflow.
- Calibrate during testing.
- Make use of larger mixture reservoirs to test the maximum buffer function.
- Use different types of sediment to make verdicts on H^*.
- Measure overflow losses to make verdicts on the separation function.

Bibliography

Arsenijević, Z., Grbavčić, Ž., Garić-Grulović, R., & Bošković-Vragolović, N. (2010). Wall effects on the velocities of a single sphere settling in a stagnant and counter-current fluid and rising in a co-current fluid. *Powder Technology*, 237-242.

Baldock, T., Tomkins, M., Nielsen, P., & Hughes, M. (2004). Settling velocity of sediments at high concentrations. *Coastal Engineering, 51*.

Basson, D., Berres, S., & Bürger, R. (2009). On models of polydisperse sedimentation with particle-size-specific hindered-settling factors. *Applied Mathematical Modelling*, 1815-1835.

Batchelor, G. (1982). Sedimentation in a dilute polydisperse system of interacting spheres. Part 1. General Theory. *J. Fluid Mech. 110*, pp. 379-408.

Berres, S., Bürger, R., & Tory, E. (2005). Applications of polydisperse sedimentation models. *Chemical Engineering Journal, 111*, pp. 105-117.

Boshoff, L. (2011). *QMM Mandena Phase 1 Geotechnical investigation-Final draft report Volume 1 of 3.* SRK Consulting Engineers & scientists.

Brown, P., & Lawler, D. (2003). Sphere Drag and Settling Velocity Revisited. *Journal of Environmental Engineering*, 222-231.

Bürger, R., García, A., Karlsen, K., & Towers, J. (2008). A kinematic model of continuous separation and classification of polydisperse suspensions. *Computers & Chemical Engineering, 32*, pp. 1173–1194.

Chandrakala, K., Gajanan , K., & Mohan , R. (2006). Effect of Operating Parameters on the Performance of Spiral. *Proceedings of the International Seminar on Mineral Processing Technology*, pp. 316 - 319.

Clifford, A. (2008). Sediment Transport Scaling for Physical Models. 1057-1065.

Coastal & Environmental Services. (2002). *Environmental impact assessment Kenmare MOMA Titanium Minerals Project in Mozambique.*

Di Felice, R. (1996). A relationship for the wall effect on the settling velocity of a sphere at any flow regime. *International Journal Multiphase Flow* , Vol.22 527:533.

Equity development. (2011). *Pathfinder Minerals: A tiger by the tail.* Equity Development.

Ettema, R., Arndt, R., Roberts, P., & Wahl, T. (2000). Hydraulic modeling: Concepts and Practice. *ASCE*.

Felice, R. D. (1999). The sedimentation velocity of dilute suspensions of nearly monosized spheres. *International Journal of Multiphase Flow* , 559-574.

Ferguson, R., & Church, M. (2004). A Simple Universal Equation For Grain Settling Velocity. *Journal of Sedimentary Geology, 74*, 933-937.

Garcia, A. (2000). *Numerical Methods for Physics - second edition.* Prentice Hall.

Garside, J., & Al-Dibouni, M. (1977). Velocity-Voidage Relationships for Fluidization and Sedimentation in Solid-Liquid Systems. *Department of Chemical Engineering*, 206-214.

Heavy minerals. (2013, 12). Retrieved 12 2014, from www.pir.sa.gov.au: http://www.pir.sa.gov.au/minerals/geological_survey_of_sa/commodities/heavy_minerals

Hirsch, C. (2007). *Numerical computation of internal & external flows Volume 1 - Fundamentals of Computational Fluid Dynamics second edition* . John Wiley & Sons .

Klerk, A. d., & Kranenburg, C. (1998). *Bezinken van zand in hopperzuigers, invloed van turbulentie en korrelverdeling. Master's thesis, Delft University of Technology, faculty of CiTG.*

Manninen, M., Taivassalo , V., & Kallio, S. (1996). On the mixture model for multiphase flow. *Valtion teknillinen tutkimuskeskus (VTT).*

Masliyah, J. (1979). Hindered settling in a mulit-species particle system . *Chemical Engineering Science, 34*, pp. 1166-1168.

Matoušek, V. (2004). *Dredge pumps and slurry transport.*

Miedema, S. (2012). *Dredging Processes - The Cutting of Sand, Clay & Rock – Theory.*

Miedema, S. (2012). *Dredging Processes The Loading Process of a Trailing Suction Hopper Dredge.*

Mirza, S., & Richardson, J. (1979). Sedimentation of suspensions of particles of two or more sizes. *Chemical Engineering Science, 34*.

Moore, P. (2011). Heavy Minerals. *International Mining*, 60-68.

Mular, A., Halbe, D., & Barrat, D. (2002). *Mineral Processing Plant - Proceedings Volume 1.* Colorado: SME.

Pietrzak, J. (2011). *An introduction to Oceanography for civil and offshore engineers.*

Rhee, C. v. (2002). *On the sedimentation process in a Trailing Suction Hopper Dredger.* Delft University of Technology.

Rhee, C. v. (2011). One dimensional sedimentation of multi-sized particles. *In 15th Transport and Sedimentation, Wroclaw, Poland*, pp. 157 – 168.

Richardson, J., & Zaki, W. (1954). Sedimentation and fluidization Part 1. *Transactions of the Institution of Chemical Engineers, 32*.

Richardson, J., & Zaki, W. (1954). The Sedimentation of a suspension of uniform spheres under conditions of viscous flow.

Rijn, L. V., Tonnon, P., Sánchez-Arcilla, A., Cáceres, I., & Grüne, J. (2011). *Scaling laws for beach and dune erosion processes.*

Rowe, P. (1987, May). A convenient empirical equation for estimation of the Richardson Zaki exponent. *Chemical Engineering Science*, pp. Vol. 42: 2795-2796.

Runge, A., Ruijg, B., Rhee, C. v., & Schrieck, G. v. (1999). Eendimensionale beschouwing van de bezinking van hooggeconcentreerde zandwatermengsels onder turbulente omstandigheden.

Slaa, S. t., Maren, S. v., & Winterwerp, J. (2012). On the hindered settling of silt water mixtures.

Turton, A., & Levenspiel, O. (1986, February 5). A Short Note on the Drag Correlation for. *Chemical Engineering*, pp. 83-86.

TZMI. (2013). *Introduction to the titanium and zircon value chains.* Victoria Park: TZ Minerals International Pty Ltd.

Veld , M. i. (2014). *Supply demand of a seperation plant.* IHC Mining.

Veld, M. i. (2014). *Surge bins at IHC sites.* IHC Mining.

Versteeg, H., & Malalasekera, W. (1995). *An introduction to computational fluid dynamics. The finite volume method.* Longman Scientific & Technical.

Wijk, J. v., Rhee, C. v., & Talmon, A. (2014). Wall friction of coarse grained sediment plugs transported in a water flow through a vertical pipe. *Ocean Engineering*.

Appendix A: Additional information

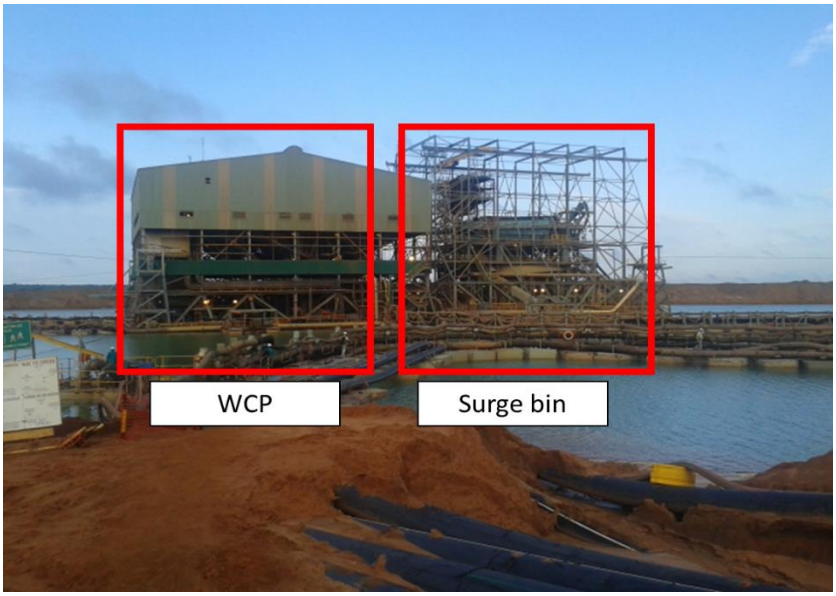

Figure A-1: Wet concentrator plant (left) and surge bin (right) in Mozambique

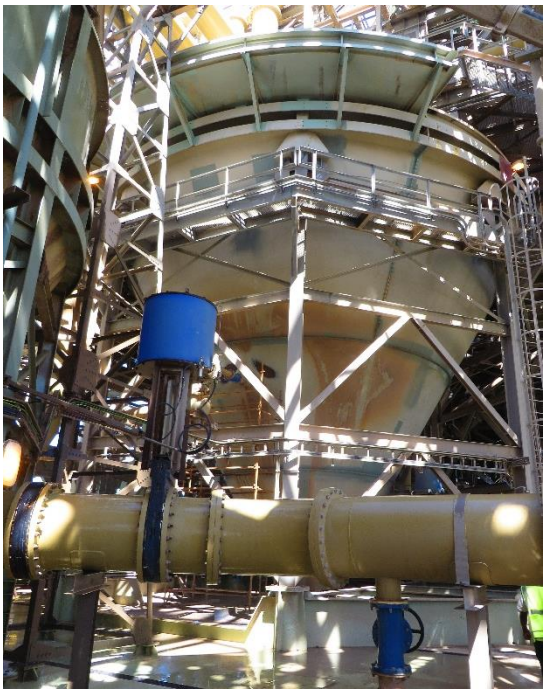

Figure A-2: Surge bin Mozambique

Graph of Ferguson & Church

Below, a graph is presented with the settling velocities calculated with the Ferguson & Church formula.

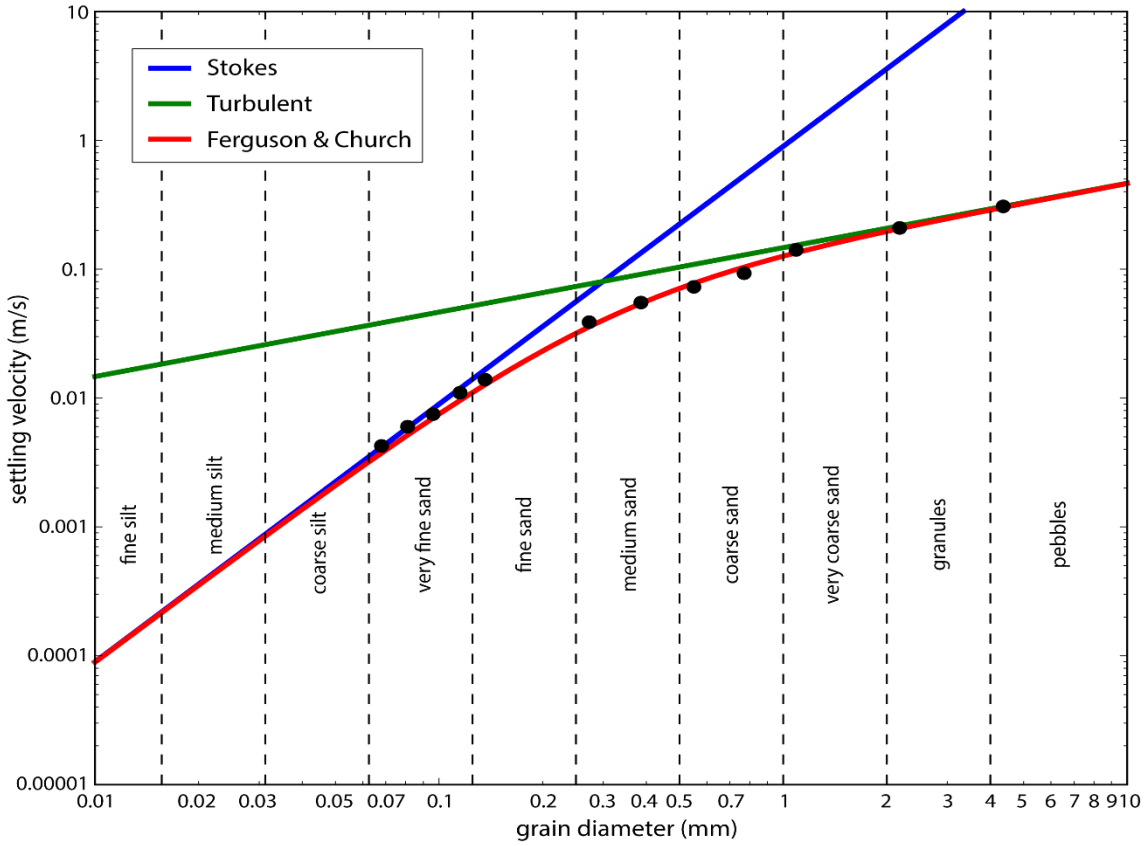

Figure A-3 Settling velocities according to Ferguson and Church , Graph is taken from www.hinderedsettling.com

Discretization:

As mentioned in the main report, the fluxes could be described through the faces of the cells. This discretization is presented below.

$$\phi_i^{n+1} = \phi_i^n + \Delta t(F_{i+1}^n + F_{i-1}^n - F_i^n) \tag{A.1}$$

The equation above describes the change in volumetric due to the fluxes that enter and leave the cell. Three fluxes can be distinguished within the brackets. The first term is the flux of sediment which enters cell i and is the amount of sediment which leaves cell $i+1$. The same holds for the second term, but then the flux comes from cell $i-1$. The last term is the amount of sand that leaves the cell itself.
Now, the fluxes can be described as follow:

$$F_i^n = \begin{cases} \frac{A_i^s}{V} v_{s,i}\phi_i & if \quad v_{s,i} > 0 \\ \frac{A_i^n}{V} v_{s,i}\phi_i & if \quad v_{s,i} < 0 \end{cases} \tag{A.2}$$

$$F_{i+1}^n = \begin{cases} \frac{A_i^n}{V} v_{s,i+1}\phi_{i+1} & if \quad v_{s,i+1} > 0 \\ 0 & if \quad v_{s,i+1} < 0 \end{cases} \tag{A.3}$$

$$F_{i-1}^n = \begin{cases} \frac{A_i^s}{V} v_{s,i-1}\phi_{i-1} & if \quad v_{s,i-1} < 0 \\ 0 & if \quad v_{s,i-1} > 0 \end{cases} \tag{A.4}$$

It can be seen here that the fluxes go to the area of the faces, compared to the method used in chapter 3. The cell face A_i^n of cell i is the same as cell face A_{i+1}^s making the physical interpretation more logical.

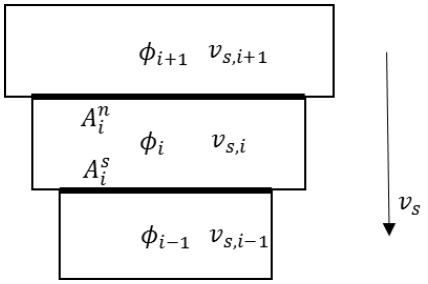

Figure A-4: Advection through cells

Appendix B: Explanatory statements on calibration and experiment

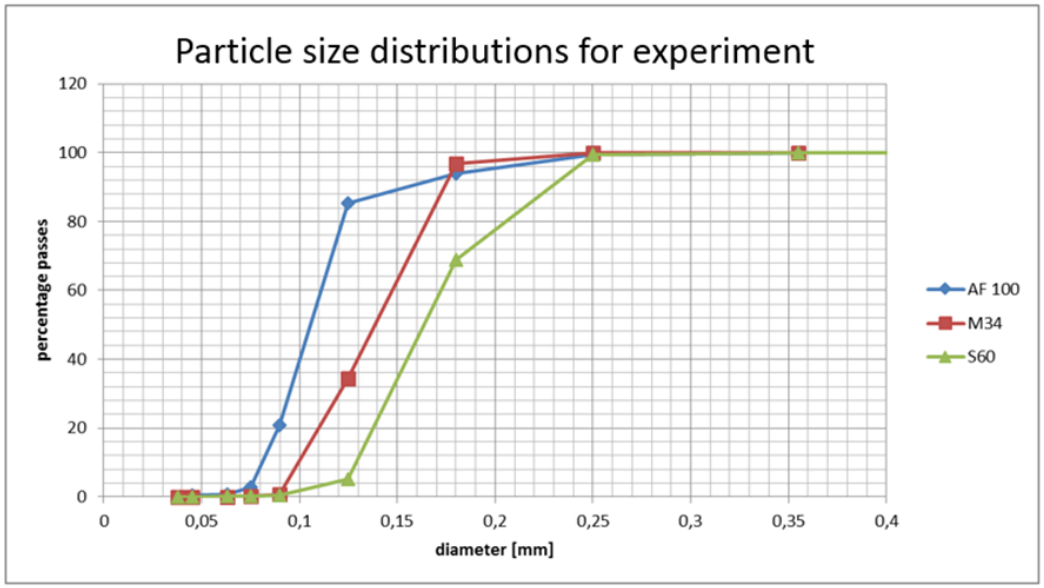

Figure B-1: PSD of 3 different types of sand for experiment

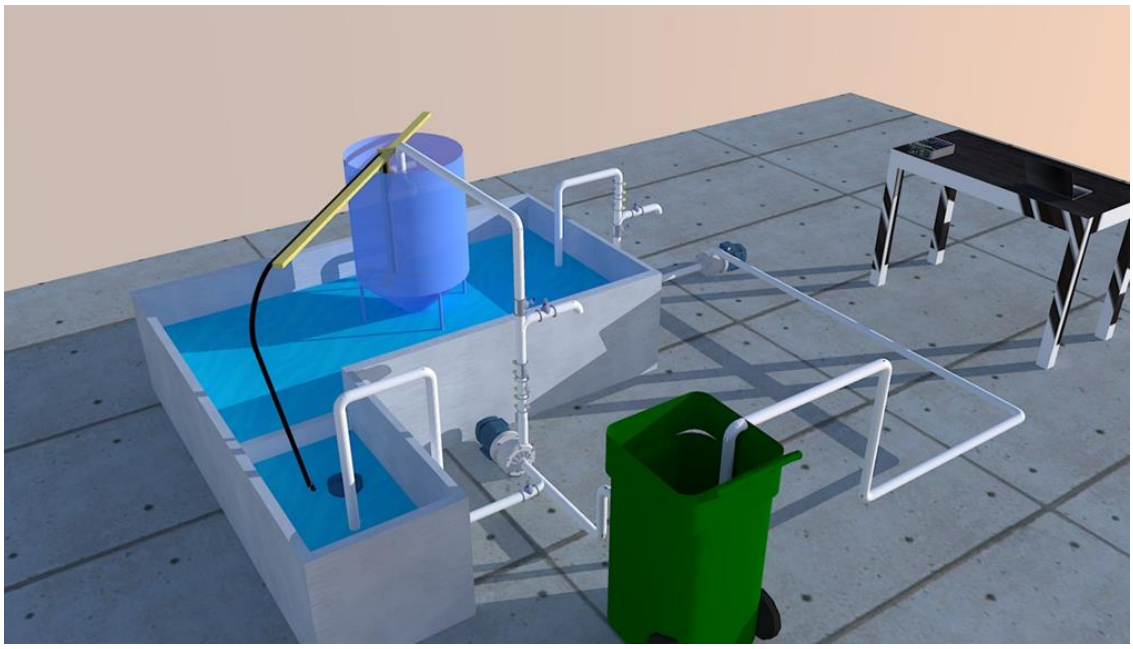

Figure B-2: Artist impression of experimental setup

Calibration setup

The different types of sensors that are used in experiment setup are elaborated in this Appendix. The calibration of the sensors plays an important part of the experiment because the correctness of the logged data is dependent of it. Information on how the sensors work and how they are calibrated is explained and elaborated in the upcoming chapter.

In the picture below, an overview is given of the calibration setup. This small loop consists of high pressure uPVC pipes with an internal diameter of 46mm. In this circuit, five sensors are placed:

- 2x CCM
- 2x Flowsensor
- 1x temperature sensor

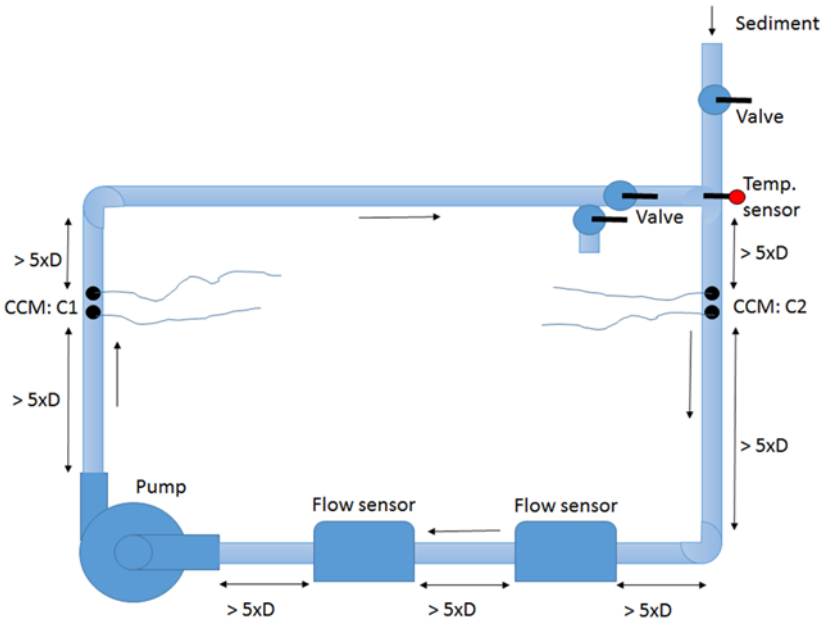

Figure B-3: Visualization of test loop

Between all bends, sensors and the pump, a minimal distance of 5 times the internal diameter is retained. The sediment which is pumped through the slurry loop, consists of very fine sand of which the PSD can be found in Figure B-1. Because the sediment is that fine, it will distribute itself homogeneously over the cross-section of the pipe if the mixture velocity is at about two times the limit deposit velocity. Secondly, the concentration sensors (CCMs) are placed in a vertical direction so that differences in the density concentration profile are minimized.

At the top right of the loop, a valve is placed. Through this valve, sediment can be inserted into the loop and different mixture densities can be obtained. Below the valve, a thermometer measures the temperature of the mixture. Because the volume of the loop is relatively small, it will heat up due to the presence of the pump.

The measuring method of the CCM is sensitive to temperature variations and mineral content of the carrier fluid, because these affect the conductivity of the carrier fluid.

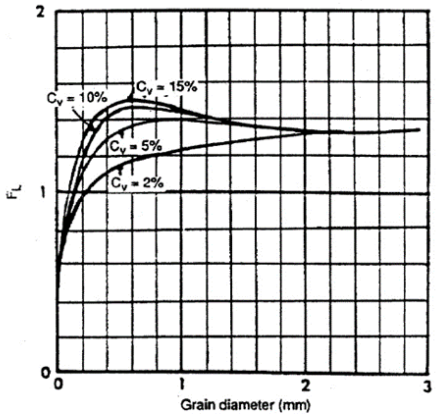

Figure B-4: Modified Froude number for the determination of the Deposit Limit Velocity according to Durand et. Al model (graph taken from Matousek).

$$V_{dl} = F_L\sqrt{2g(S_s - 1)d} \tag{B.1}$$

The formula presented above is used to determine the deposit limit velocity of the sand. In this formula:

- F_L is the modified Froude number. The highest value of the graph is taken: F_L=1.5
- d is the grain diameter in mm
- S_s is the relative density of the sediment

Solving this equation leads to a deposit limit velocity of 1.5 m/s and, thus, the mixture velocity is set to 3 m/s.

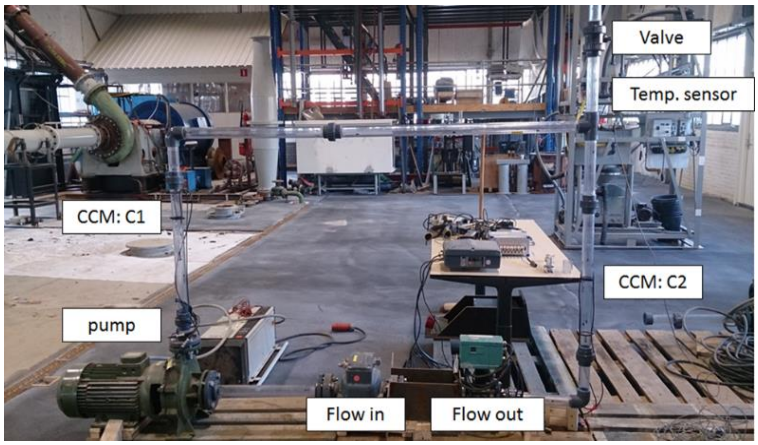

Figure B-5: picture of calibration loop

Density sensors: CCM

The technique used for these instruments is to measure the electrical resistance of the mixture. This technique has the potential to measure the amount of sand in pipelines. Fundamentally, the method measures the electrical conductivity of the sand-slurry across the pipe. Since sand is non-conductive, the concentration can be calculated from the measured conductivity. The measuring method is sensitive to temperature variations and mineral content of the carrier fluid, because these affect the conductivity of the carrier fluid. Furthermore, the technique is not influenced by pressure, flow velocity or other variations.

To measure the concentration of sand in the pipes, so called CCMs (conductivity concentration measurement) are used. The principle of the used technique is quite logical to understand. Two titanium screws are placed (at about 1 cm of each other) in the pipeline, in such a way that the tips are going fully through the wall. When measuring the electrical current that goes through the two points, the mixture density can be derived because the amount of sand will disturb the conductivity of the carrier fluid.
In the picture below, the two titanium screws can be identified. To be sure that the electrical current goes through the inner side of the pipe, the screws are sealed with a special silicon layer.

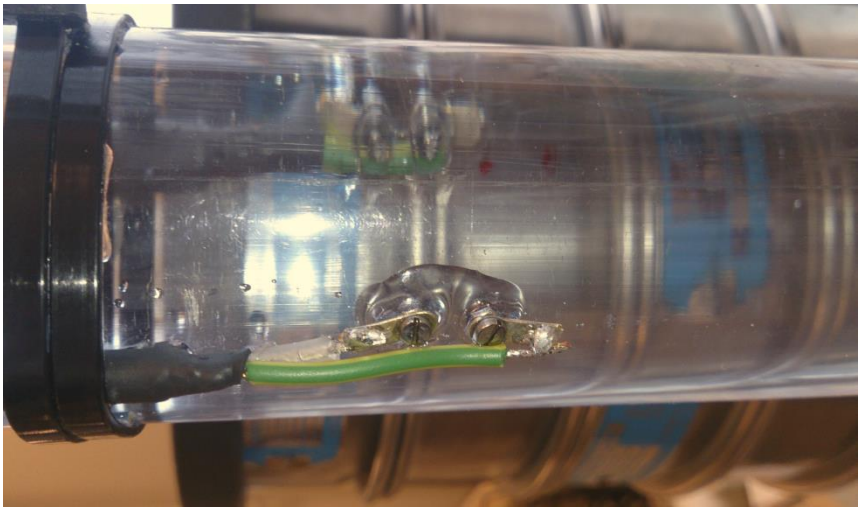

Figure B-6: CCM installed in pipelines

The CCM which is used to measure the inflowing concentration the surge bin, is indicated by "C1". The conductivity is measured on two sides of the pipe as can be seen in the photograph above. The couple of screws will be named as C1.1 and C1.2 because they will be calibrated individually.
The same holds for the CCMs which will measure the concentration in the output of the surge bin. The CCM is indicated with C2 and the couples of screws are marked C2.1 and C2.2.
The CCM sensors are installed by Deltares. Because the distance between the two titanium screws is not "100% exactly" equal, the measured conductivity will be different for each sensor.

The CCMs are in turn connected to the GCM which collects and amplifies the signals from the different CCMs. With the "Range" button, the amplification of the signal can be adjusted. The GCM is on its turn connected with a data logger and a computer. The output signals of the GCM are measured in mV and stored on the computer via Dewesoft dataloggers.

To determine the mixture density in the surge bin itself, use is made of CCM poles. The poles are using the same conductivity technique as the CCMs in the pipes, the only difference is that a pole consists of multiple couples on a row.

The poles are placed in a vertical way in the surge bin in a way that the concentration over the height can be measured. Unfortunately, a decision has to be made about the locations in surge bin which need to be measured, because the channels on the data loggers are limited. In the pictures below a visualization and a real picture of the probes can be seen.

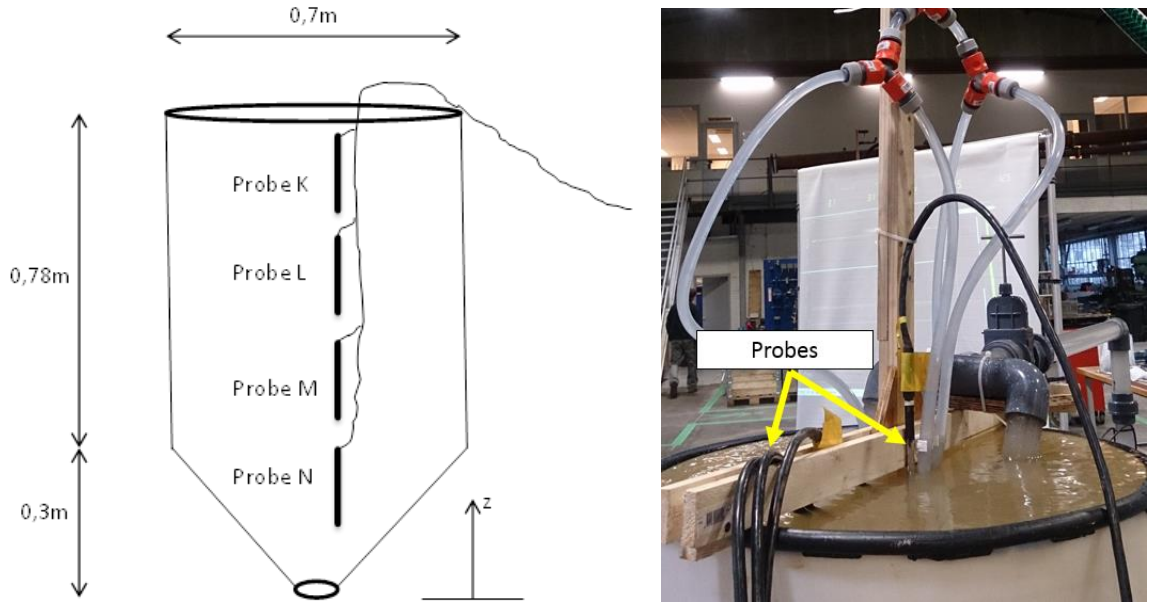

Figure B-7: Installed probes in the surge bin, visualization (left) and picture (right)

Flow sensors

The flow sensors which are used have been rented from Deltares and the Delft Technical University. Both sensors are capable to measure slurry flows. The flow sensors used, make use of electromagnetic induction of which the exact working principle is beyond the scope of this thesis. However, a brief explanation of the working principle is that in the sensor, a magnetic field is created and channeled into the fluid which is flowing through the pipe. The flow of the conductive liquid through the magnetic field will generate a voltage signal which is sensed by conductive sensors placed inside. When the fluid moves faster, a higher voltage is generated which can be translated into the mixture velocity. Because the diameter of the pipe is known, the flow can be determined as a result. In the calibration loop they are placed one after each other to check whether they deliver the same results. In the experiment setup, the Deltares flow meter is used to measure the incoming flow, while the TU Delft flow sensor is used to measure the outgoing flow.

A Real Transit Time sensor from MTI Measurements&Diagnostics is used to calibrate the flow meters. During the calibration tests, the Real Transit Time sensor is monitored and possible variations of the flow sensors can be distinguished.

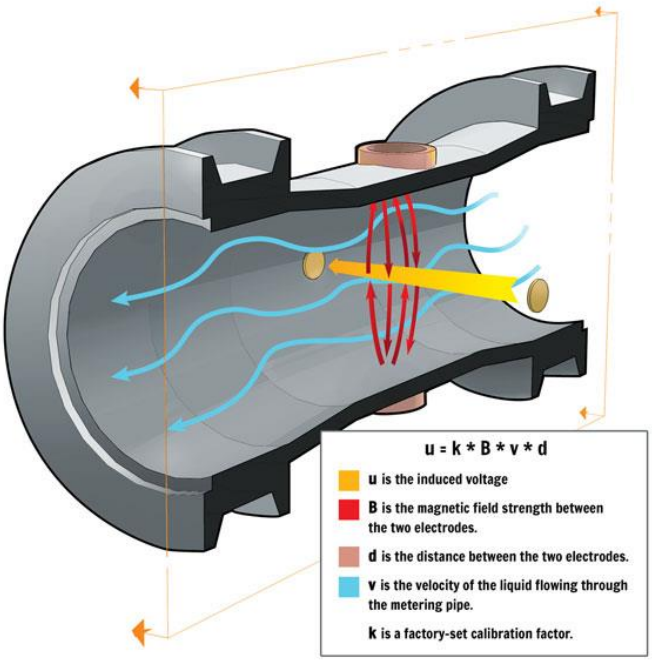

Figure B-8: working principle of magnetic flow sensor

The flow sensor from the TU Delft is limited to measure a maximum flow of 5 liters per second. This value equals an average flow velocity of 3 m/s. The sensor has 20% tolerance so peak values of 6 liters per second can be measured. The sensor will give an "overload error" if the flow exceeds the 6 liter per second value. If this maximum value is exceeded no data will be stored.

The inflow is measured with a Foxboro flow sensor from Deltares. During calibration tests it became clear that this sensor reacts much faster on flow fluctuations than the Flowtec Variomag. Because the experiment will be executed with constant flows, the delayed response of the sensor is not of importance.

Figure B -9: Flowtec Variomag left and Foxboro flow sensor right

The calibration of the jet is done during the experiment itself and not in the calibration setup. Jet water is pumped from the overflow basin into the surge bin by a submersible pump. In contrast to the centrifugal pumps, the flow of a submersible pump is hard to regulate since it only has an on/off tap. To determine the

flow, the jet pump was turned on while the outflow of the surge bin was closed. Since no flow meter is installed, the flow is determined by measuring the time needed to fill a bucket of 20 liter. This process is executed 5 times after which the average value is determined. This process is executed each time when the jetflow had to be adjusted. The results of the maximum jetflow are shown in Table B-1.

Table B-1: determination of the maximum jetflow

	Test 1	Test 2	Test 3	Test 4	Test 5	Average
Volume bucket (liter)	20	20	20	20	20	
Time (sec)	57	58	59	59	58	
Flow liter/sec	0.35	0.34	0.34	0.34	0.34	0.34

The average value of 0.34 liter per second is the maximum flow of the jet. A ball valve is installed so the flow can be reduced, however, a ball valve is not the most appropriate valve to regulate the flow. A more convenient way to regulate the flow was to install a gate valve and, to measure the flow, to install a flow sensor on the jet hose.

Calibration of the CCMs

Calibrations tests have been executed twice during the experiment. Once before the experiment and once after. The reason for the second calibration test was that process water could be used from the experiment. Furthermore, the temperature of the water during the experiment was known since it varied from $13 - 15.5$ degrees Celcius. Therefore the second calibration tests could be executed within this temperature range.

As described in the previous paragraph, the results CCMs are influenced by mineral contents in the carrier fluid (ions) and temperature deviations. The increase of ions in the carrier fluid is the result of dissolved salt particles that are present in the M34 sand, but also by dissolved metal ions from the pump impellers and rust of the metal overflow basin.
Therefore, process water of the experiment is used for the calibration of the sensors. In the steps below, the procedure that is followed for the calibration of the CCMs is explained.

1. The calibration loop is filled with process water from the experiment.
2. A certain amount of dry sand is added. The amount of sand corresponds with a certain volumetric concentration. In total, seven calibrations tests are executed: 0%, 5%, 10%, 15%, 20%, 25% and 35% of volumetric concentrations.
3. The mixture is pumped through the loop with an average flow velocity of 3m/s to achieve a homogeneous mixture.
4. The conductivity and the temperature are logged.
5. After logging the process water (with increased ions because of the added sand) is collected so it can be compared with the reference process water.
6. The conductivity of this “new” process is measured.
7. Step 1 is repeated with another amount of sand.

The amount of sand for a certain volumetric concentration is determined with the following formula:

$$Amount\ of\ sand\ = C_v * V_{testloop} * \rho_{sand} \quad \text{(B.2)}$$

Where:

- $Amount\ of\ sand$ is in $[kg]$
- $V_{testloop}$ is the volume of the calibration loop and is equal to 11.3 liters
- ρ_{sand} is density of sand $= 2.65\ kg/dm^3$
- C_v is the volumetric concentration

The underlying thought behind step 6 is that the amount of ions in the process water will increase because dry sand is added. Subsequently, extra ions will dissolve in the water which will affect the conductivity. When the conductivity of the water is measured, it can be compared with the original conductivity of the process water.

Calibration results

The software which is used for the data logging is Dewesoft which processes all the incoming signals and stores them in predefined files. In the graphs below, the logged information for each volumetric concentration $(0\%, 5\%, 10\%, 15\%, 20\%, 25\%, 35\%)$ is plotted for each sensor.

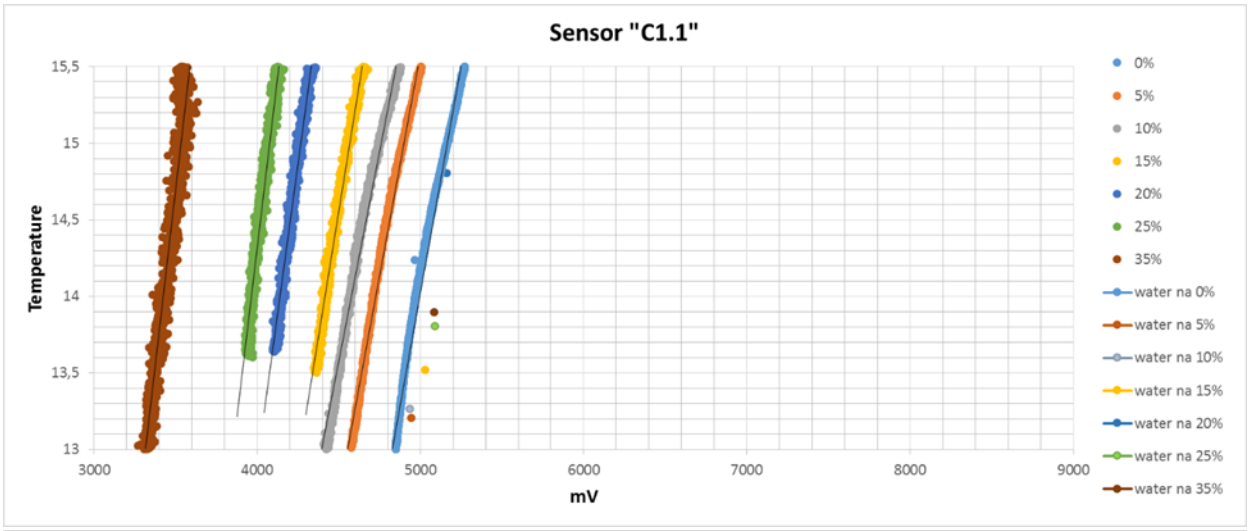
Sensor "C1.1"
Temperature
15,5
15
14,5
14
13,5
13
3000
4000
5000
6000
7000
8000
9000
mV
0%
5%
10%
15%
20%
25%
35%
water na 0%
water na 5%
water na 10%
water na 15%
water na 20%
water na 25%
water na 35%

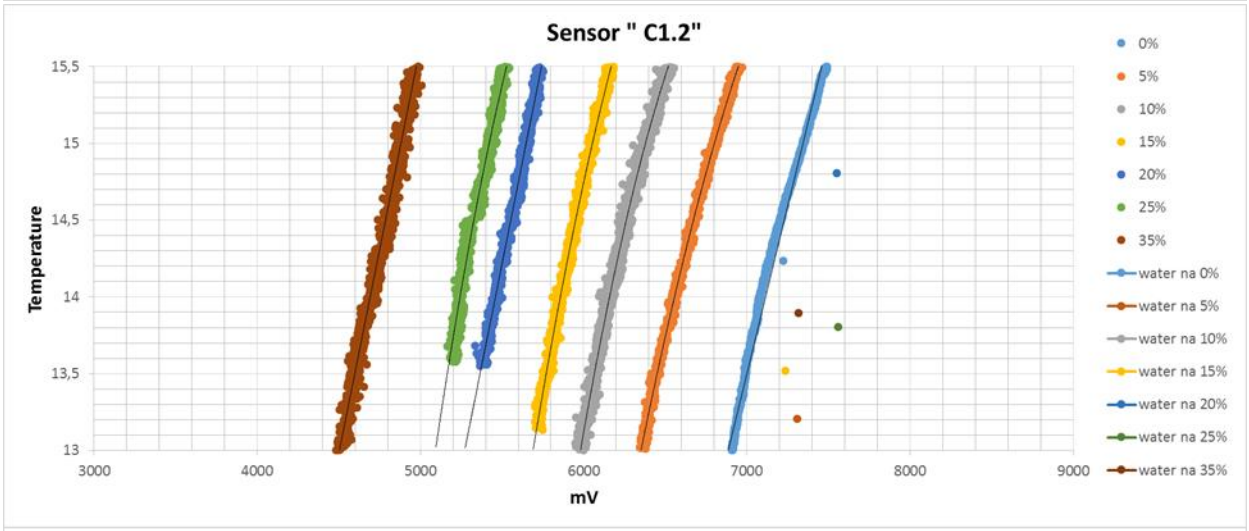
Sensor " C1.2"
Temperature
15,5
15
14,5
14
13,5
13
3000
4000
5000
6000
7000
8000
9000
mV
0%
5%
10%
15%
20%
25%
35%
water na 0%
water na 5%
water na 10%
water na 15%
water na 20%
water na 25%
water na 35%

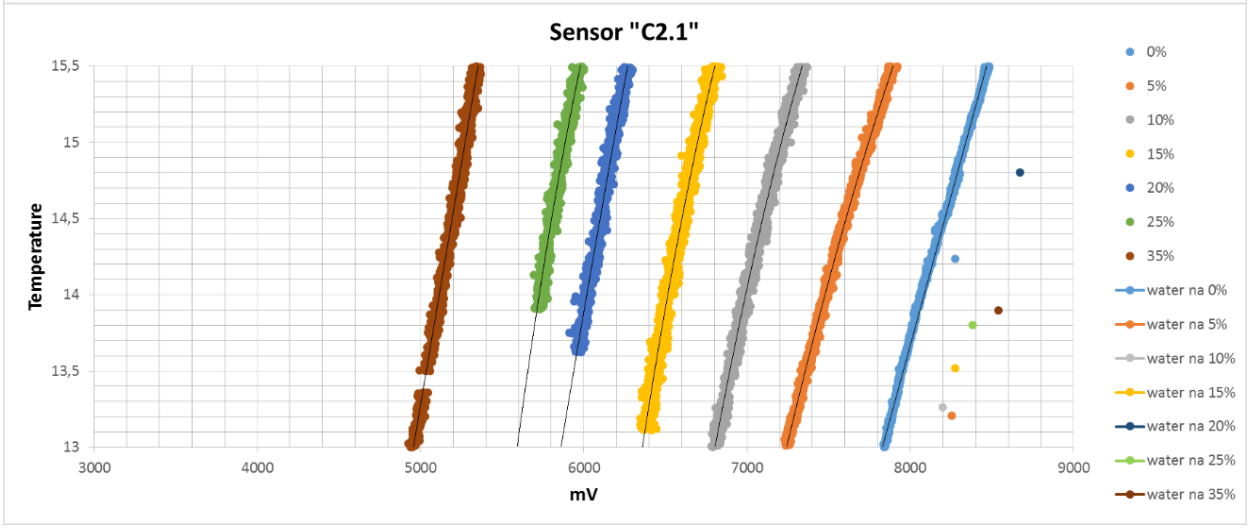
Sensor "C2.1"
Temperature
15,5
15
14,5
14
13,5
13
3000
4000
5000
6000
7000
8000
9000
mV
0%
5%
10%
15%
20%
25%
35%
water na 0%
water na 5%
water na 10%
water na 15%
water na 20%
water na 25%
water na 35%

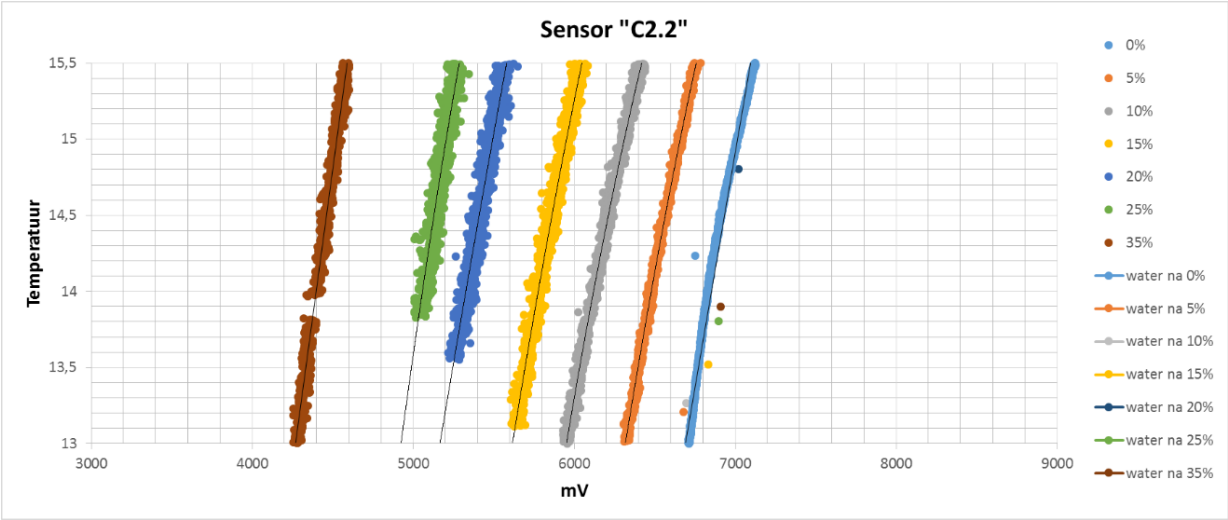

Figure B-10: 4 graphs showing the results of the calibration for the 4 CCM 's placed in the pipes

In these graphs, the measured electric potential difference (in millivolts) is plotted on the horizontal axis against the temperature (in degrees Celsius) on the vertical axis. The different dots which are plotted are the values measured from the water as described in step 6 of this chapter and the values can be seen in Table B-2.

Table B-2: Results of the conductivity of water before and after the calibration

	C1.1 mV	C1.2 mV	C2.1 mV	C2.2 mV	Temp degC
Water 0%	4966	7225	8274	6751	14.2
	5013	7138	8133	6646	
Difference	-46	87	142	105	
water 5%	4942	7307	8252	6678	13.2
processwater	4870	6941	7887	6517	
Difference	72	366	365	161	
Water 10%	4937	7308	8199	6697	13.3
processwater	4876	6949	7897	6521	
Difference	61	359	303	176	
Water 15%	5028	7236	8274	6832	13.5
processwater	4904	6993	7950	6550	
Difference	124	244	324	282	
Water 20%	5162	7550	8670	7020	14.8
processwater	5120	7290	8287	6751	
Difference	42	260	383	269	
Water 25%	5091	7561	8381	6897	13.8
processwater	4942	7047	8021	6584	
Difference	149	513	361	312	
Water 35%	5086	7316	8539	6910	13.9
processwater	5013	7138	8033	6596	
Difference	73	178	507	314	

Knowing that the conductivity of the water increases when the amount of ions increases, it was expected that this relation became visible after a data analyses. However, when analyzing the results above, this relation is not true for every sensor.

For example:
Looking at differences between the conductivity of the water (25% and 35%) of sensor C1.2 and C2.1:

Sensor C1.2 measures a higher conductivity of the 25% water compared to 35% water while sensor C2.1 shows an increase (which was expected).

These "unlogical" results, could be explained by several arguments such as:

- The water was not stirred well enough.
- Very fine particles settled on a titanium screw and influenced the conductivity.
- A very small air bubble between the titanium screws influenced the conductivity.
- The amount of salt and impurities in each sandbag is not identical.

Because of the unexpected results as described above, it has been decided not to correct the measured datasets but to keep them as they are. However, it should be kept in mind that deviations are present in the measurements. The maximum deviation is in the order of 7.5% volumetric concentration.

Table B-3: Deviations measured on the correction of water

Sensor	Largest correction of water [mV]	Average increase mV per 1% C_v	Maximum deviation [% C_v]
C1.1	149	44	3.3
C1.2	513	69	7.5
C2.1	507	84	6.0
C2.2	314	70	4.5

Generated formulas:
Now, from the datasets, formulas are created so the volumetric concentration can be calculated as a function of the measured temperature and potential difference (conductivity).

$$C_v = f(T, V) \tag{B.3}$$

In the next chapters use is made of the standard deviation. The standard deviation is a measure of how spread out numbers are and is calculated by taking the square root of the variance:

$$\sigma = \sqrt{\frac{\sum(x_i - \bar{x})^2}{n_x}} \tag{B.4}$$

Where n_x is the amount of numbers in the dataset and $\bar{x}$ is the average value of the dataset.
First, a function is created for the temperature. Looking at the graphs it can be seen that the best fit through each concentration (each color), would be an exponential function. However, in the graphs it can be seen that the black linear line gives a good fit as well. The standard deviation found in the temperature range (from 13 to 15,5 degrees Celsius) has a maximum 2,2% volumetric concentration.

Table B-4: Deviations measured in the temperature range from 13 – 15.5 degrees

Sensor	Standard deviation σ [mV]	Average increase mV per 1% C_v	Deviation [% C_v]
C1.1	86	44	1.9
C1.2	154	69	2.2
C2.1	130	84	1.5
C2.2	107	70	1.5

To create the formula for the concentration, the influence of the temperature is taken as a linear function. The slope of this function is taken as the average value of the linear function of the 0% and 35% datasets. In addition the function goes through the 14 degrees Celcius point of the corresponding concentration.

Example given: for sensor C2.1 the increase of conductivity per degree Celcius becomes 195mV. This is the average of the slopes of 0% and 35%. This value will be used further to explain the final equation.

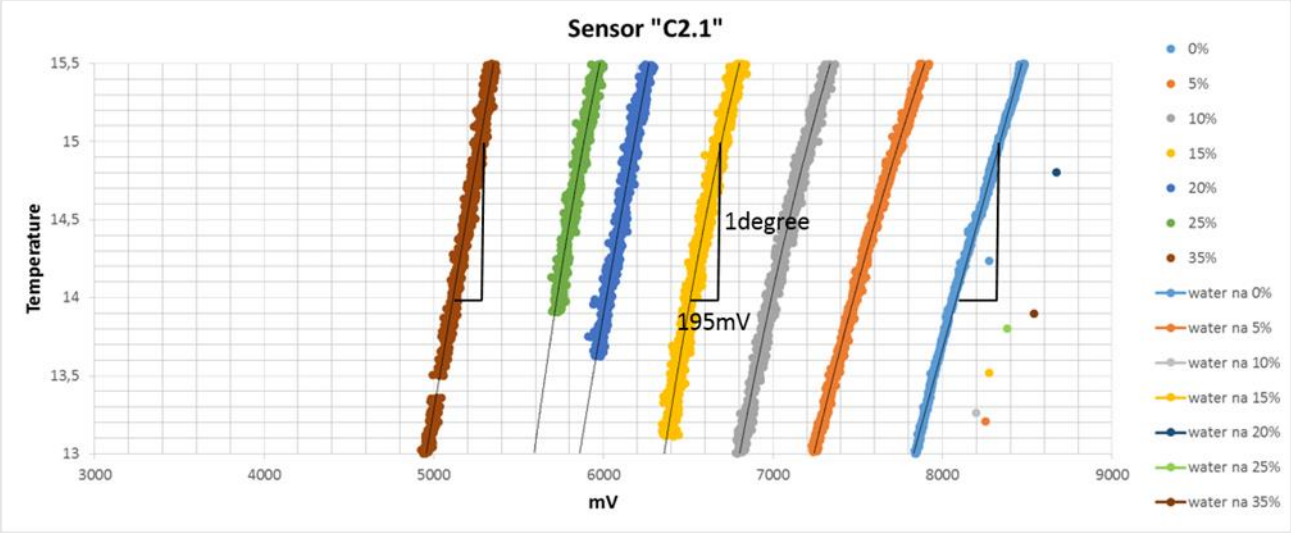

Figure B-11: Increase of conductivity due to temperature increase

Potential difference

Now, a function has to be created which relates the measured millivolts to a certain volumetric concentration. For simplicity of this report, the steps taken are only elaborated for 1 sensor.

Elaboration sensor C1.2:

So far, the measured datasets are linearized in such a way that they have the same slope and, thus, are parallel. Now, a function will be created that can calculate the values in between the measured datasets. If the intersections of the linearized equations with y=14 are plotted, Figure B-12 is obtained.

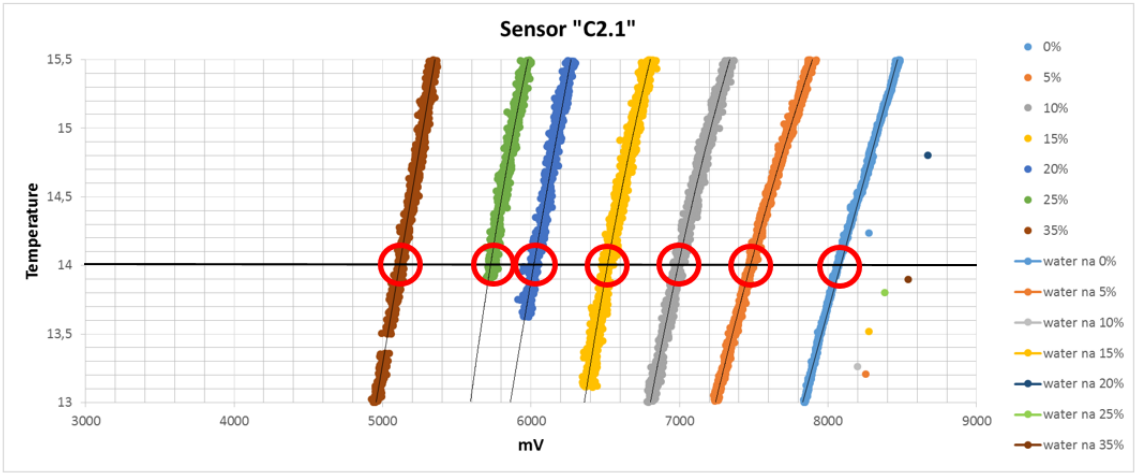

Figure B-12: Intersections at 14 degrees Celcius

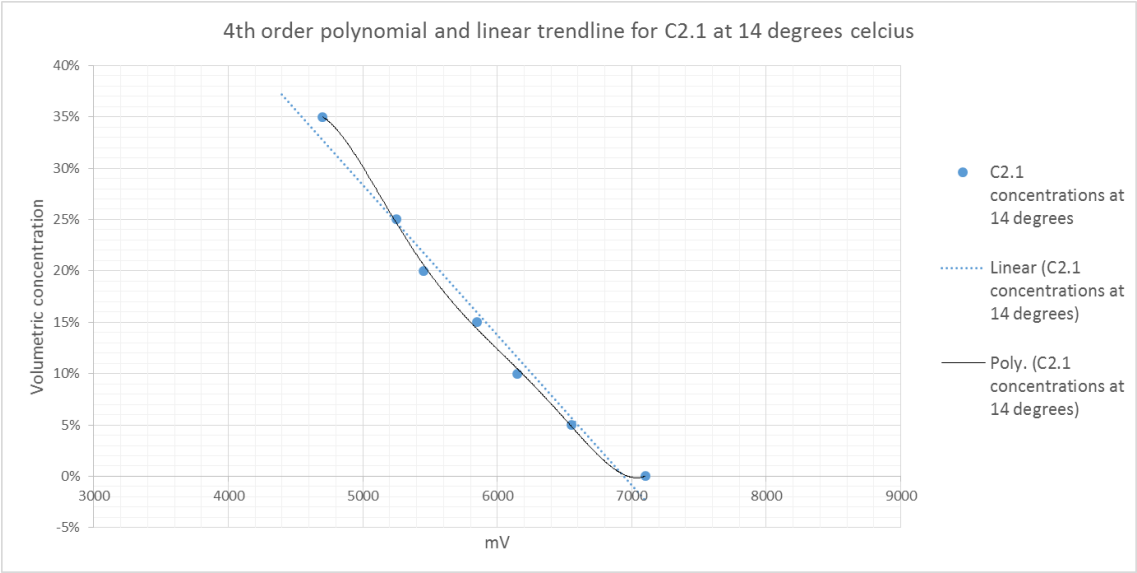

Figure B-13: Functions to determine the concentration: High order polynomial and linear function

In Figure B-13, the plotted dots are the intersections of the colored lines in Figure B-12 with y=14. High order polynomial functions have been generated to create functions that fit the plotted dots best. For sensor C2.1, it can be seen that the fourth order polynomial approaches the dots very well. However, these polynomials generate good values for interpolations, but for extrapolation the function is not desirable. In addition to the polynomial, a linear function is plotted as well and seems to approximate the dots pretty well. Small deviations seem to be encountered.

For each sensor, higher order polynomial functions are generated because from a theoretical point of view, these will give the best results as they approach the measured values better than the linearized equations. Nevertheless, it seems that when these polynomial functions are used in Dewesoft, large deviations are encountered and mass balances differ way too much.

When the linearized functions are used, these differences are reduced significantly the mass balances are better maintained. These arguments are decisive to use the linearized equations.

For sensor C2.1 the linear equation is given by:

$$y = -0{,}000111163810991878x + 0{,}870814523710712 \quad \text{(B.5)}$$

Where y represent the volumetric concentration and x is the measured conductivity. As mentioned previously, a correction has to be made depending on the measured temperature. Therefore this equation becomes:

$$y = -0.000111163810991878 * (x + (14 - T_{measured}) * 195) + 0.870814523710712 \quad \text{(B.6)}$$

Scatter plots

To check whether the generated formulas fit the raw data, a scatter plot for each sensor is made. This scatter plot should be interpreted the following way: on the x-axis the exact volumetric concentration. On the y-axis, the results are plotted from the formula which solves the raw data.

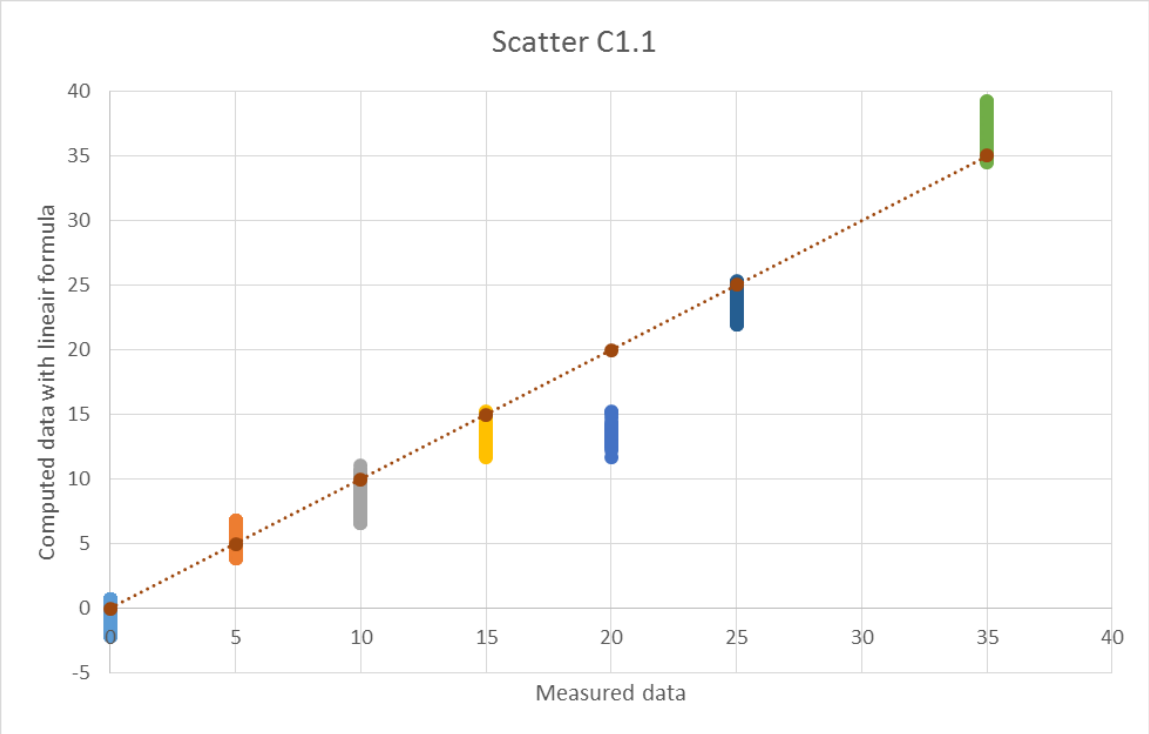

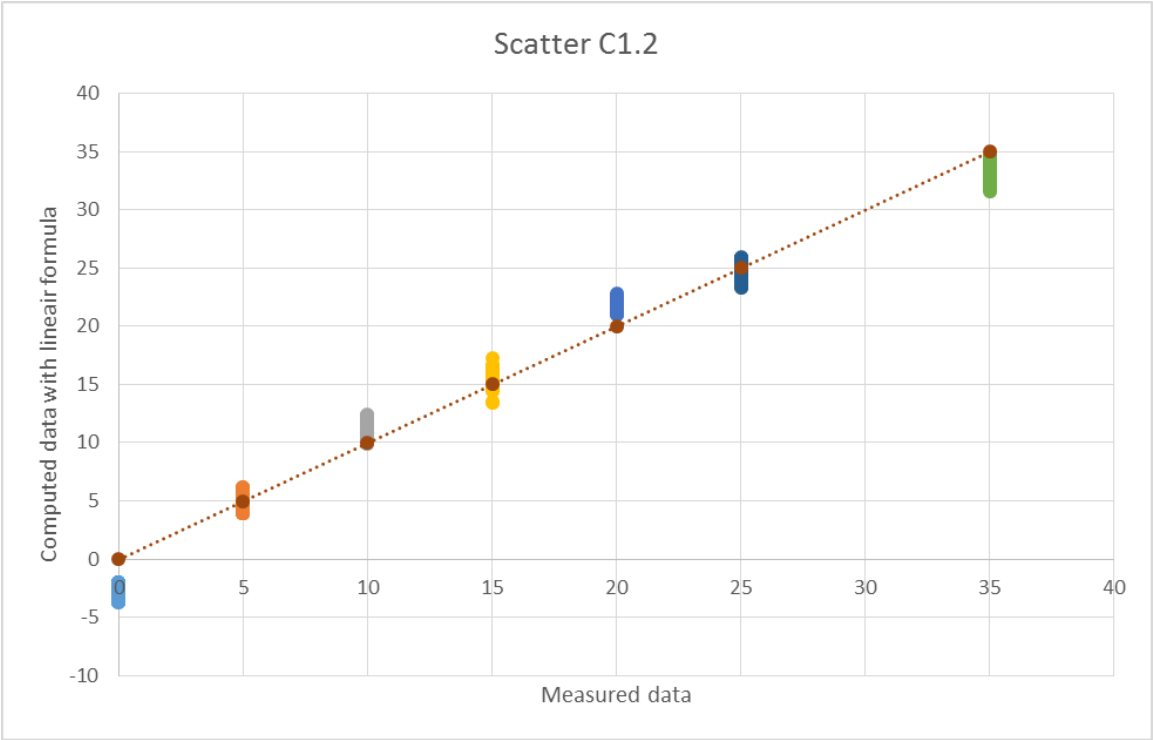
Scatter C1.2
Computed data with lineair formula
Measured data
40
35
30
25
20
15
10
5
0
-5
-10
0
5
10
15
20
25
30
35
40

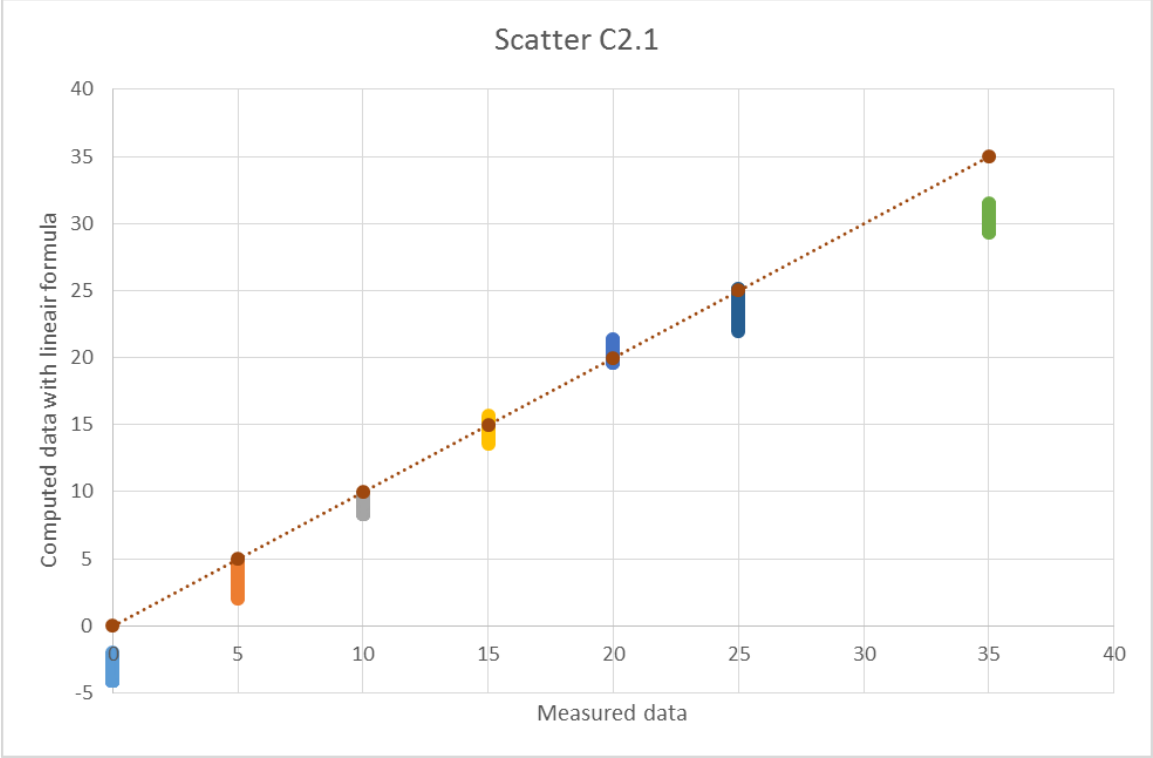
Scatter C2.1
Computed data with lineair formula
Measured data
40
35
30
25
20
15
10
5
0
-5
0
5
10
15
20
25
30
35
40

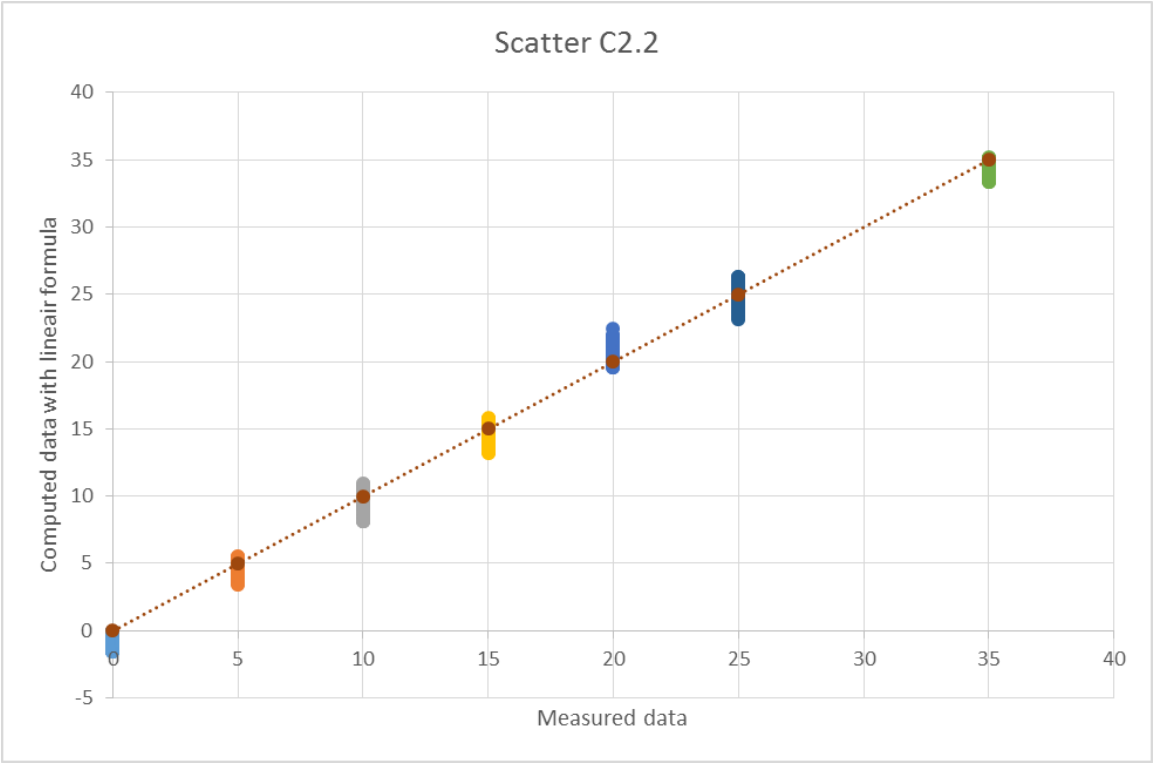

Figure B-14: 4 Scatter plots showing how the generated formulas fit the measured data

It can be concluded that the generated functions deliver good results because the calculated values approach the theoretical very well. In order to see how much the computed datasets vary from the theoretical values, the standard deviation of the calculated dataset, relative to the theoretical value, is determined. These values are presented in Table B-5.

Table B-5: Standard deviations of the computed values relative to the theoretical values

Sensor	σ 0%	σ 5%	σ 10%	σ 15%	σ 20%	σ 25%	σ 35%
C1.1	0.84	1.20	1.26	1.91	6.71	1.12	1.71
C1.2	2.69	2.29	3.36	0.86	1.85	0.47	2.13
C2.1	2.98	1.90	0.86	1.21	0.53	1.36	8.26
C2.2	0.68	2.13	0.72	0.81	0.95	0.46	0.70

It can be concluded that the deviations are acceptable since the average standard deviation lays around 2%. For two cases the standard deviations reach values of 6.71% and 8.26%.
The electric conductivity probes in the surge bin are calibrated in a different, less complicated way. The values for the zero concentration could easily be determined with the process water in the surge bin. To determine concentration values, the probes are put in baskets filled with a sand-water mixture of which the volumetric concentration is determined in advance. This leads to two known points for the concentration. To determine the values in between, a simple linear relation is used. The direct effect of temperature variations is not taken in account compared to the CCMs placed in the pipes.

Appendix C: Model & experimental results

Introduction

All scenarios described in the main report have been carried out with high attention and precision. When impurities during the data logging were experienced or noticed (air bubbles, flow problems), the batch was performed again. Despite the attention paid, the flows of scenario (batch 1 and 2) have a small deviation relative to the planned value. Batch 4 was more difficult to create than expected.

The equations for the sensors, as they are derived in 6.2, are programmed in Dewesoft and subsequently, the logged data is exported to Excel files which will form the input files for the 1.5D model. The volumetric concentrations which are measured with the experiment, are used as the incoming concentration profiles for the model. In addition, the inflow, outflow and jetflow can be programmed and the model is ready for use. As a result, the program generates a concentration profile of the outgoing flow which can be compared with the data measured with the experiment.

This procedure is repeated for all the 24 experimental datasets.

Statistics

To make the analyses between the computed and measured data insightful, several statistical values are calculated for all the datasets. By analyzing the results and these statistical values, a verdict of the validation can be made.

The maximum derivation is nothing more than the maximum, absolute difference between the measured and calculated values of the outgoing concentration. It must be noticed that this number doesn't say anything about the reliability of the model.

The standard deviation and formula are already elaborated in Appendix B.

The R squared value is an indication of how well data points are fitting a curve. In this case: how well does the computed curve fit the measured curve? The R squared value is calculated using the Pearson Correlation which is a correlation between two random variables. Pearson's correlation is defined as:

$$R(X,Y) = \frac{cov(X,Y)}{\sigma_X \sigma_Y} \tag{C.1}$$

Where σ_X and σ_Y are the standard deviations of the measured and calculated datasets. The covariance is a measure how two variables change together and is defined as:

$$cov(X,Y) = \frac{\sum_{i=1}^{n}(x_i - \bar{x})(y_i - \bar{y})}{n} \tag{C.2}$$

Filling in the formulas of the covariance and the standard deviation in the Pearson correlation, leads to the following relation:

$$R(X,Y) = \frac{\sum_{i=1}^{n}(x_i - \bar{x})(y_i - \bar{y})}{\sqrt{\sum_{i=1}^{n}(x_i - \bar{x})^2 \sum_{i=1}^{n}(y_i - \bar{y})^2}} \qquad \text{(C.3)}$$

Now, the R squared value can be determined as $R^2\ (X,Y)$. The values for R squared have a range between 0 and 1 and $R^2 = 1$ indicates that the computed data fits the measured data perfectly.

Explanation on graphs:

The created graphs and deviations are explained in the illustration below.

1. General information of the experiment is given such as water temperature, average flows, batch and scenario numbers.

2. Is the plotted data of the experiment. The blue line represents the concentration at the outflow while the orange line represent the concentration at the inflow. The orange line is used as an input signal for the 1.5D model.

3. Shows the computed concentration at the outflow of the model (blue line) and the measured data from the experiment.

4. Gives the error between the computed and measured data. This graph is obtained if the blue line is subtracted from the orange line in number 3). From this graph, the maximum deviation is determined.

5. Shows a summary of the calculated statistics.

Results of measured and computed data

Scenario number:	**1**	Jet: [l/s]	0.35	Average temp: [°C]	14.0
Batch number:	**1**	Flow in: [l/s]	2.9	Max temp: [°C]	14.1
Duration experiment: [s]	920	Flow out: [l/s]	1.7	Min temp: [°C]	13.9

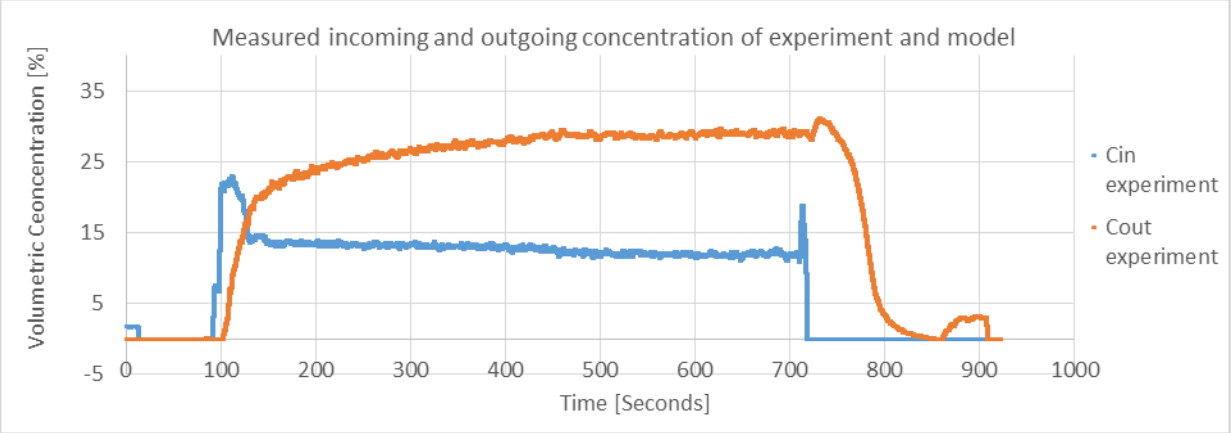

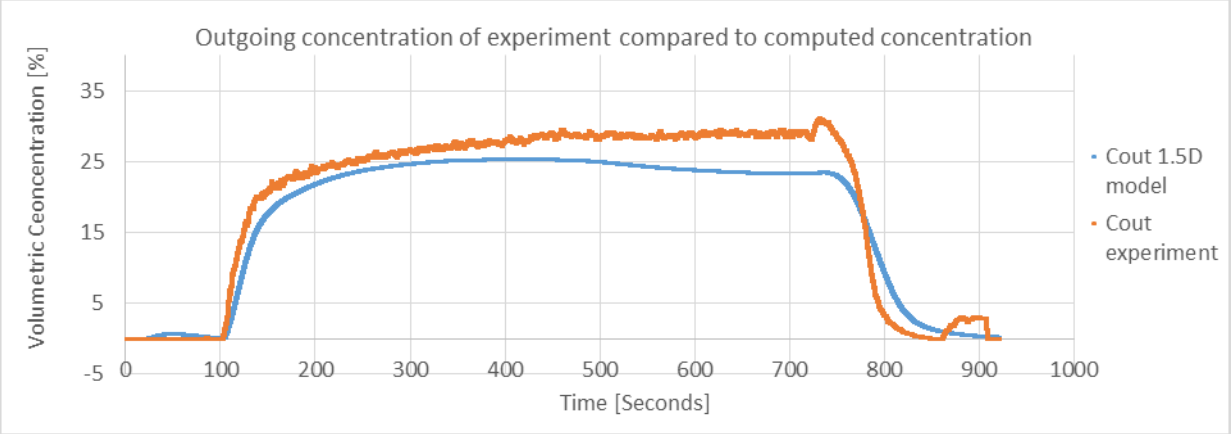

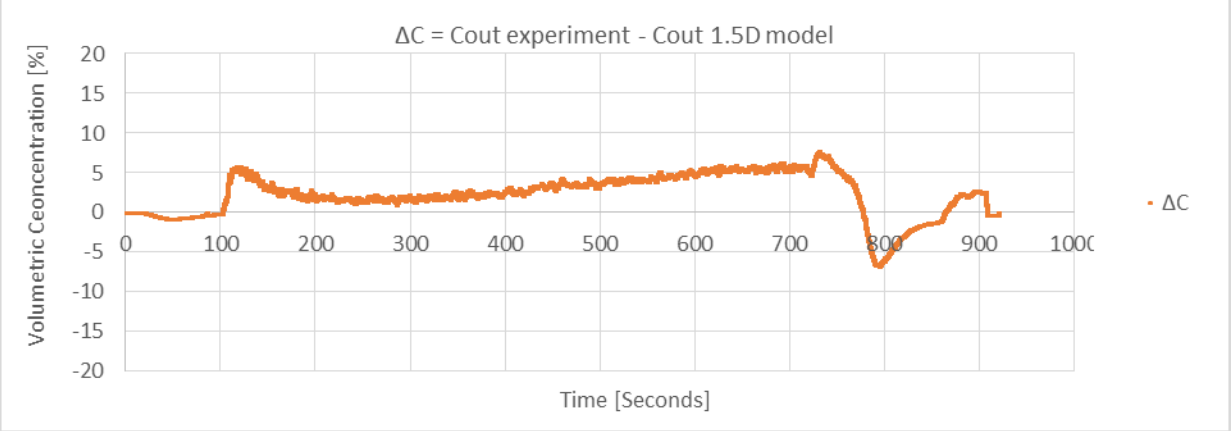

Results:

Maximum deviation: [%Cv]	7.7
Standard deviation: [%Cv]	2.7
R^2: [-]	0.97

Results of measured and computed data

Scenario number:	**1**	Jet: [l/s]	0.35	Average temp: [°C]	14.5
Batch number:	**2**	Flow in: [l/s]	3.0	Max temp: [°C]	14.6
Duration experiment: [s]	707	Flow out: [l/s]	1.8	Min temp: [°C]	14.4

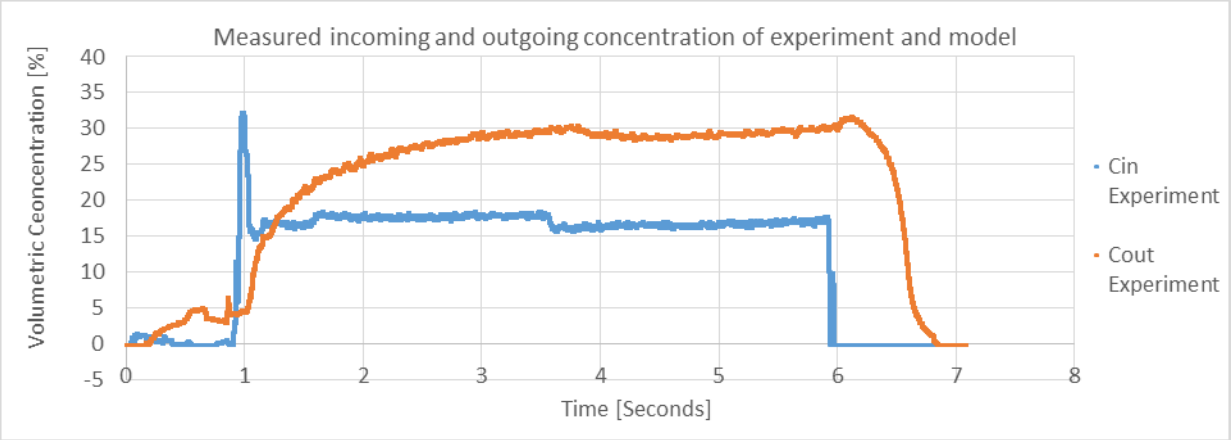

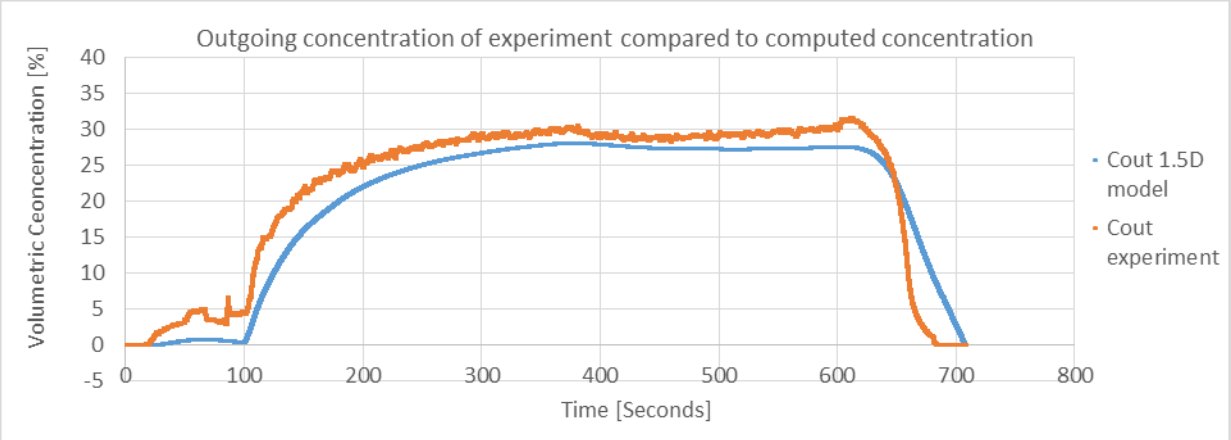

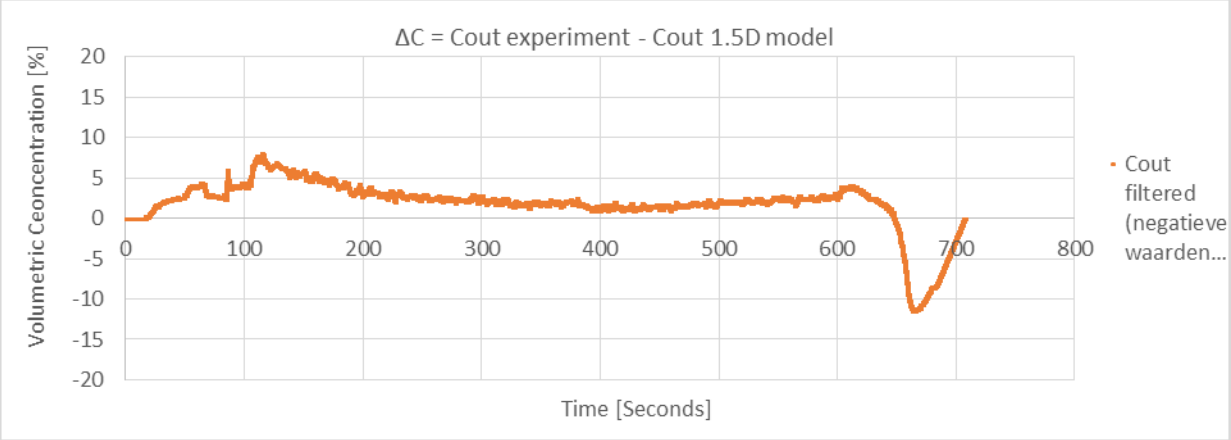

Results:

Maximum deviation: [%Cv]	11.6
Standard deviation: [%Cv]	3.1
R^2: [-]	0.92

Results of measured and computed data

Scenario number:	**1**	Jet: [l/s]	0.35	Average temp: [°C]	15.0
Batch number:	**3**	Flow in: [l/s]	2.9	Max temp: [°C]	15.1
Duration experiment: [s]	847	Flow out: [l/s]	1.9	Min temp: [°C]	15.0

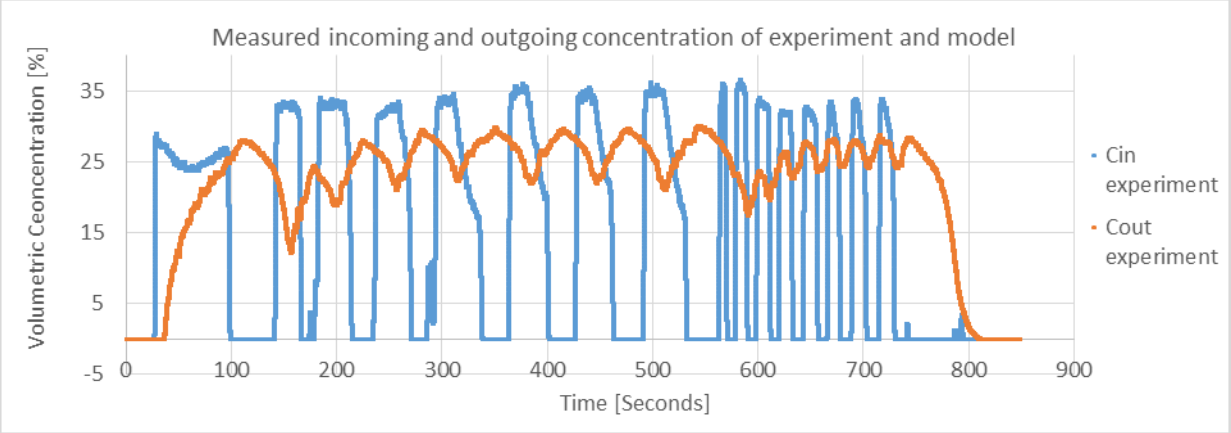

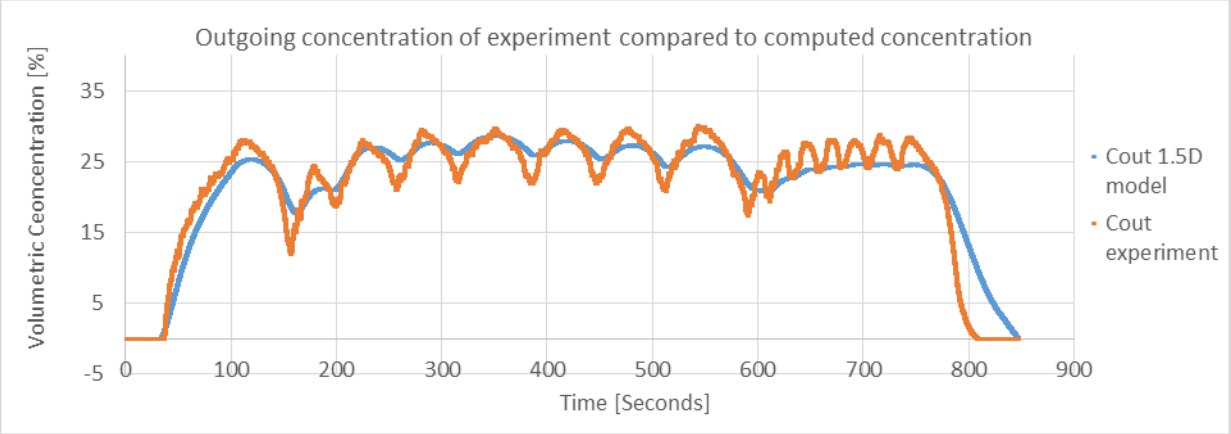

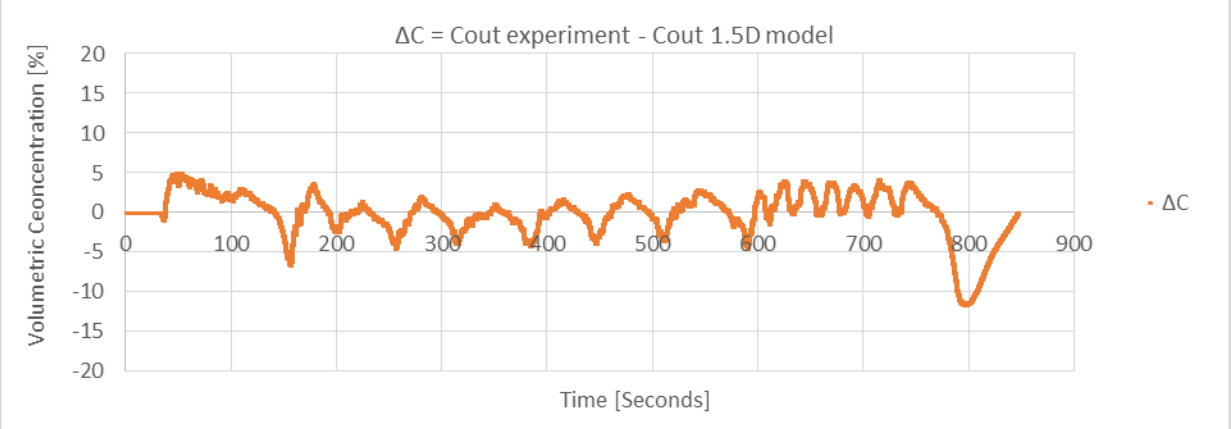

Results:

Maximum deviation: [%Cv]	11.6
Standard deviation: [%Cv]	3.0
R^2: [-]	0.89

Results of measured and computed data

Scenario number:	**1**	Jet: [l/s]	0.35	Average temp: [°C]	15.2
Batch number:	**4**	Flow in: [l/s]	2.9	Max temp: [°C]	15.3
Duration experiment: [s]	993	Flow out: [l/s]	1.8	Min temp: [°C]	15.1

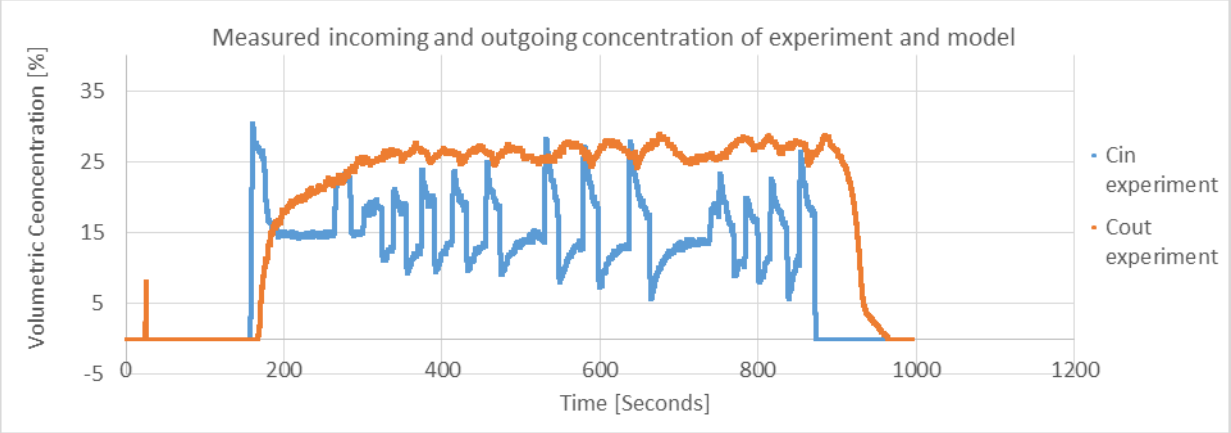

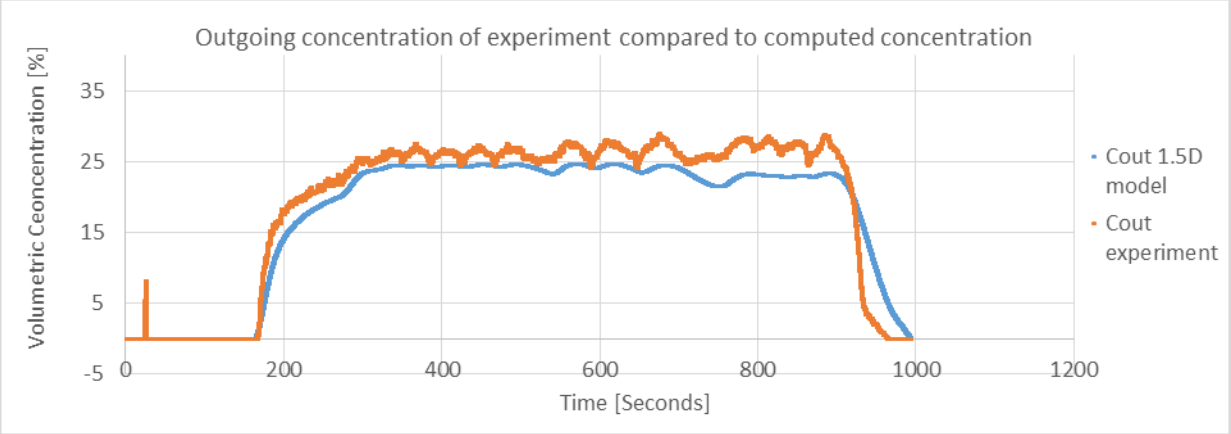

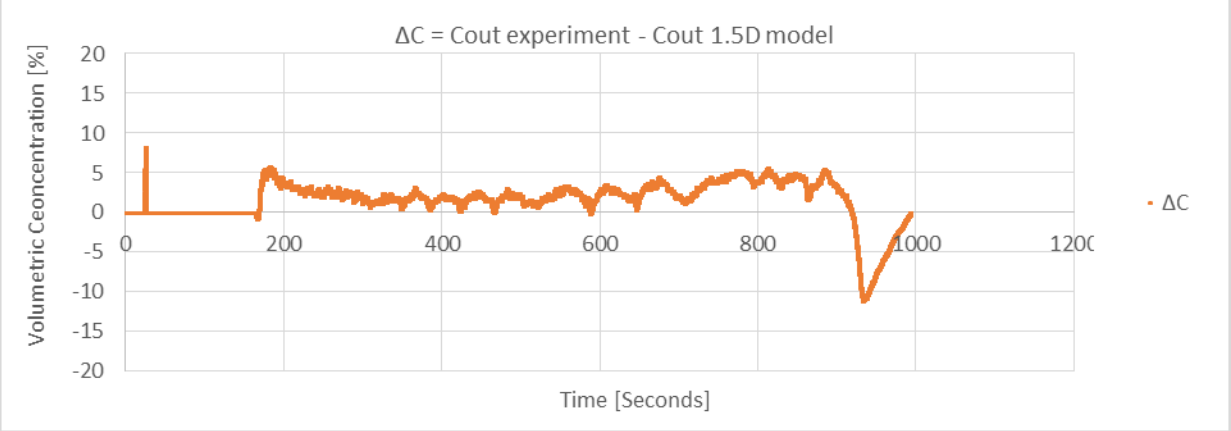

Results:

Maximum deviation: [%Cv]	11.1
Standard deviation: [%Cv]	2.9
R^2: [-]	0.96

Results of measured and computed data

Scenario number:	**1**	Jet: [l/s]	0.35	Average temp: [°C]	15.3
Batch number:	**5**	Flow in: [l/s]	3.0	Max temp: [°C]	15.4
Duration experiment: [s]	318	Flow out: [l/s]	1.9	Min temp: [°C]	15.3

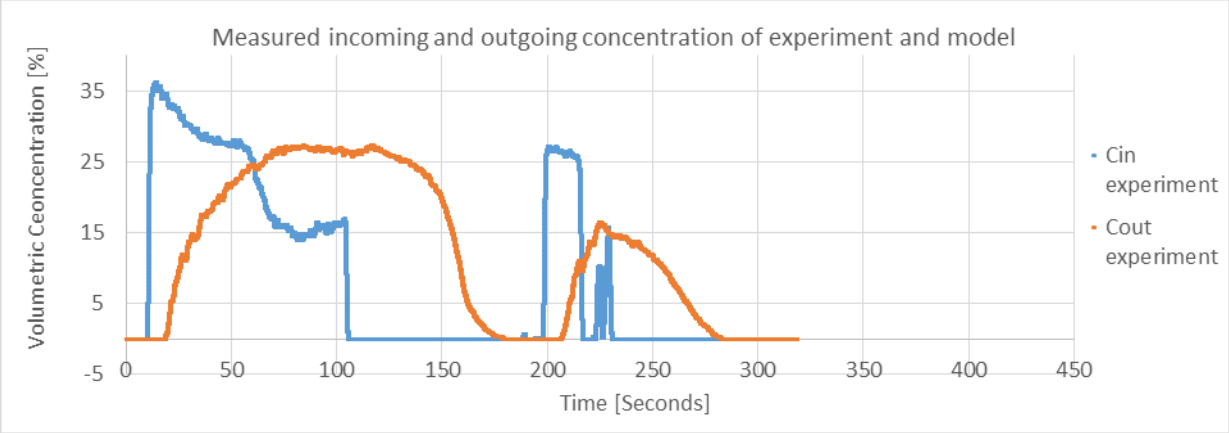

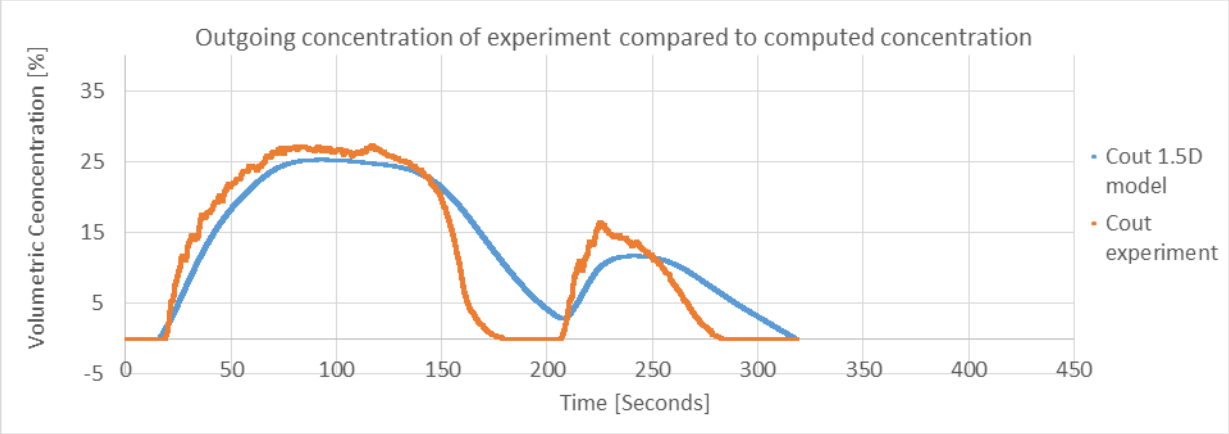

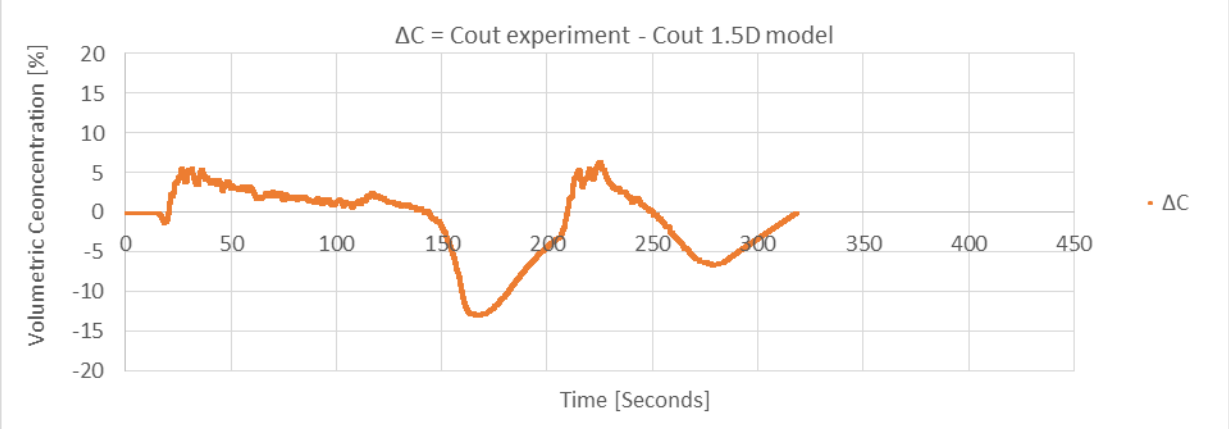

Results:

Maximum deviation: [%Cv]	12.9
Standard deviation: [%Cv]	4.7
R^2: [-]	0.84

Results of measured and computed data

Scenario number:	**1**	Jet: [l/s]	0.35	Average temp: [°C]	14.5
Batch number:	**6**	Flow in: [l/s]	3.0	Max temp: [°C]	14.6
Duration experiment: [s]	562	Flow out: [l/s]	1.9	Min temp: [°C]	14.5

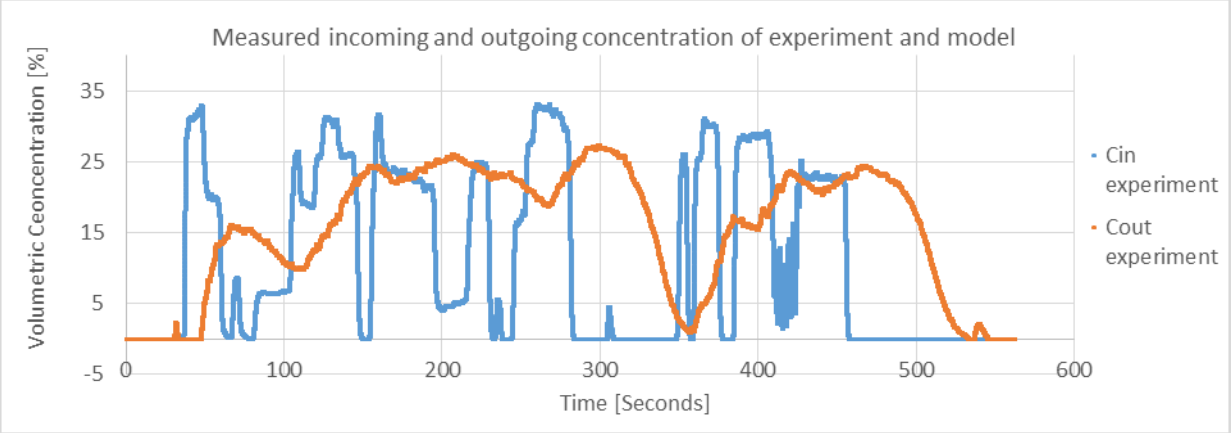

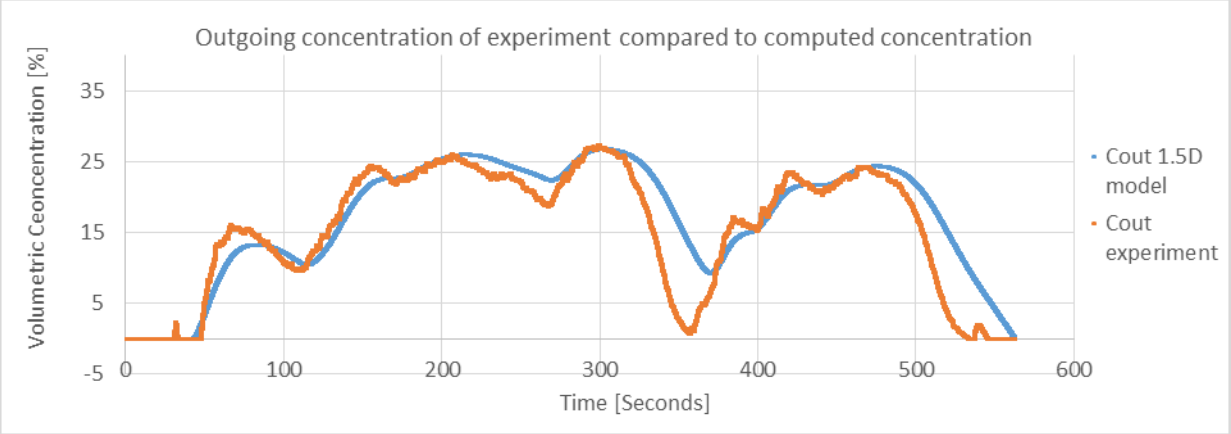

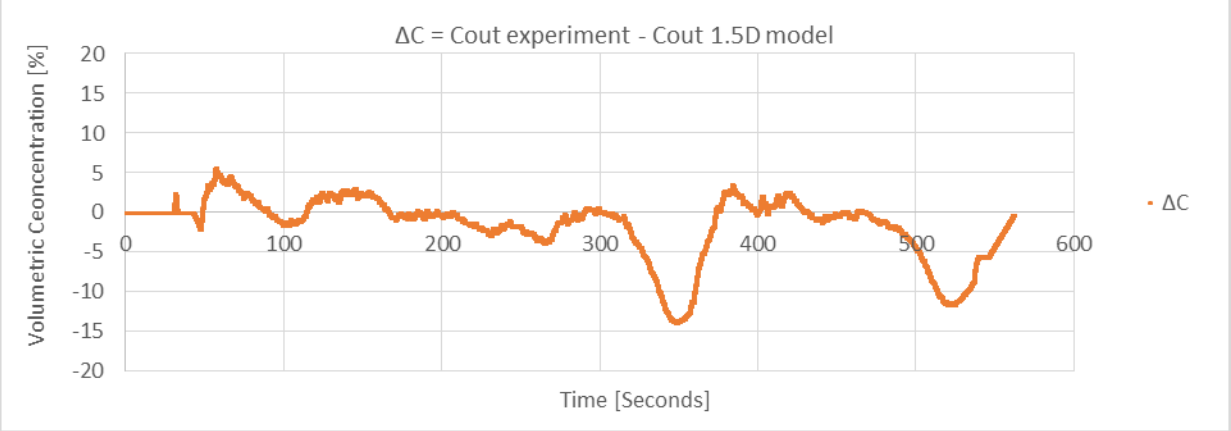

Results:

Maximum deviation: [%Cv]	14.0
Standard deviation: [%Cv]	3.9
R^2: [-]	0.83

Results of measured and computed data

Scenario number:	**3**	Jet: [l/s]	0.28	Average temp: [°C]	14.7
Batch number:	**1**	Flow in: [l/s]	2.2	Max temp: [°C]	14.8
Duration experiment: [s]	374	Flow out: [l/s]	1.5	Min temp: [°C]	14.6

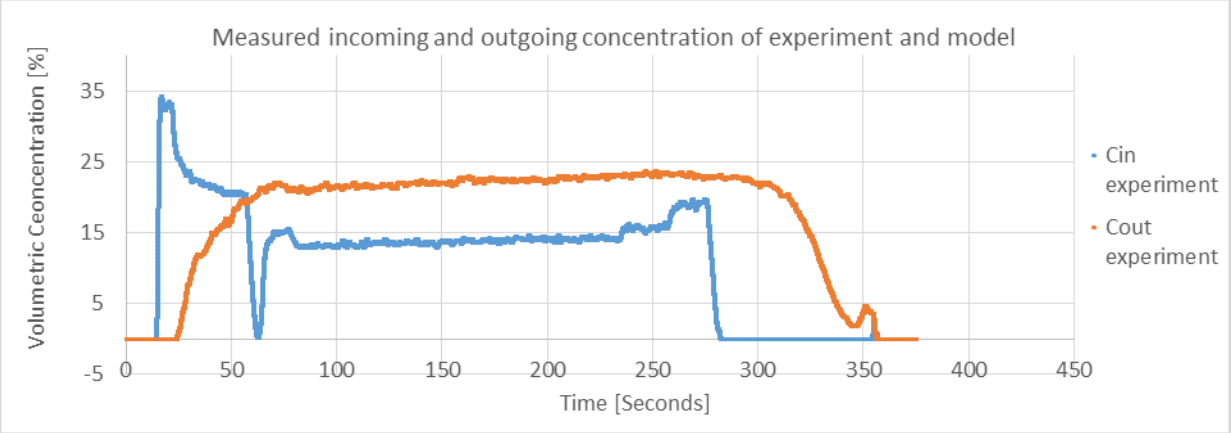

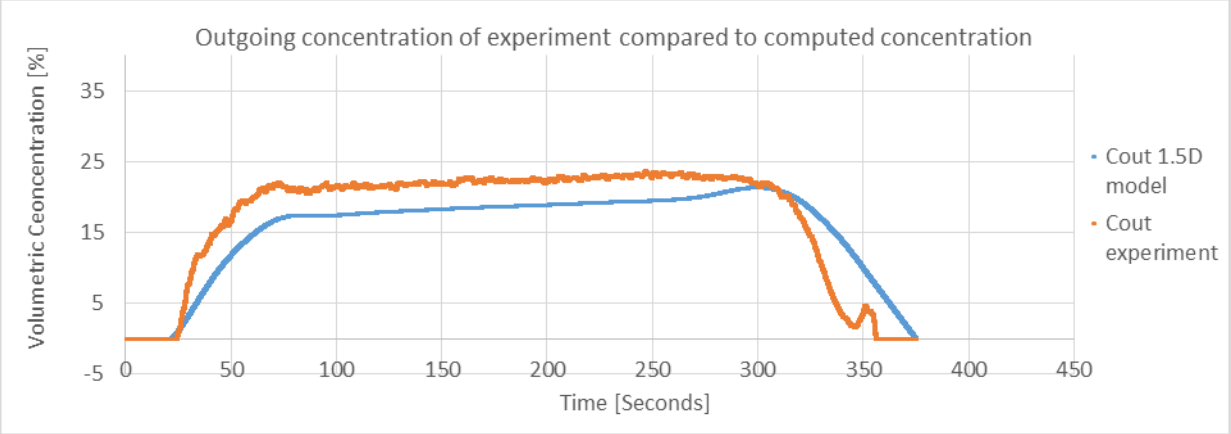

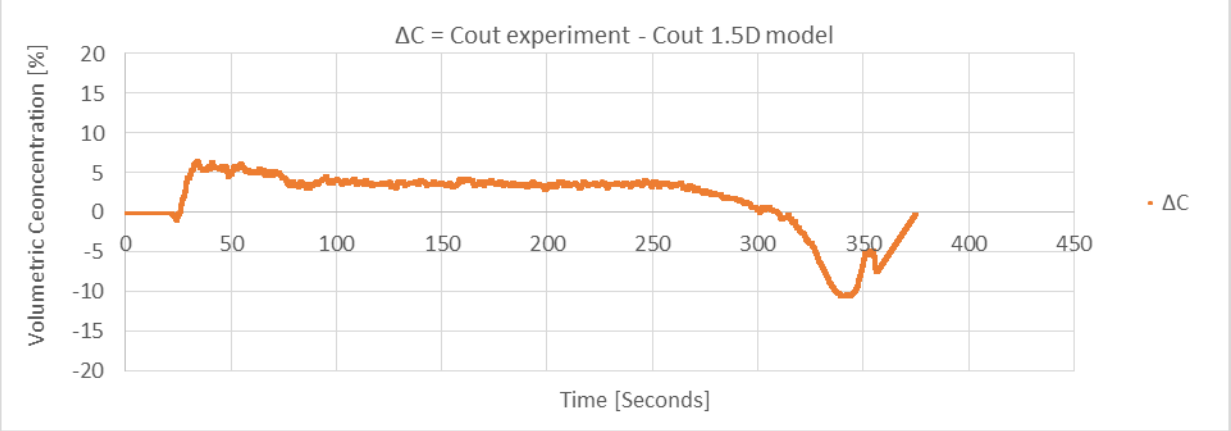

Results:

Maximum deviation: [%Cv]	10.5
Standard deviation: [%Cv]	3.8
R^2: [-]	0.83

Results of measured and computed data

Scenario number:	**3**	Jet: [l/s]	0.28	Average temp: [°C]	14.9
Batch number:	**2**	Flow in: [l/s]	2.2	Max temp: [°C]	14.9
Duration experiment: [s]	387	Flow out: [l/s]	1.5	Min temp: [°C]	14.8

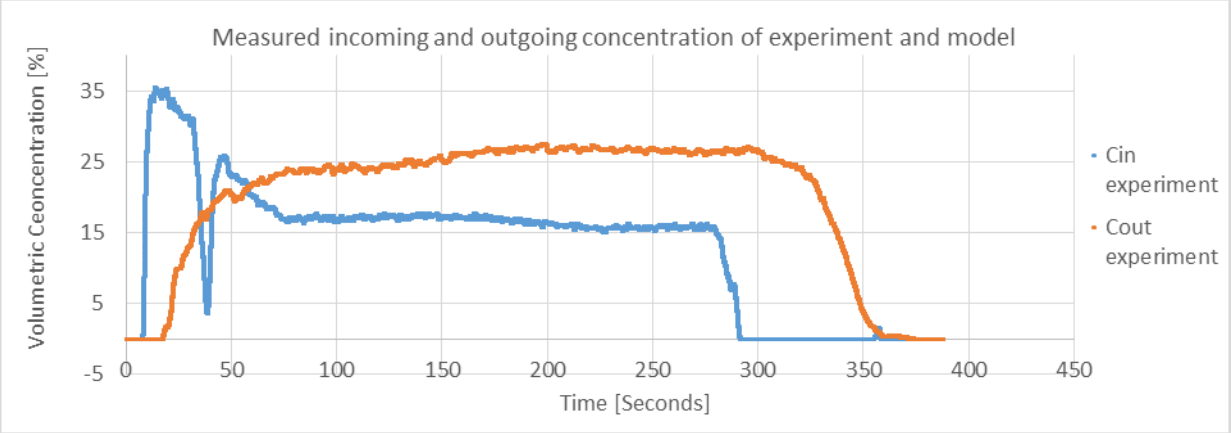

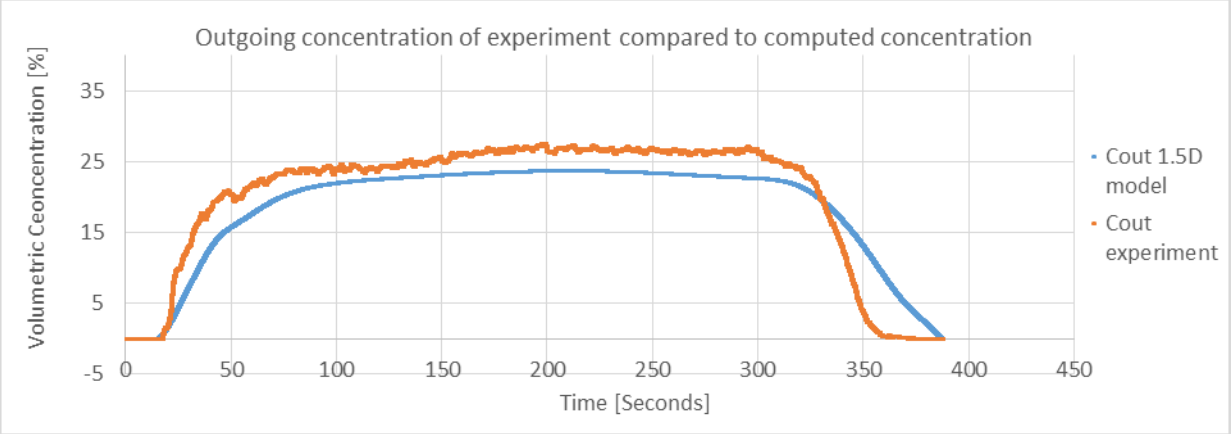

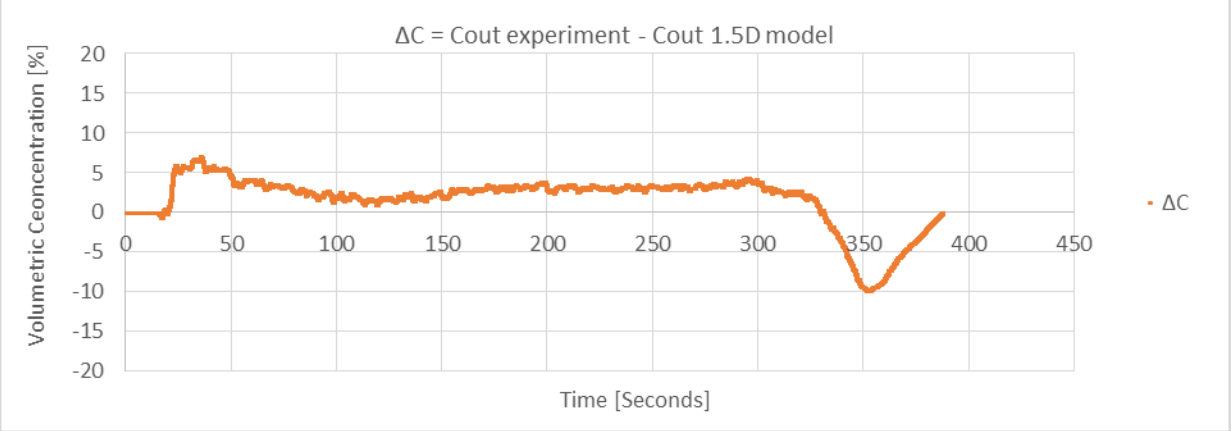

Results:

Maximum deviation: [%Cv]	9.9
Standard deviation: [%Cv]	3.3
R^2: [-]	0.91

Results of measured and computed data

Scenario number:	**3**	Jet: [l/s]	0.28	Average temp: [°C]	14.5
Batch number:	**3**	Flow in: [l/s]	2.2	Max temp: [°C]	14.7
Duration experiment: [s]	1068	Flow out: [l/s]	1.5	Min temp: [°C]	14.4

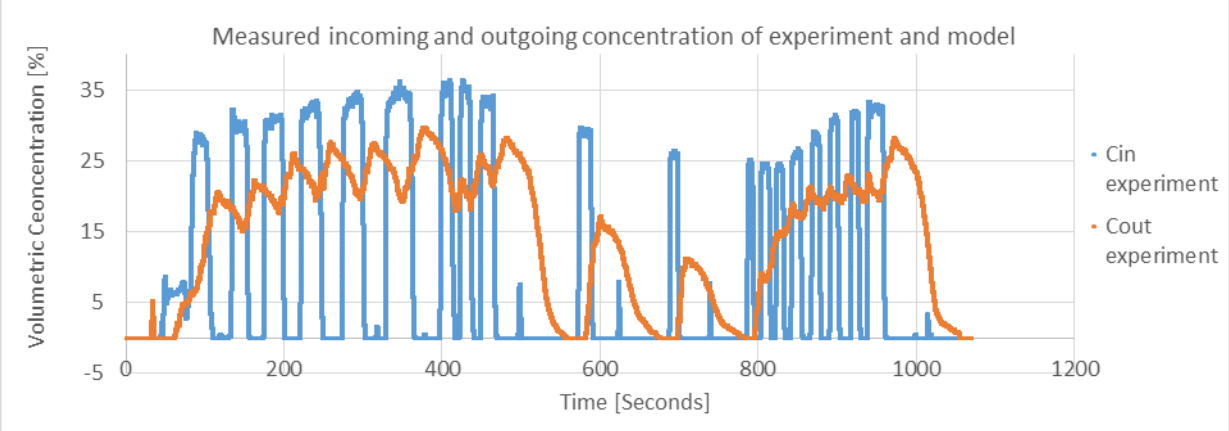

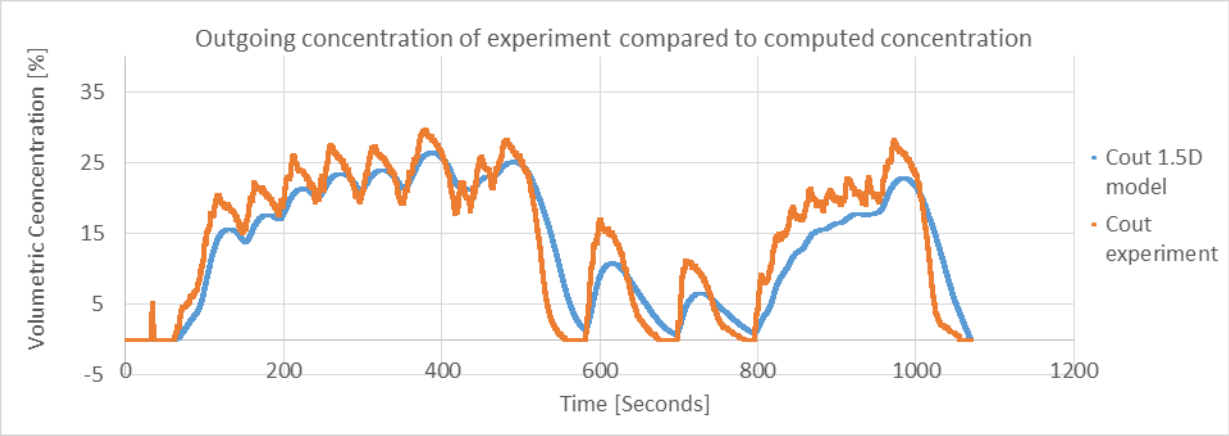

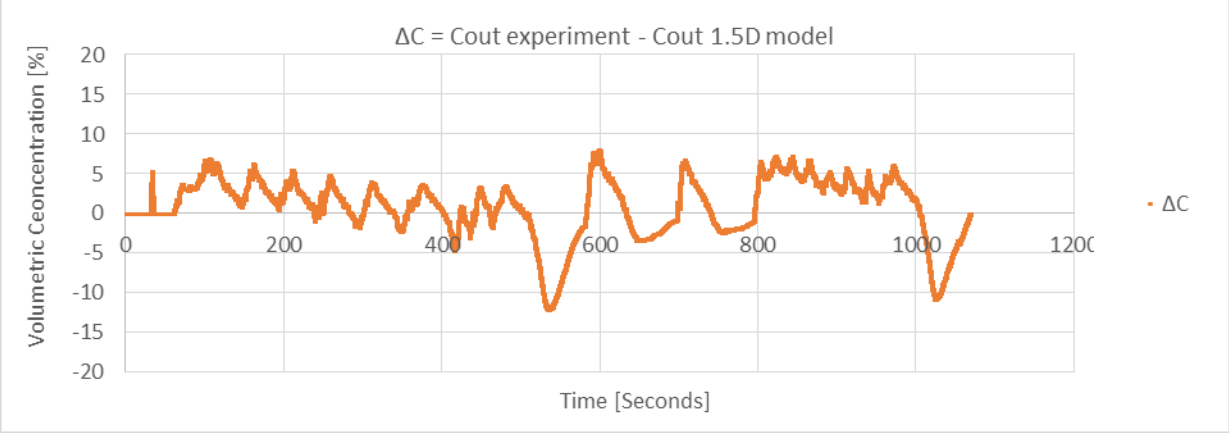

Results:

Maximum deviation: [%Cv]	12.2
Standard deviation: [%Cv]	3.9
R^2: [-]	0.85

Results of measured and computed data

Scenario number:	**3**	Jet: [l/s]	0.28	Average temp: [°C]	14.9
Batch number:	**4**	Flow in: [l/s]	2.2	Max temp: [°C]	14.9
Duration experiment: [s]	383	Flow out: [l/s]	1.5	Min temp: [°C]	14.8

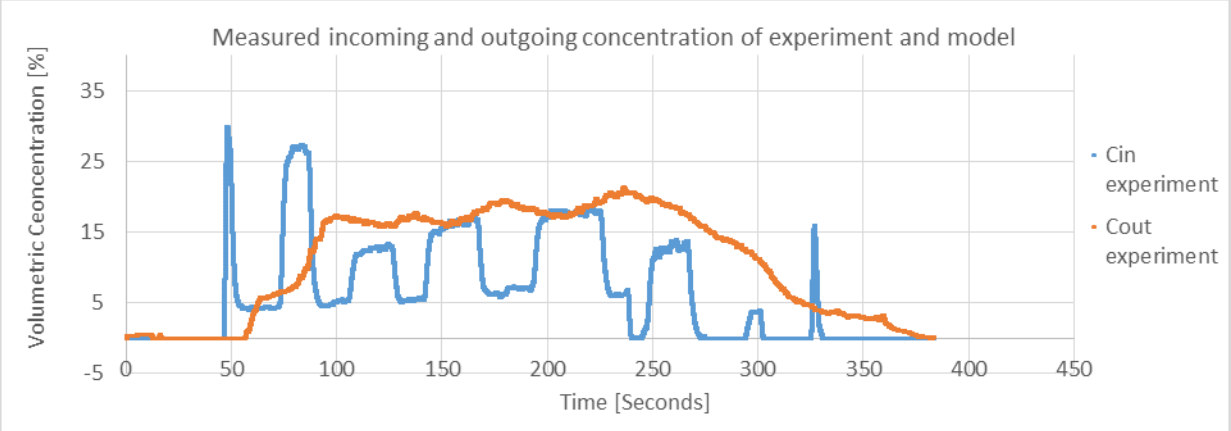

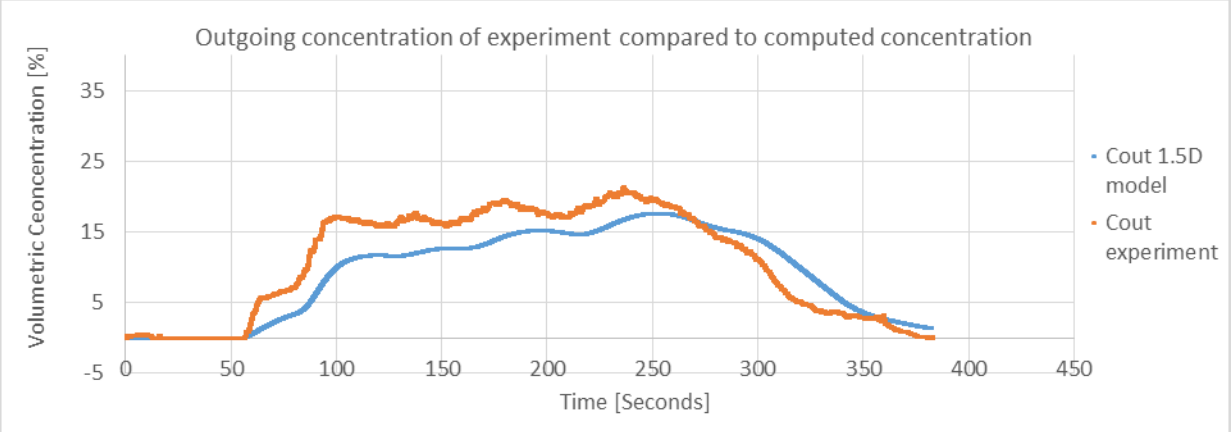

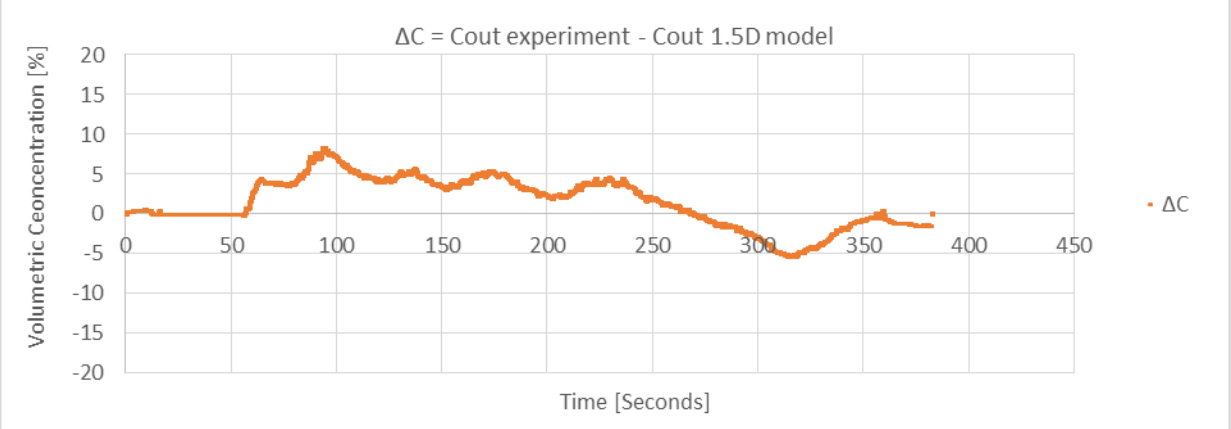

Results:

Maximum deviation: [%Cv]	8.4
Standard deviation: [%Cv]	3.2
R^2: [-]	0.84

Results of measured and computed data

Scenario number:	**3**	Jet: [l/s]	0.28	Average temp: [°C]	14.9
Batch number:	**5**	Flow in: [l/s]	2.2	Max temp: [°C]	14.9
Duration experiment: [s]	443	Flow out: [l/s]	1.5	Min temp: [°C]	14.8

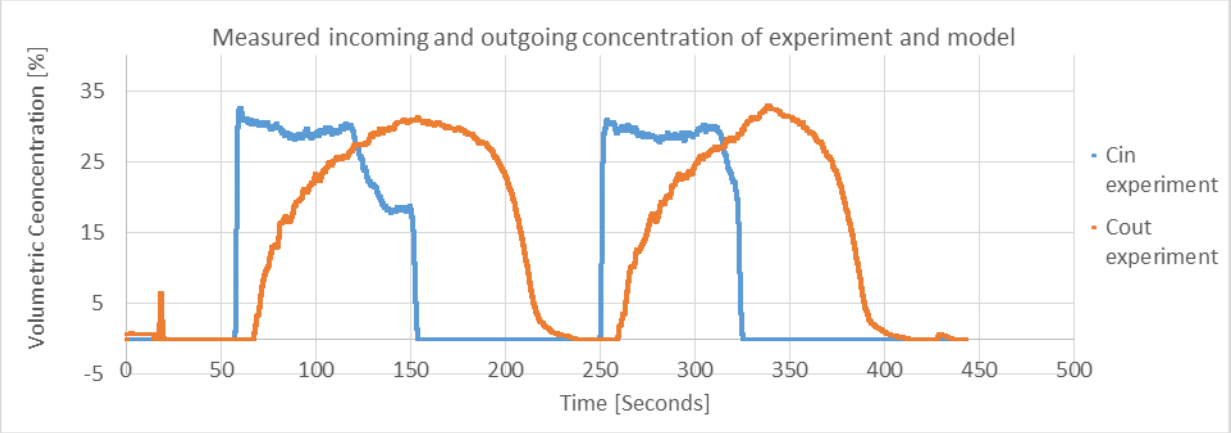

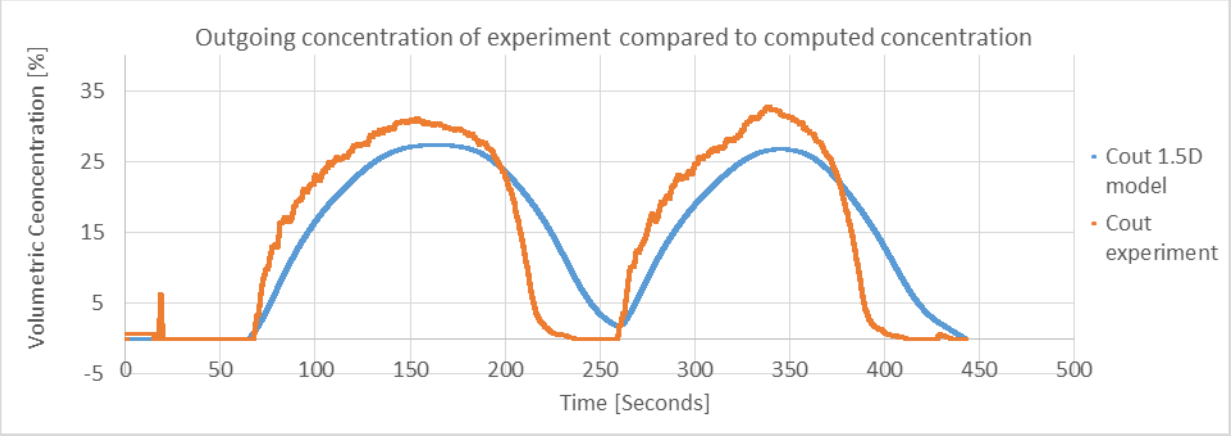

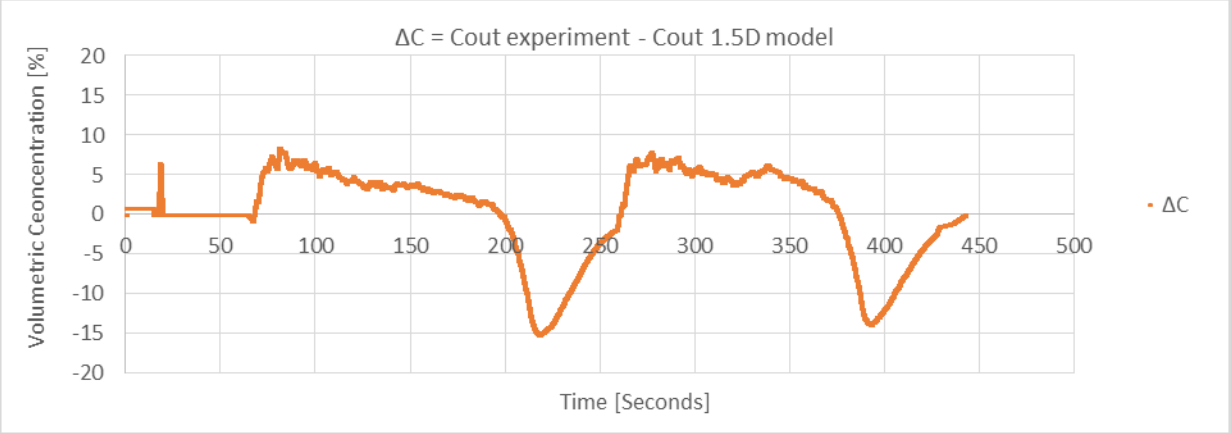

Results:

Maximum deviation: [%Cv]	15.1
Standard deviation: [%Cv]	5.7
R^2: [-]	0.82

Results of measured and computed data

Scenario number:	**3**	Jet: [l/s]	0.28	Average temp: [°C]	14.7
Batch number:	**6**	Flow in: [l/s]	2.2	Max temp: [°C]	14.8
Duration experiment: [s]	729	Flow out: [l/s]	1.5	Min temp: [°C]	14.6

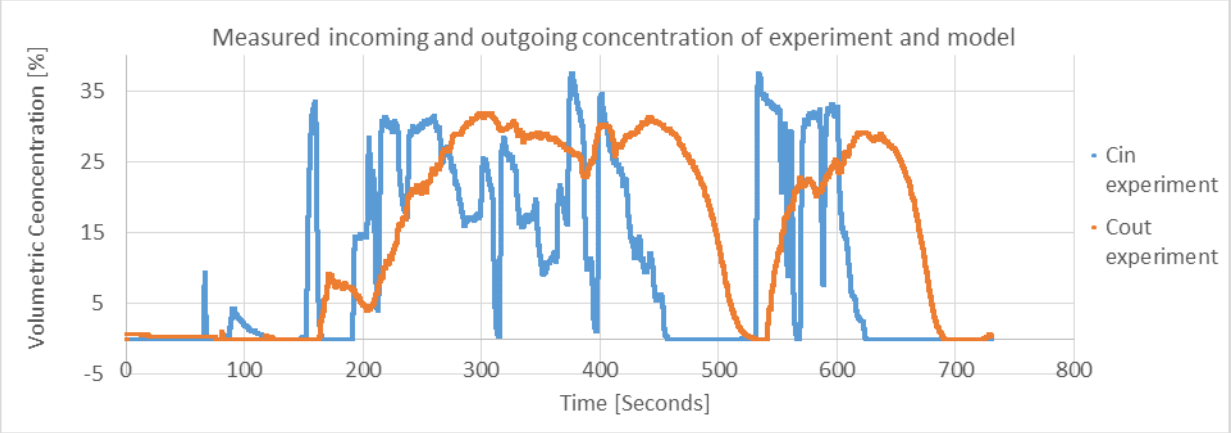

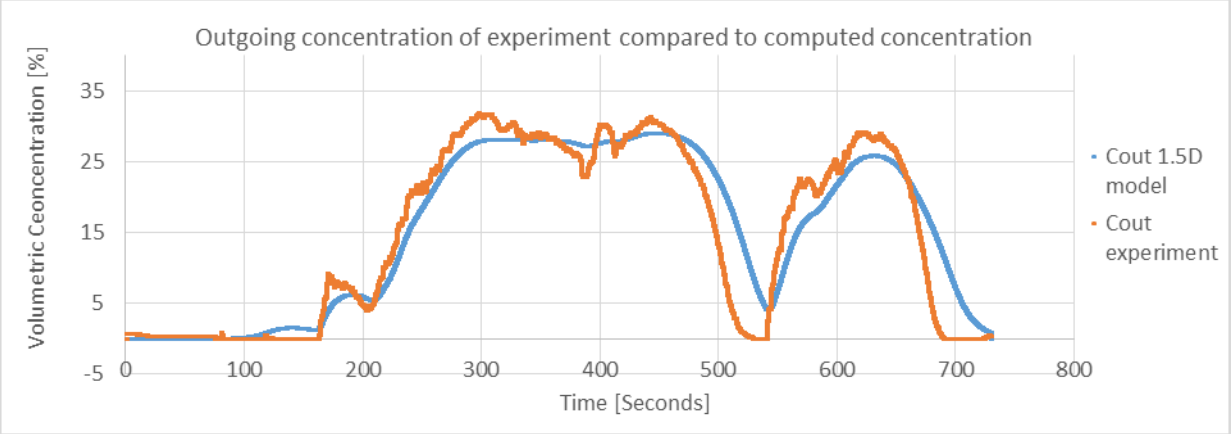

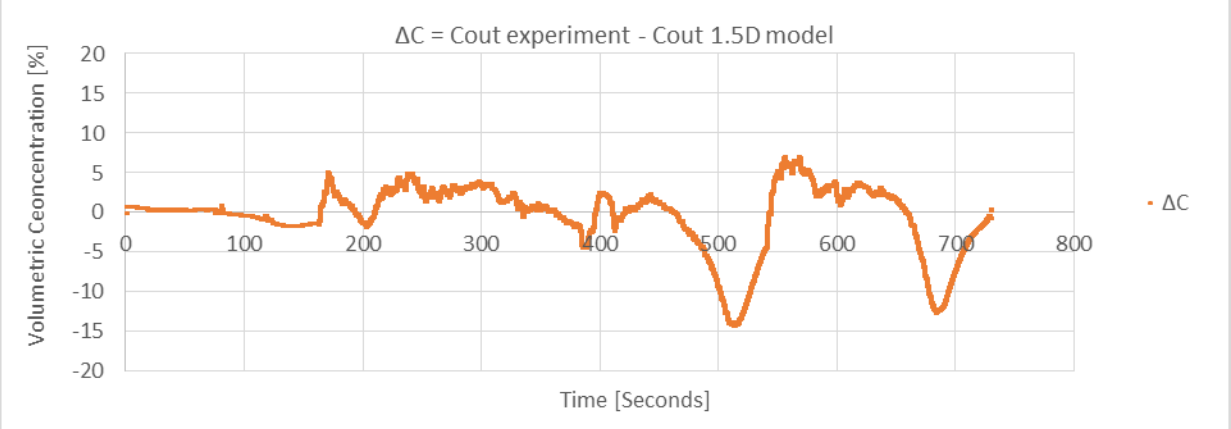

Results:

Maximum deviation: [%Cv]	14.2
Standard deviation: [%Cv]	4.2
R^2: [-]	0.90

Results of measured and computed data

Scenario number:	**5**	Jet: [l/s]	0.00	Average temp: [°C]	13.6
Batch number:	**1**	Flow in: [l/s]	2.9	Max temp: [°C]	13.6
Duration experiment: [s]	498	Flow out: [l/s]	1.8	Min temp: [°C]	13.5

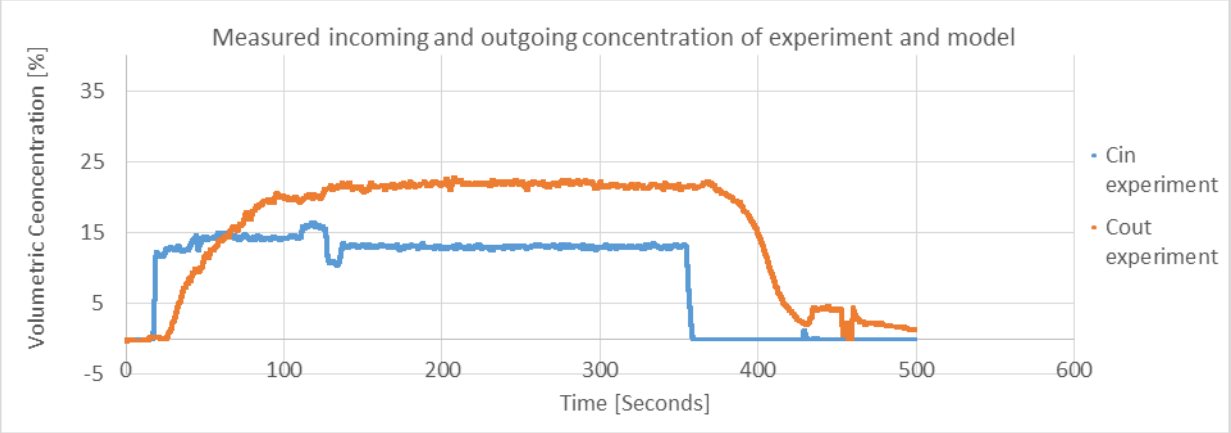

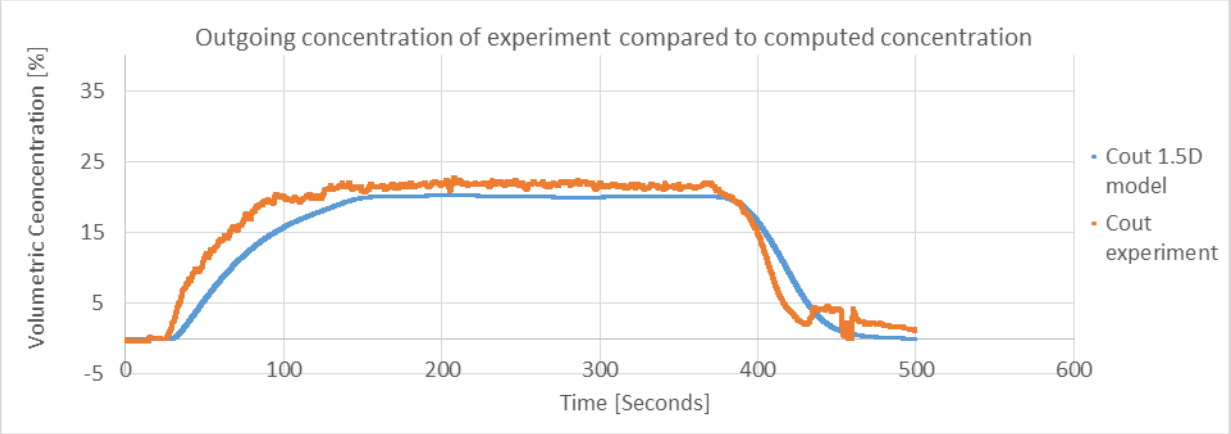

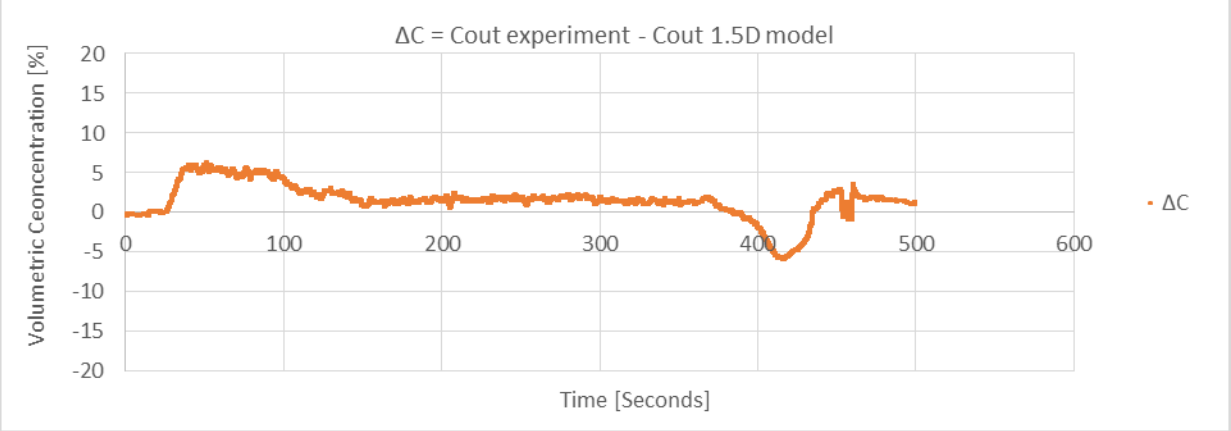

Results:

Maximum deviation: [%Cv]	6.4
Standard deviation: [%Cv]	2.2
R^2: [-]	0.93

Results of measured and computed data

Scenario number:	**5**	Jet: [l/s]	0.00	Average temp: [°C]	13.8
Batch number:	**2**	Flow in: [l/s]	2.9	Max temp: [°C]	13.8
Duration experiment: [s]	651	Flow out: [l/s]	1.8	Min temp: [°C]	13.7

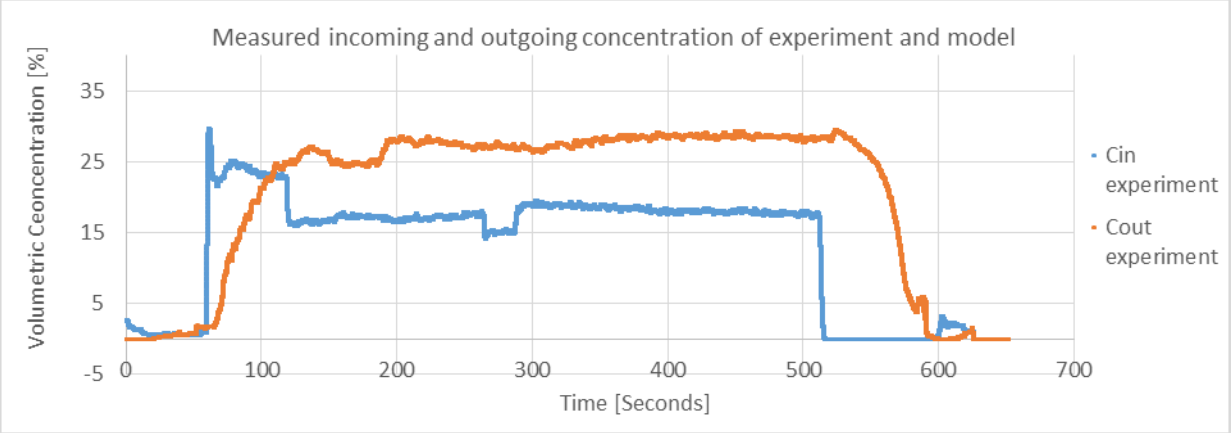

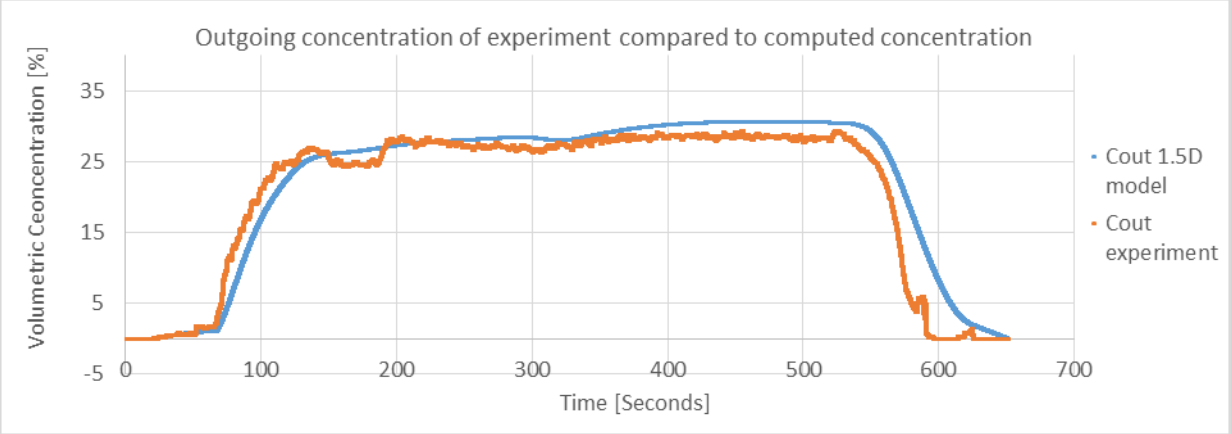

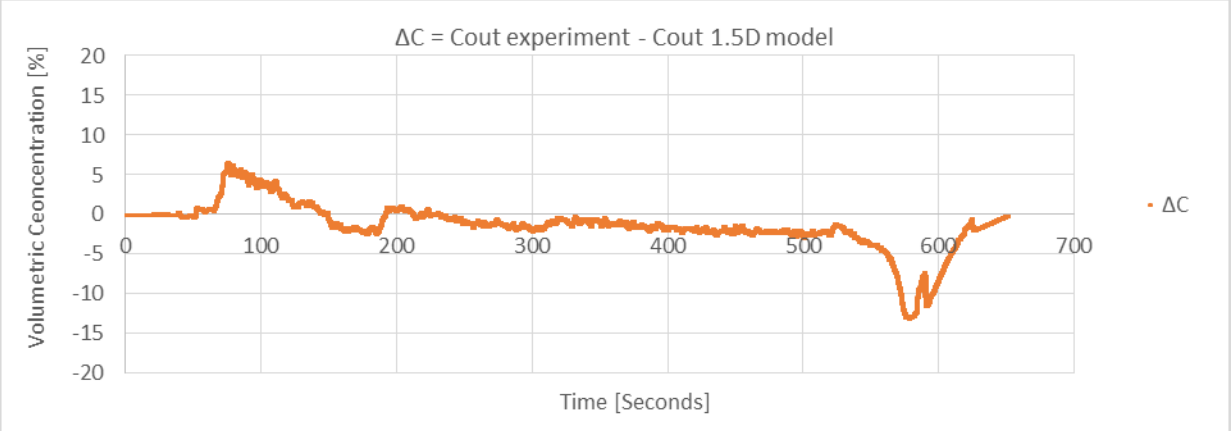

Results:

Maximum deviation: [%Cv]	13.0
Standard deviation: [%Cv]	2.9
R^2: [-]	0.93

Results of measured and computed data

Scenario number:	**5**	Jet: [l/s]	0.00	Average temp: [°C]	13.9
Batch number:	**3**	Flow in: [l/s]	2.9	Max temp: [°C]	14.0
Duration experiment: [s]	745	Flow out: [l/s]	1.9	Min temp: [°C]	13.8

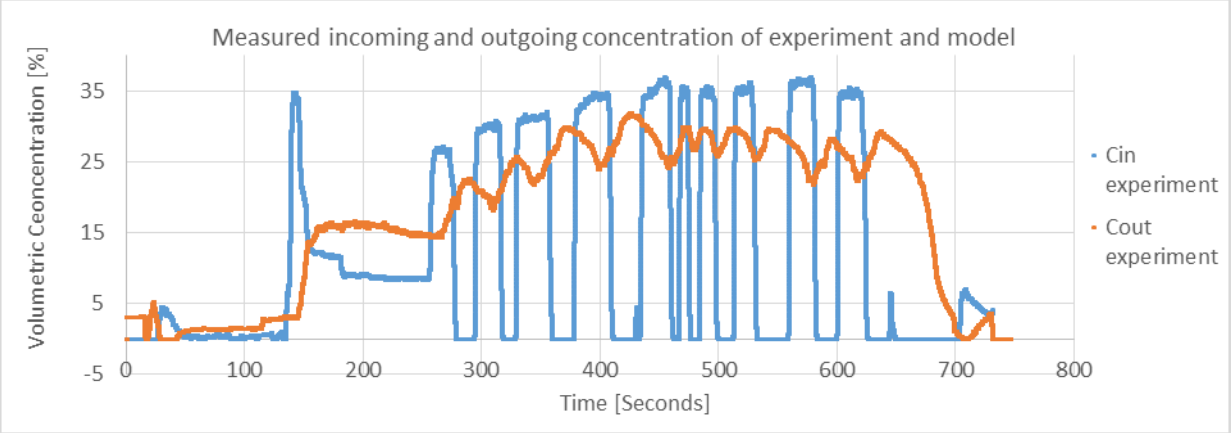

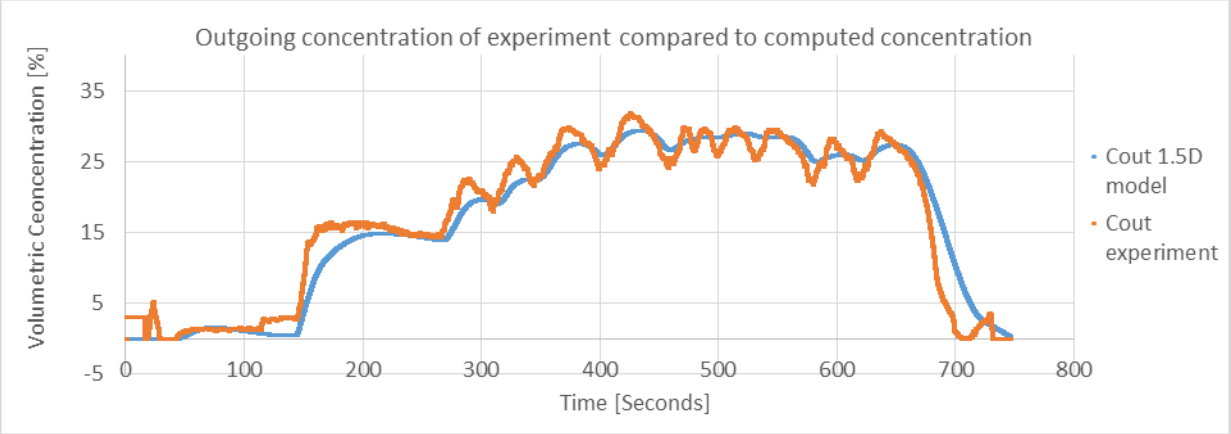

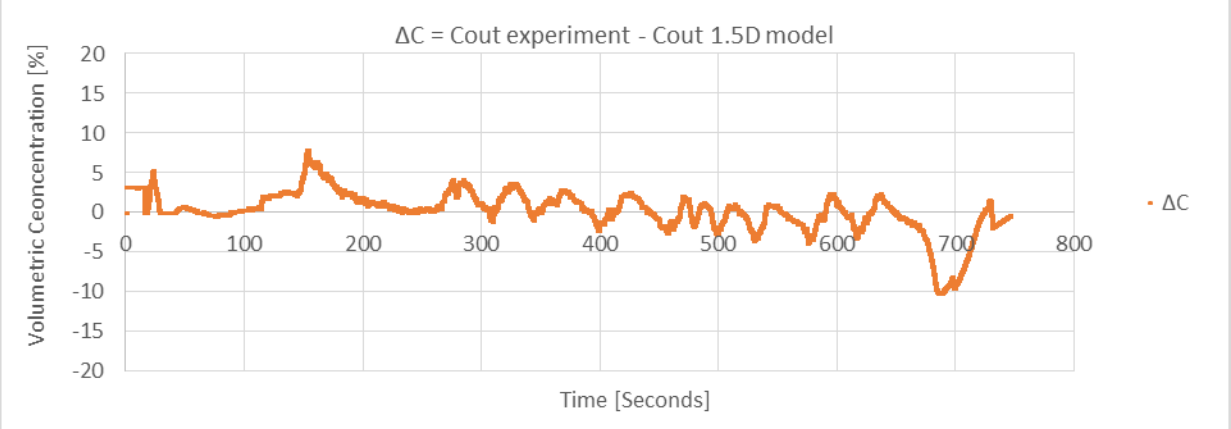

Results:

Maximum deviation: [%Cv]	10.2
Standard deviation: [%Cv]	2.6
R^2: [-]	0.94

Results of measured and computed data

Scenario number:	**5**	Jet: [l/s]	0.00	Average temp: [°C]	14.0
Batch number:	**4**	Flow in: [l/s]	3.0	Max temp: [°C]	14.1
Duration experiment: [s]	973	Flow out: [l/s]	2.0	Min temp: [°C]	13.9

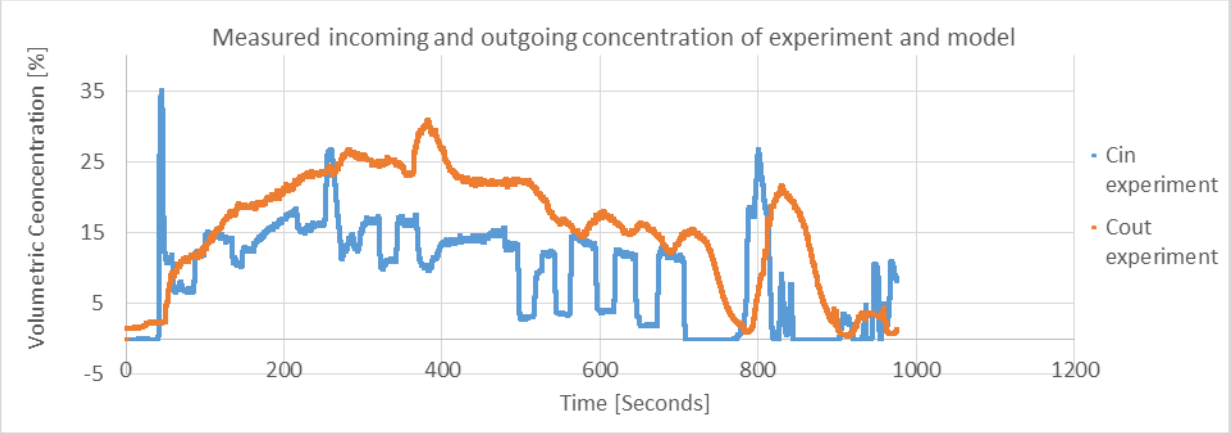

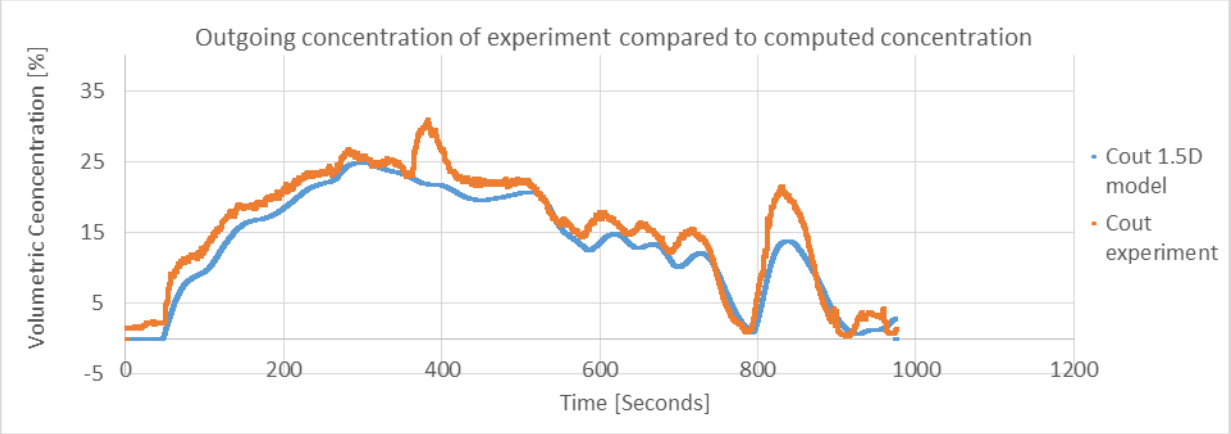

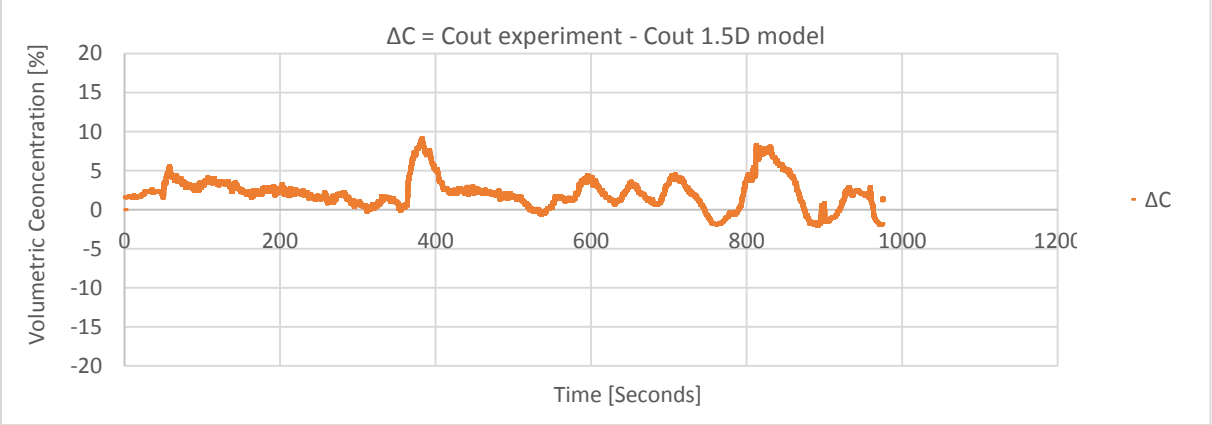

Results:

Maximum deviation: [%Cv]	9.2
Standard deviation: [%Cv]	2.0
R^2: [-]	0.94

Results of measured and computed data

Scenario number:	**5**	Jet: [l/s]	0.00	Average temp: [°C]	14.2
Batch number:	**5**	Flow in: [l/s]	2.8	Max temp: [°C]	14.2
Duration experiment: [s]	232	Flow out: [l/s]	2.0	Min temp: [°C]	14.1

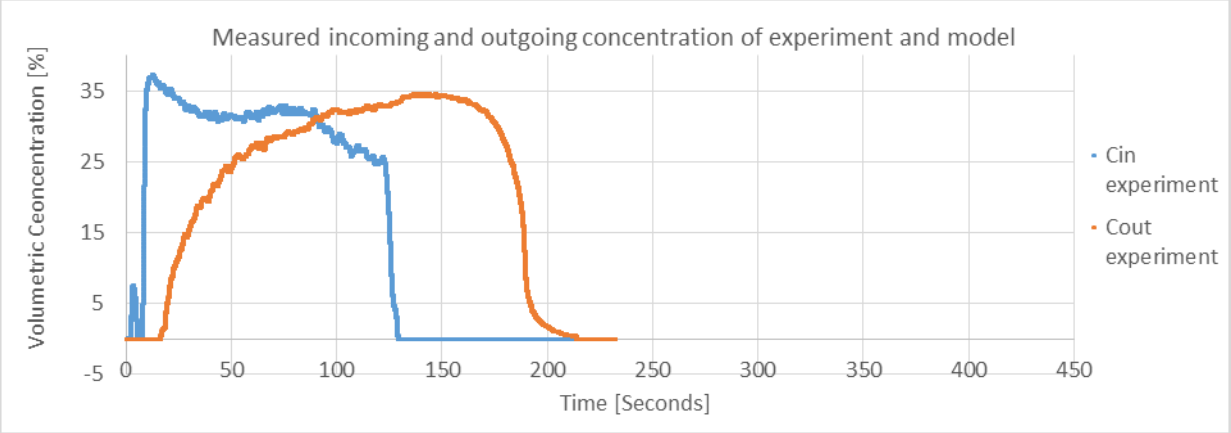

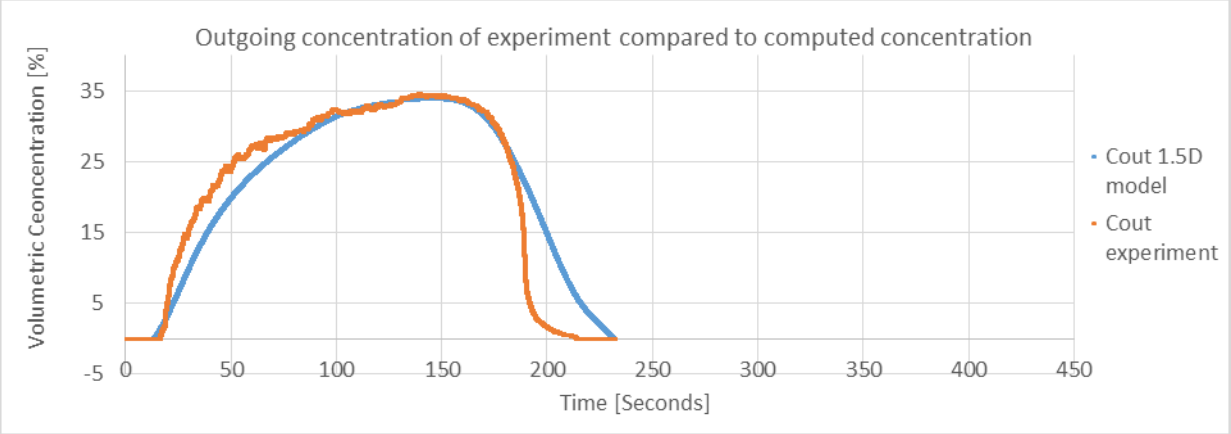

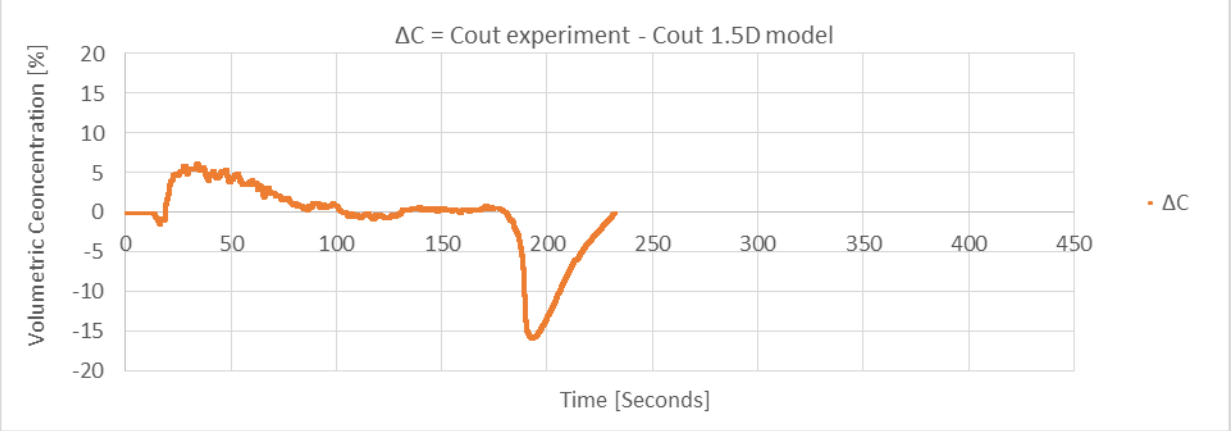

Results:

Maximum deviation: [%Cv]	15.9
Standard deviation: [%Cv]	4.6
R^2: [-]	0.89

Results of measured and computed data

Scenario number:	**5**	Jet: [l/s]	0.00	Average temp: [°C]	14.7
Batch number:	**6**	Flow in: [l/s]	3.0	Max temp: [°C]	14.8
Duration experiment: [s]	411	Flow out: [l/s]	1.9	Min temp: [°C]	14.7

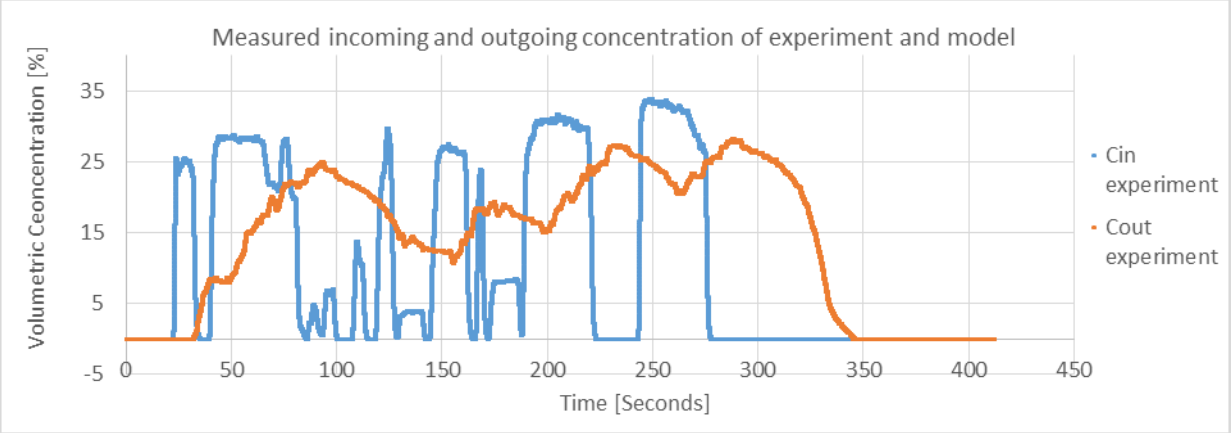

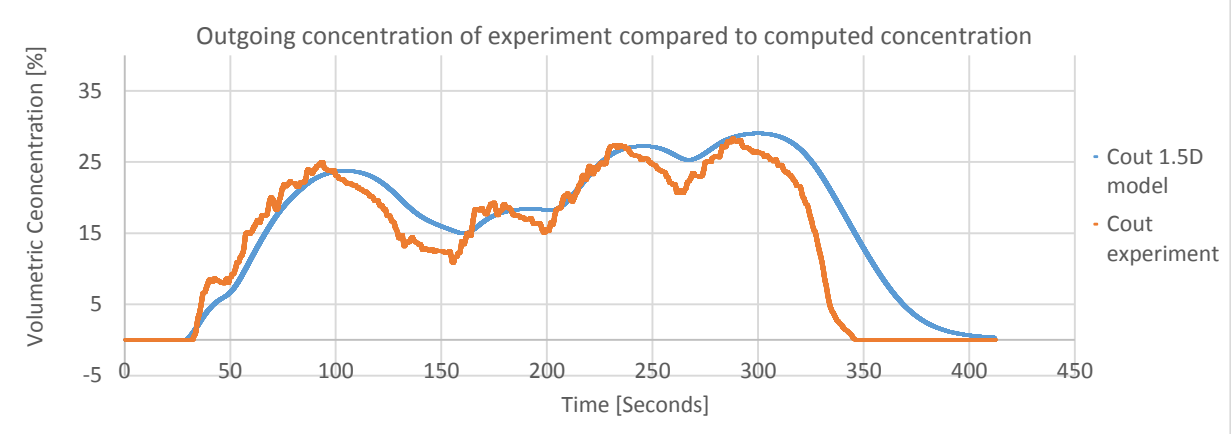

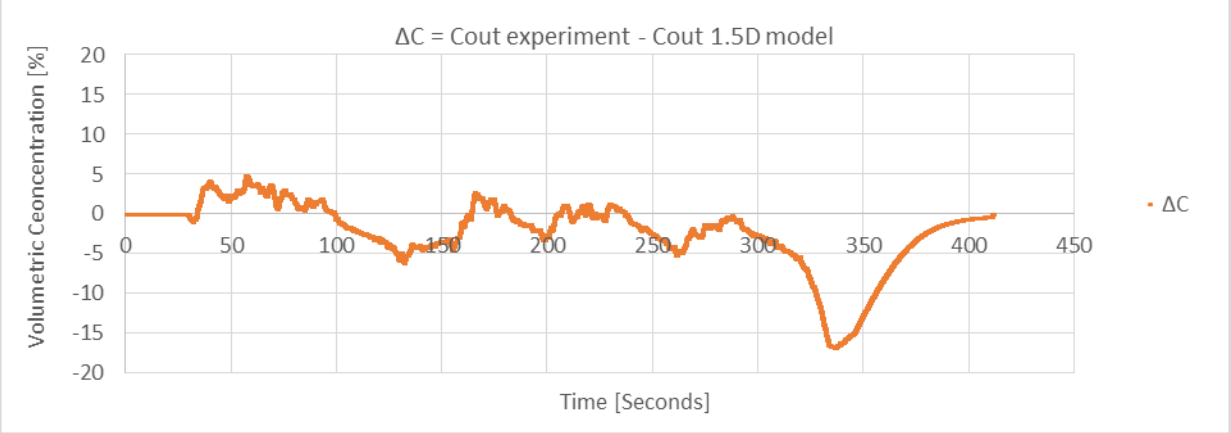

Results:

Maximum deviation: [%Cv]	16.7
Standard deviation: [%Cv]	4.1
R^2: [-]	0.84

Results of measured and computed data

Scenario number:	**6**	Jet: [l/s]	0.35	Average temp: [°C]	14.8
Batch number:	**1**	Flow in: [l/s]	3.0	Max temp: [°C]	14.9
Duration experiment: [s]	379	Flow out: [l/s]	2.5	Min temp: [°C]	14.7

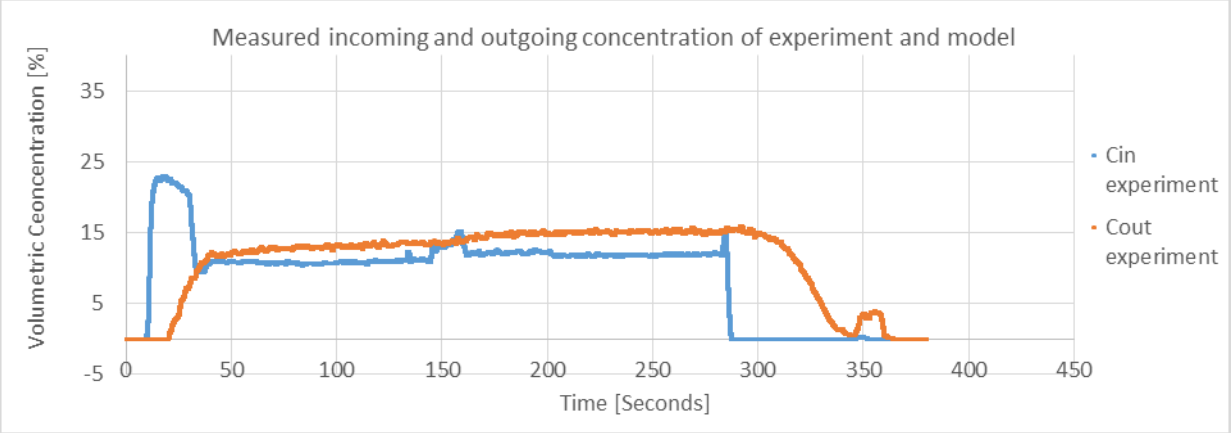

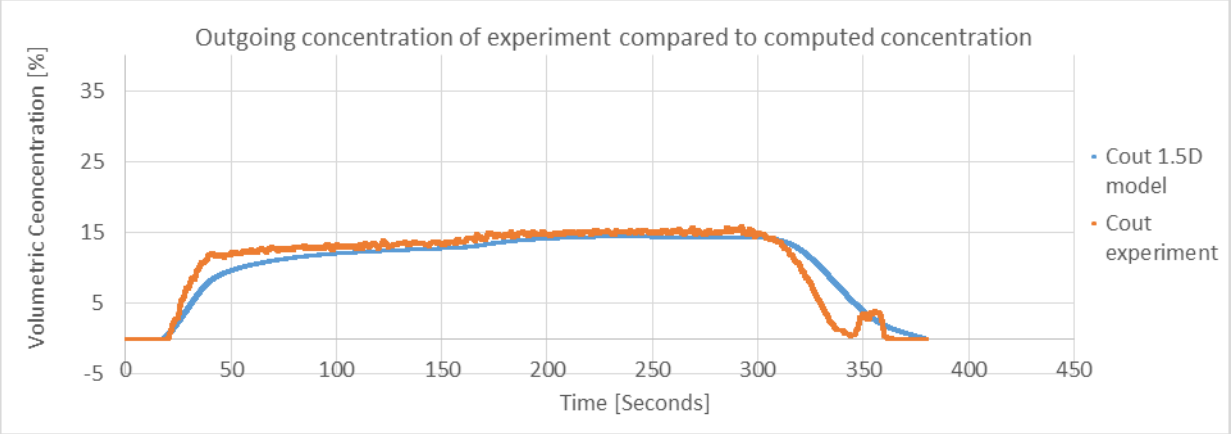

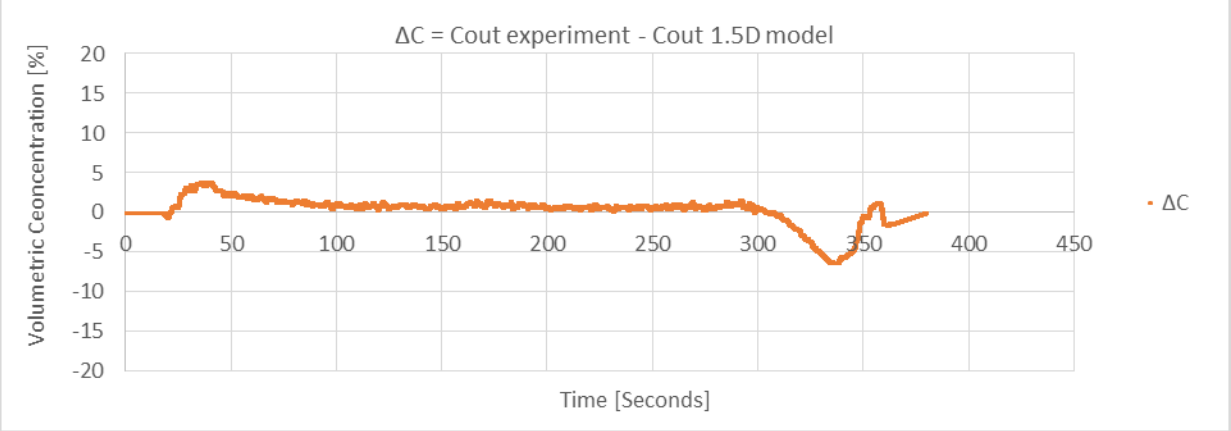

Results:

Maximum deviation: [%Cv]	6.4
Standard deviation: [%Cv]	1.9
R^2: [-]	0.90

Results of measured and computed data

Scenario number:	**6**	Jet: [l/s]	0.35	Average temp: [°C]	14.9
Batch number:	**2**	Flow in: [l/s]	3.0	Max temp: [°C]	15.0
Duration experiment: [s]	357	Flow out: [l/s]	2.5	Min temp: [°C]	14.9

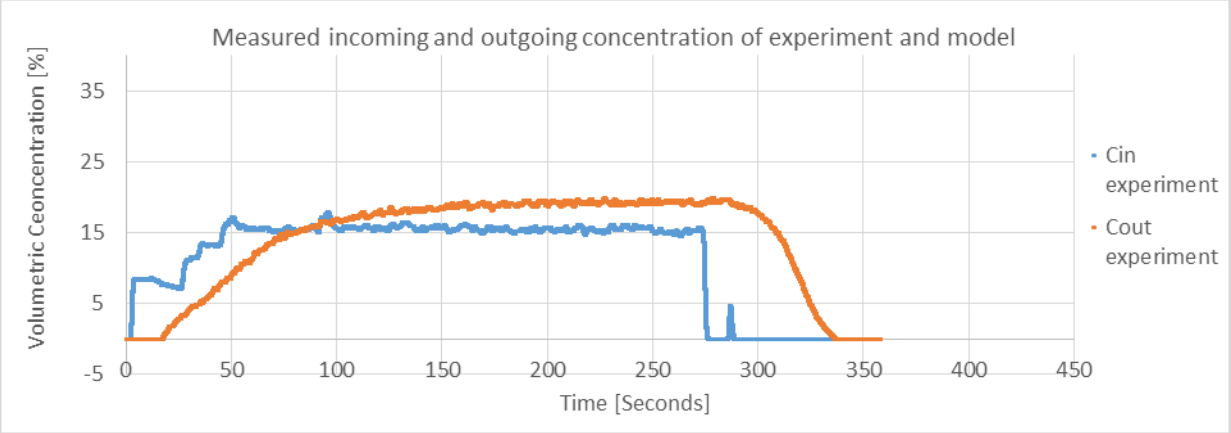

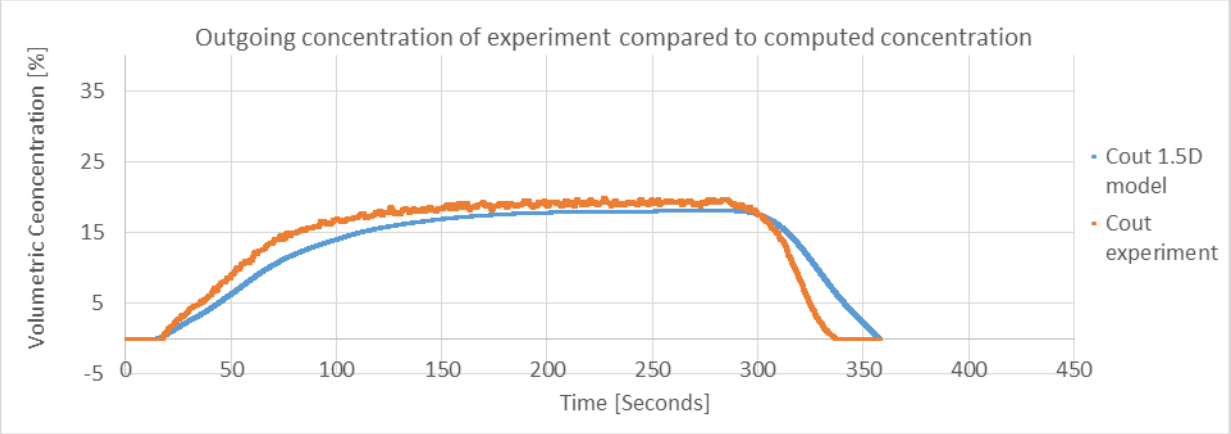

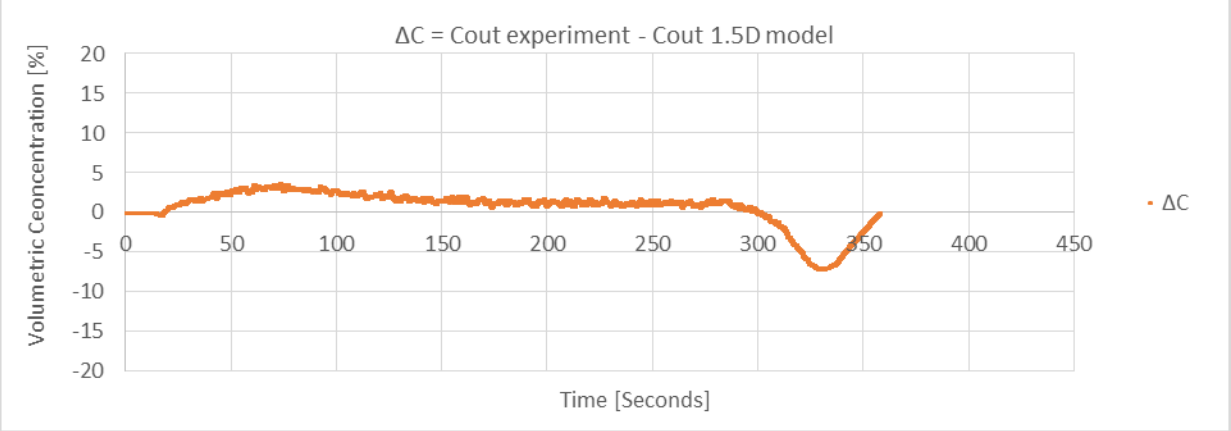

Results:

Maximum deviation: [%Cv]	7.1
Standard deviation: [%Cv]	2.4
R^2: [-]	0.90

Results of measured and computed data

Scenario number:	**6**	Jet: [l/s]	0.35	Average temp: [°C]	15.0
Batch number:	**3**	Flow in: [l/s]	2.9	Max temp: [°C]	15.1
Duration experiment: [s]	445	Flow out: [l/s]	2.5	Min temp: [°C]	14.9

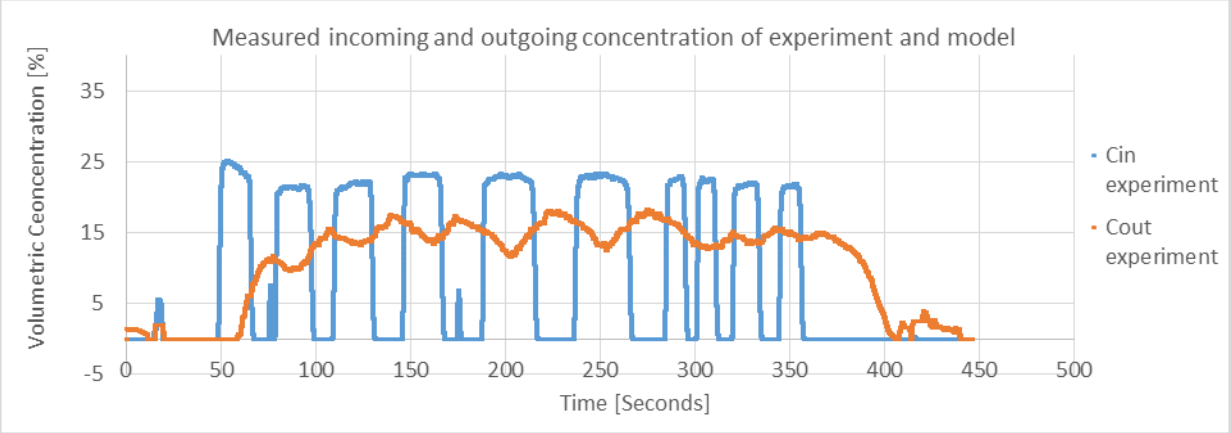

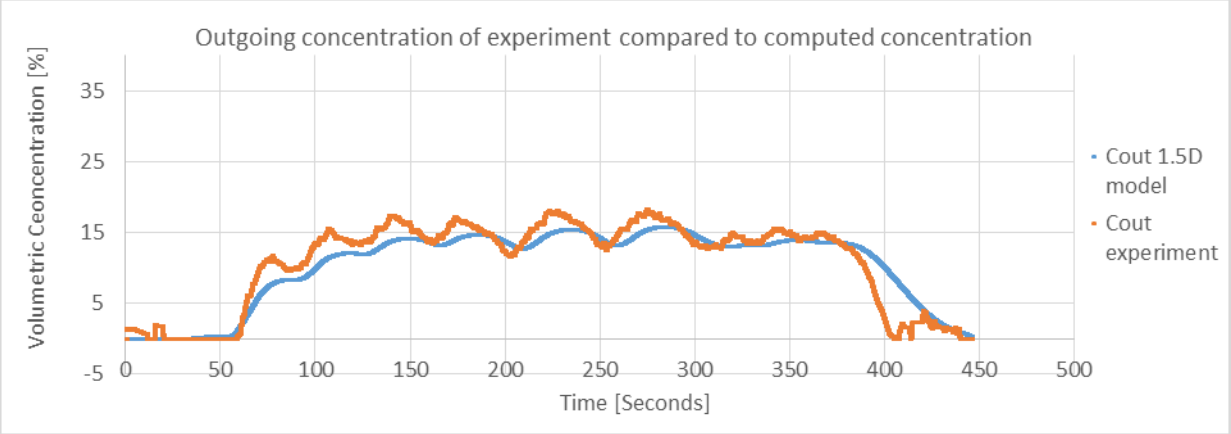

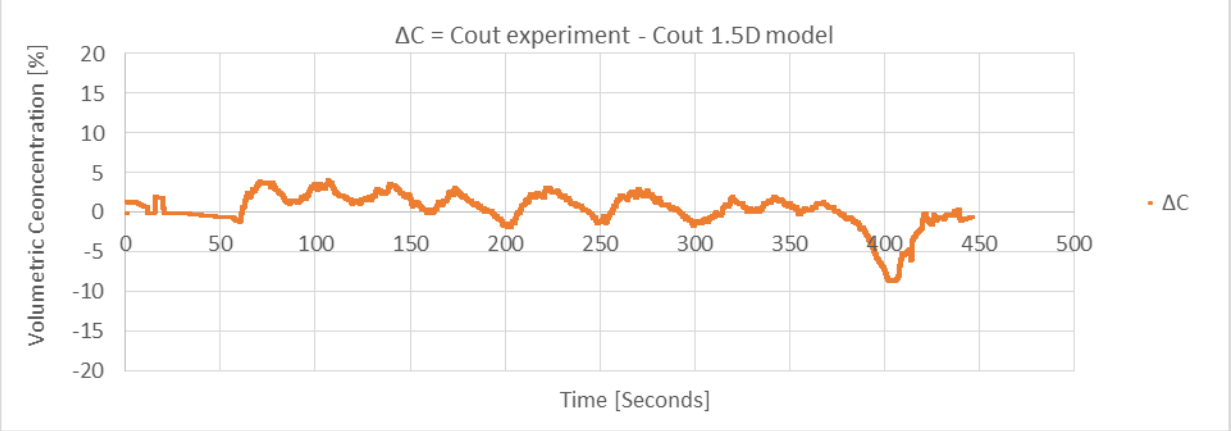

Results:

Maximum deviation: [%Cv]	8.6
Standard deviation: [%Cv]	2.4
R^2: [-]	0.89

Results of measured and computed data

Scenario number:	**6**	Jet: [l/s]	0.35	Average temp: [°C]	15.1
Batch number:	**4**	Flow in: [l/s]	3.1	Max temp: [°C]	15.2
Duration experiment: [s]	497	Flow out: [l/s]	2.5	Min temp: [°C]	15.0

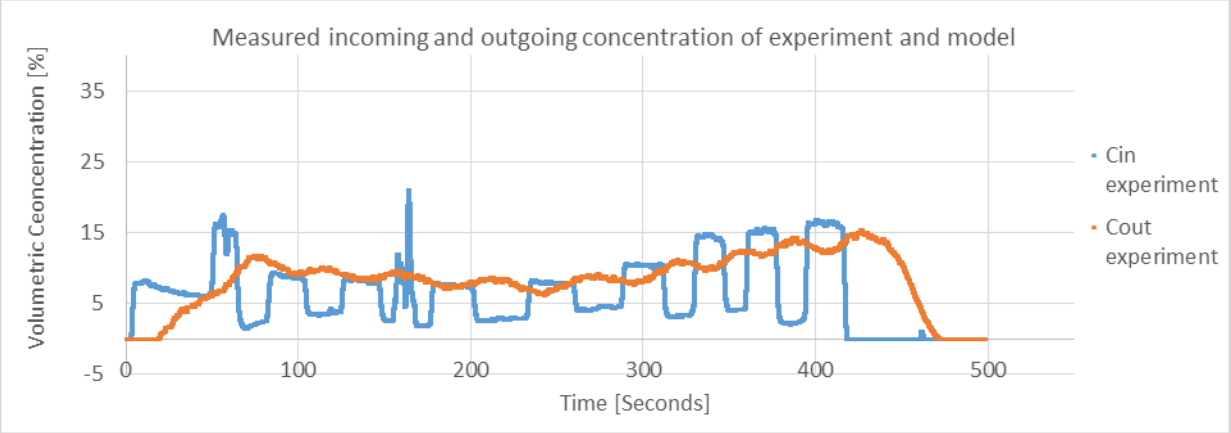

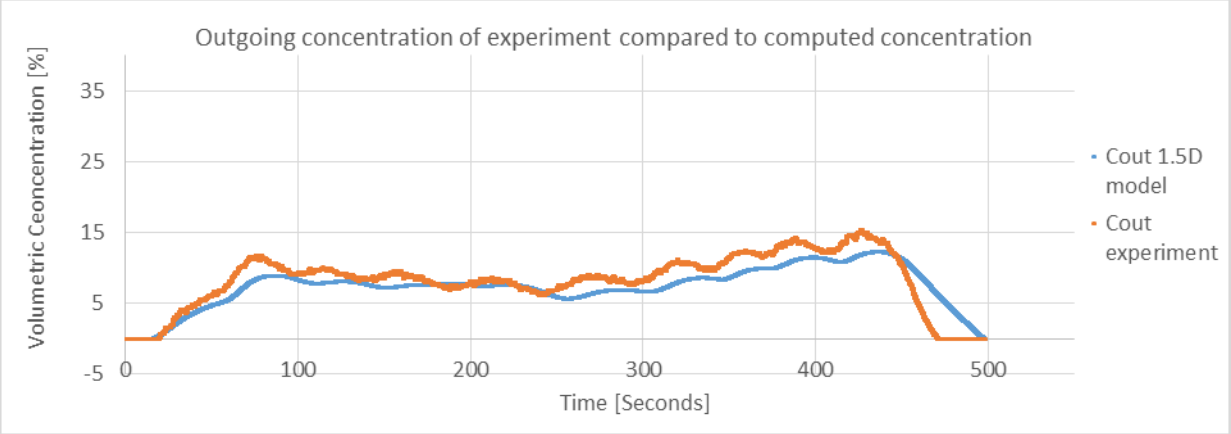

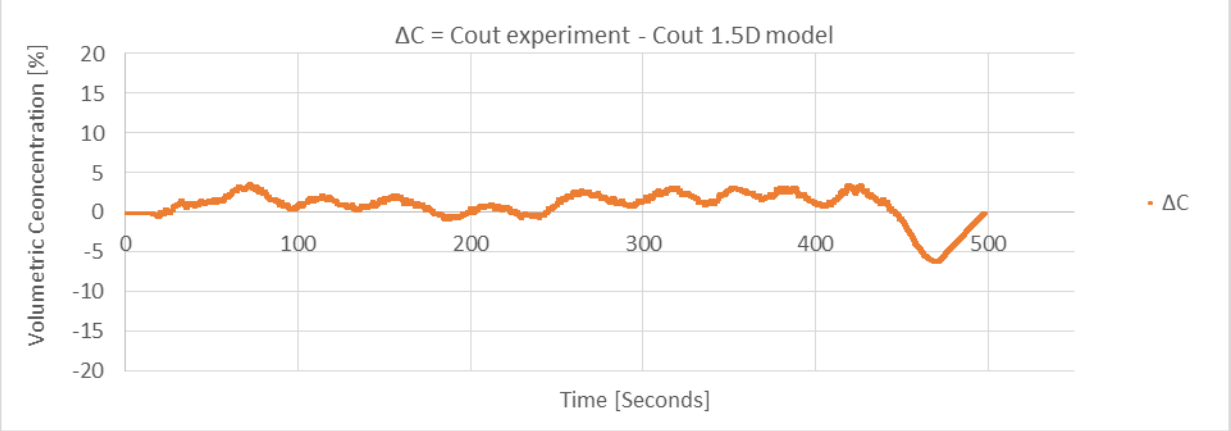

Results:

Maximum deviation: [%Cv]	6.1
Standard deviation: [%Cv]	2.0
R^2: [-]	0.80

Results of measured and computed data

Scenario number:	**6**	Jet: [l/s]	0.35	Average temp: [°C]	15.3
Batch number:	**5**	Flow in: [l/s]	3.0	Max temp: [°C]	15.3
Duration experiment: [s]	253	Flow out: [l/s]	2.5	Min temp: [°C]	15.2

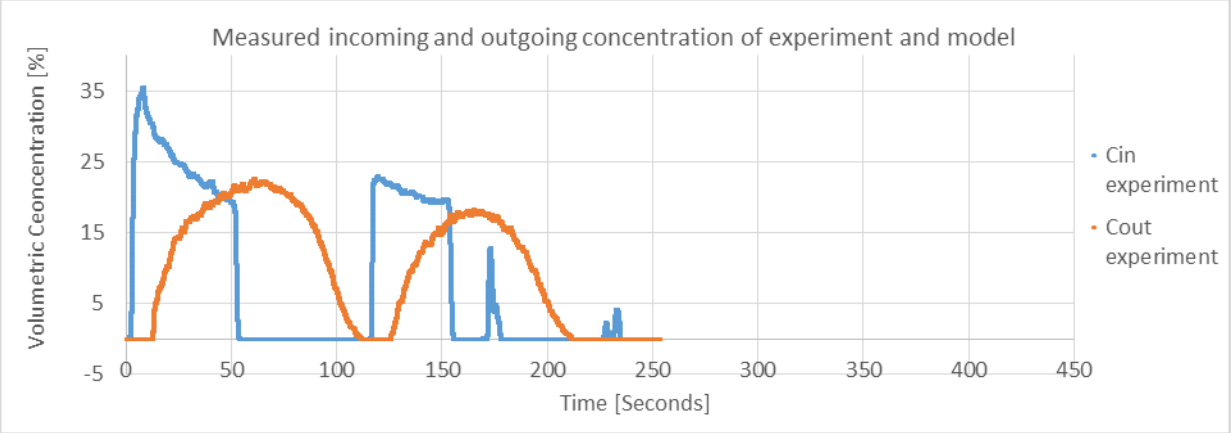

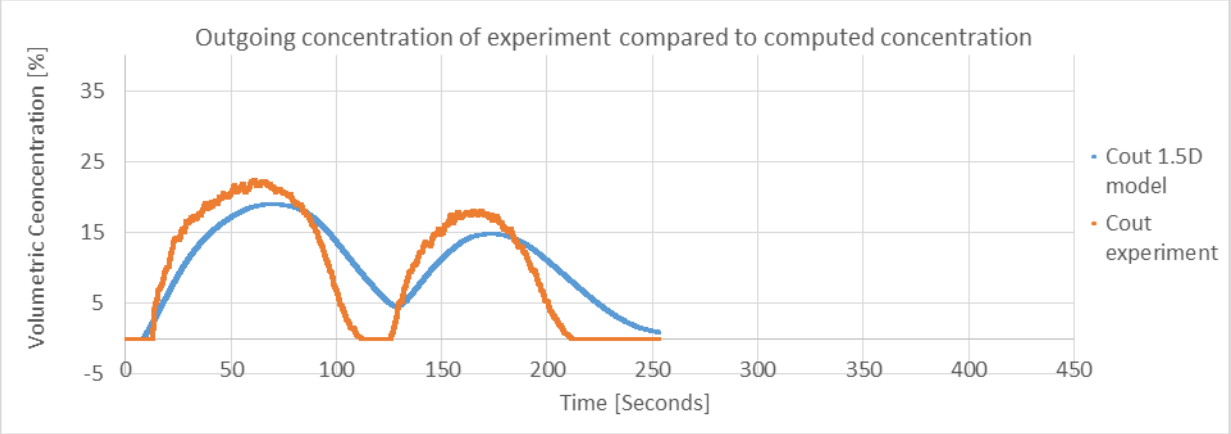

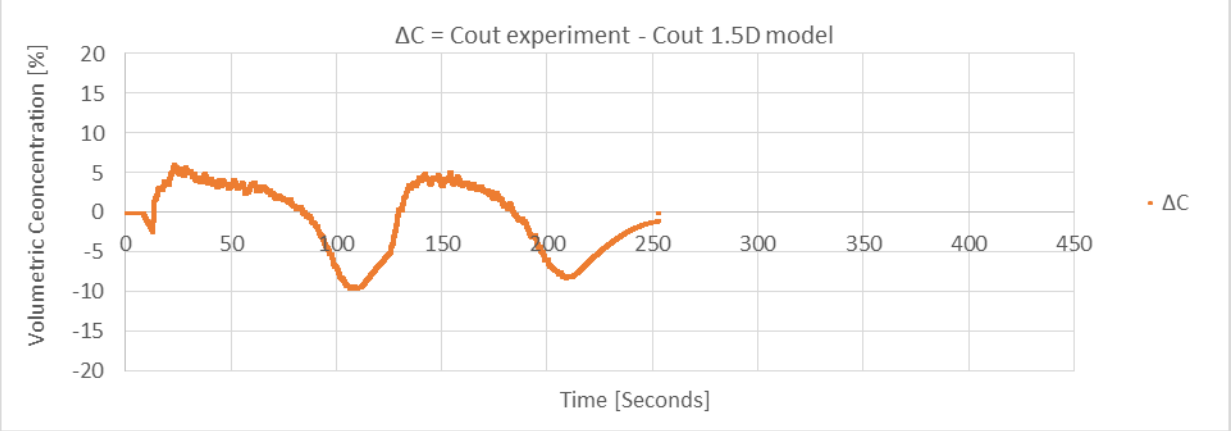

Results:

Maximum deviation: [%Cv]	9.6
Standard deviation: [%Cv]	4.7
R^2: [-]	0.76

Results of measured and computed data

Scenario number:	**6**	Jet: [l/s]	0.35	Average temp: [°C]	15.2
Batch number:	**6**	Flow in: [l/s]	3.0	Max temp: [°C]	15.3
Duration experiment: [s]	373	Flow out: [l/s]	2.6	Min temp: [°C]	15.2

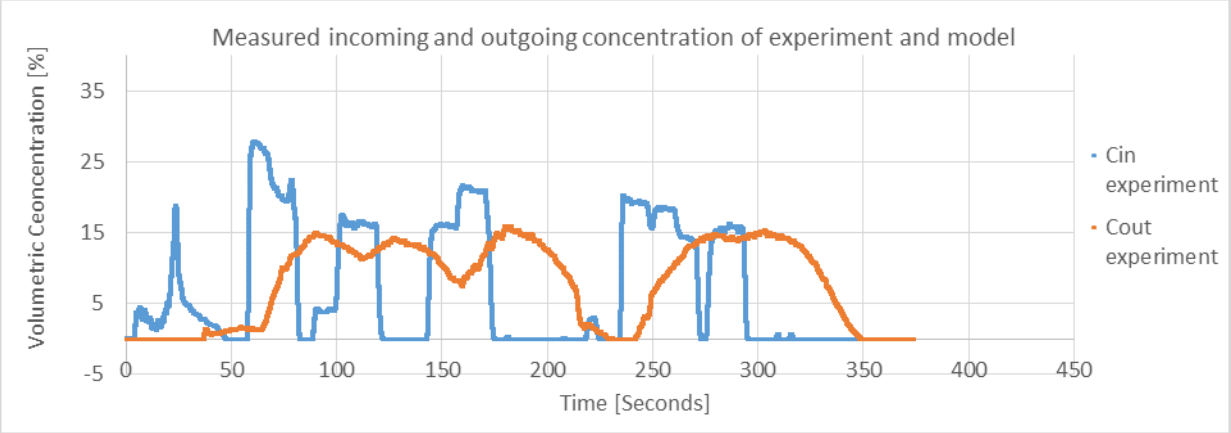

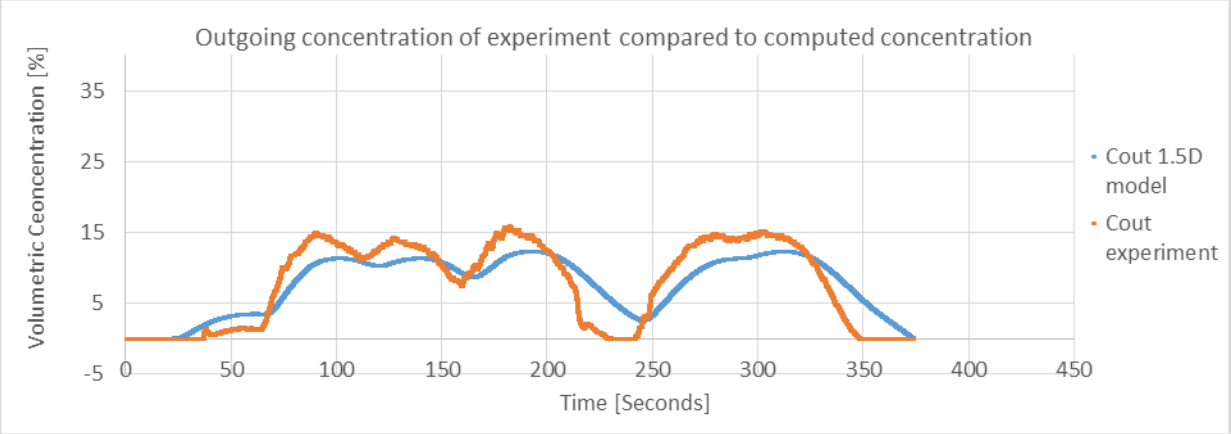

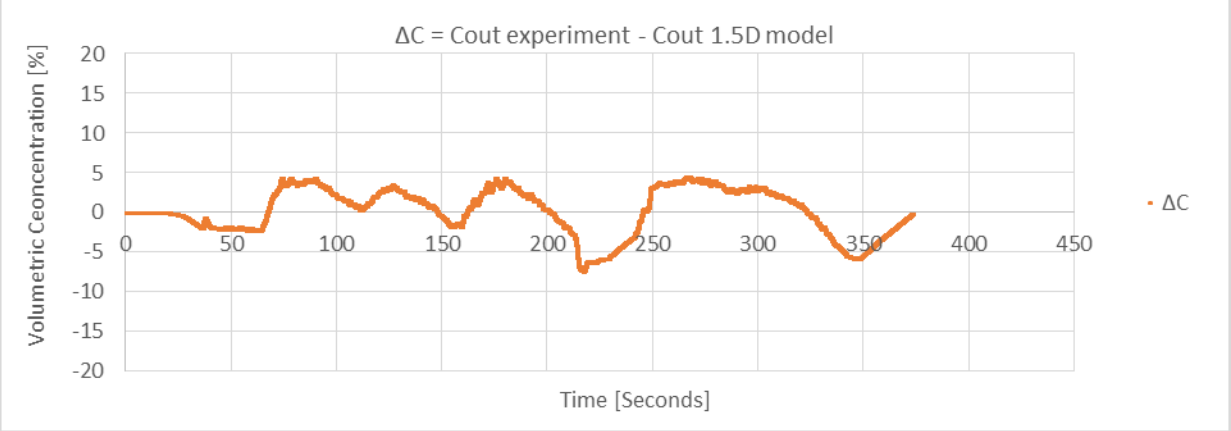

Results:

Maximum deviation: [%Cv]	7.4
Standard deviation: [%Cv]	3.1
R^2: [-]	0.84

Pulsating jet results

Figure C-1 on the next page, shows the results of the pulsating jet on the outgoing concentration. More data is available of the pulsating jet but not further analyzed in this report. Compared to all of the previous simulation, this dataset could not be compared with the 1.5D model because it only works with a constant value for the jetflow. As mentioned in the recommendations of the main report, it is advisable to add a function in the program so this value can obtain multiple values during a simulation.

During the execution of the experiment, the following parameters are used:

- $Q_{inflow} = 2{,}8\ l/s$
- $Q_{outflow} = 1{,}8\ l/s$
- $Q_{jet} = 0{,}38\ l/s$
- Jet interval: $20\ sec$ and $30\ sec$ (see **Figure C-1**)

When looking at the results as presented in **Figure C-1** several interesting remarks can be observed:

- The effect of turning on/off the jet can be seen in the outgoing concentration profile.
- When the jet is turned on the concentration in the outflow suddenly decreases and vice versa.
- The frequency of the pulsating jet can be seen in the outgoing concentration profile.
- The deviations on the outgoing concentration due to the jet are in the order 1-2% C_v.

Conclusion & recommendation

A pulsating jet has effect on the concentration in the outflow. It is advisable to implement this fluctuating jet in the 1.5D model and to investigate what the effects are on the concentration in the outflow.

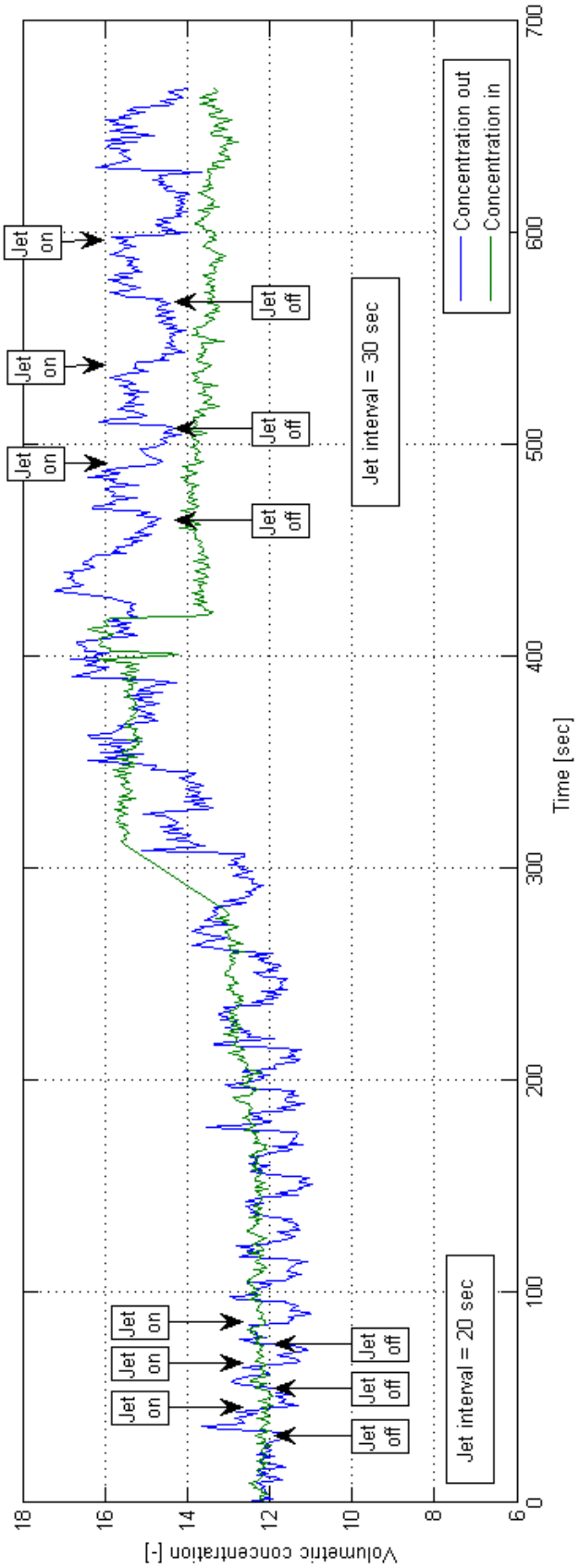

Figure C-1: results of fluctuating jet on the outgoing concentration